Tuning Aromaticity in Superacidic Media

Alexander Nitzer

Dissertation zur Erlangung des Doktorgrades

der Fakultät für Chemie und Pharmazie

der Ludwig-Maximilians-Universität München

Tuning Aromaticity in Superacidic Media

Alexander Nitzer

aus

Moskau, Russische Föderation

2022

Erklärung

Diese Dissertation wurde im Sinne von §7 der Promotionsordnung vom 28.November 2011 von Herrn Prof. Dr. Andreas Kornath betreut.

Eidesstattliche Versicherung

Diese Dissertation wurde selbstständig und ohne unerlaubte Hilfe erarbeitet.

München, den 12.09.2022

Alexander Nitzer

Dissertation eingereicht am	17.08.2022
1. Gutachter	Prof. Dr. A. J. Kornath
2. Gutachter	Prof. Dr. T. M. Klapötke
Mündliche Prüfung am	07.09.2022

„Don`t just have an idea – have all of them.”

Niv-Mizzet

Danksagung

Vielen Leuten gebührt Dank, ohne sie wäre diese Arbeit nicht zu Stande gekommen, ich hoffe sie alle in den folgenden Sätzen zu erwähnen.

Sehr großer Dank gilt Herrn Prof. Kornath für die Betreuung dieser Arbeit. Den Forschungsfreiraum, die Projektvielfalt auch über die reine akademische Forschung hinaus, die Möglichkeit sich zu entwickeln, die Unterstützung bei vielerlei Problemen, dafür bin überaus dankbar.

Des Weiteren danke ich Herrn Prof. Klapötke für die Übernahme der Zweitkorrektur dieser Arbeit.

Ich danke dem ganzen Arbeitskreis für die schöne Zeit, sei es zur Bachelor-, Master- oder Doktorarbeit: Domi, Michi, Ines, Yvonne, Manu, Flo, Chris, Alan, Steffi, Marie, Basti, Dirk und Valentin. Wir hatten eine schöne Zeit, ich werde mit einem lachenden und einem weinenden Auge zurückblicken.

Ich danke Chris für das Lösen vieler meiner Kristallstrukturen sowie später das Beibringen dessen. Herrn Prof. Karaghiosoff und Herrn Dr. Krumm danke ich dabei für die Unterstützung, zudem bei jeglicher Fachfrage, die seiner Expertise bedurfte. Frau Breitenstein gebührt Dank für die unermüdliche Unterstützung bei den NMR-Messungen.

Ralf, Karl und vor allem Thomas danke ich für die wissenschaftliche Ausbildung und schöne Zeit in Los Angeles, die mir sehr geholfen hat.

Gaby danke ich für Unterstützung und vor allem für Verständnis, in jeglicher Hinsicht.

Meinen fünf Praktikanten gebührt großer Dank, vieles von dieser Arbeit ist durch sie möglich geworden − Martin, Robert, Pauline, Malte und Julian − euch vielen Dank.

Meinen Freunden danke ich für die vielen schönen Erlebnisse, die wir in und München hatten, den Beistand in den nicht immer einfachen Jahren, schön dass wir uns kennengelernt haben.

Der größte Dank gebührt meinen Eltern – die Unterstützung, die Liebe, einfach alles.

Table of Contents

1. Introduction 1
2. Objectives 6
3. Results 8
   - 3.1 Tricarboxybenzenes 8
   - 3.2 1,3,5-Tricyano- and 1,3,5-Triaminobenzene 13
   - 3.3 1,2,4,5-Tetracarboxybenzene 16
   - 3.4 Trihydroxybenzenes and 1,3,5-Trimethoxybenzene 17
   - 3.5 Cyanuric acid and Urazole 24
   - 3.6 Diaminomaleonitrile 27
4. Conclusion and Summary 31
5. Citations 33
6. Appendix 35
   - 6.1 List of Publications, Drafts and Conference Contributions 35
     - 6.1.1 Publications 35
     - 6.1.2 Drafts 35
     - 6.1.3 Conference contributions 36
7. Papers and Drafts
   - 7.1 Third time is a charm – protonating tricarboxybenzenes 37
   - 7.2 Two room-temperature stable trications – Triprotonated triamino- and tricyanobenzene 45
   - 7.3 A small room temperature stable tetracation 53
   - 7.4 Preparation of a room temperature stable cyclohexenyl carboxonium dication 58
   - 7.5 Arenium, oxononium and arenium oxonium cations – Protonation of 1,2,3- and 1,2,4-trihydroxybenzene 64
   - 7.6 Increasing aromaticity by protonation 71
   - 7.7 N, C, O – distribution of charge in protonated urazole 77
   - 7.8 Diaminomaleonitrile – mono-, di- …and tetraprotonation?! 82

1. Introduction

Aromaticity – this term is controversially discussed by chemists for more than a century. The expression was first mentioned by A. W. Hofmann in 1857, when he described the existence of insolinic acid, a compound derived from the purification of cuminic acid, as one of the monobasic aromatic acids.[1] The olfactory characteristics, meaning the distinct smell was already associated with many substances and then defined aromatic. Hofmann's student, A. Kekulé, has proposed propose a concept of greatest importance.[2] Benzene, C_6H_6, is the aromatic compound par excellence, being the key building block to an enormous variety of molecules. Kekulé also addressed this molecule, as its structure was yet unknown. First, he proposed sausage-like structures to be present (Figure 1).[3]

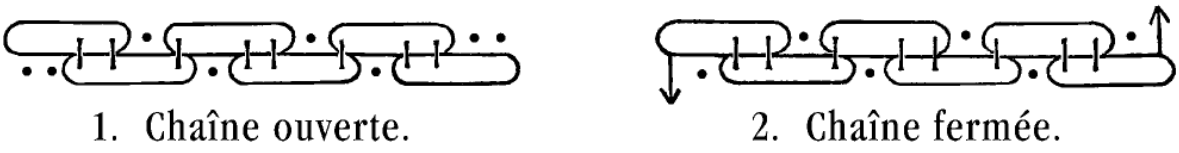

Figure 1. Kekulé's sausage formulas for open and closed chains in benzene.[2-3]

He dreamed of an ouroboros later, a snake eating its own tail, and write the well-known hexagon structures with three double bonds, a cyclohexatriene (Figure 2).[4] The double and single bonds exchange places rapidly, which somewhat describes the different behavior of benzenes compared to olefines.[5]

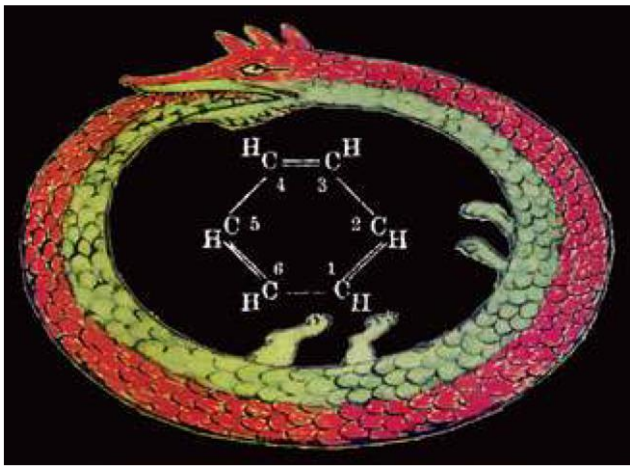

Figure 2. The ouroboros - a serpent eating its tail, the inspiration for Kekulé's breakthrough.[6]

This difference is easily observable when comparing the hydrogenation of benzene to that of cyclohexene and cyclohexadiene. The experimentally found heat of reaction to form cyclohexane from cyclohexene is −118 kJ/mol. If a cyclohexatriene structure, an olefine-like species, was present in benzene, it should be three times the energy from the hydrogenation of cyclohexene, adding to −354 kJ/mol. It is much less in reality, only −206 kJ/mol are needed.[6]

This difference of 148 kJ/mol had to be addressed. J. Thiele described the nature of unsaturated and aromatic compounds in 1899.[7] Based on Kekulé's theory, he denoted compounds with conjugated double bonds and assign partial valences to each atom. If an even partial valence were present, the system is conjugated. With the partial valences, the concept of magnetism was brought into the topic of aromatic compounds, which becomes important at a later stage. Linus Pauling used quantum chemical[8] and experimental data to quantify resonance energies,[9] further explaining the resonance of aromatic compounds.[10] The double bonds inside the benzene ring merged to the well-known ring. The resonance stabilization amounts to the calculated difference of 148 kJ/mol. The invention of X-ray diffraction enabled the exact measurement of bond lengths. The carbon bonds of benzene were found to be equisized, in length between carbon single and double bonds.[11] Thus one important criterium of aromaticity was measured: The bond equalization. Later, it was found that aromatic compounds in general are stabilized by π-π interactions, which are attractive interactions between two π-systems.[11b]

But what is aromaticity, what compound qualifies for it, how can it be quantified? E. Hückel was given an explanation: The MO scheme of benzene leads to the formation of a π-system, the electrons from the 2p orbitals of each carbon are delocalized above and below the ring plane.[12] A correlation between number of π-electrons and aromaticity was done, ultimately leading to Hückel's rule. A cyclic system would be aromatic, if 4n+2 π-electrons were present. If 4n π-electrons were found, it would be antiaromatic, which results in lowered stability and higher reactivity of such compound. If neither of them was true, a compound would be non-aromatic. That aromaticity does not depend on the number of atoms, but the number of delocalized electrons inside the ring has been shown with the two following examples. Besides the cyclopentadienyl anion, the cycloheptatrienyl (tropylium) cation was prepared, which

does confirm Hückel's rule.[13] The quantifiying of aromaticity started from the concept of magnetic ring current, first proposed by London[14] and extended by Pople and Untch.[15] Based on Hückel's rule, a ring exhibits a quantifiable diamagnetic ring current for aromatic compounds like benzene or a paramagnetic one for non- or antiaromatic compounds, for example pentalene or heptalene. The newly invented NMR spectroscopy[16] gave suitable experimental data, enabling the testing of those theories. The ^{1}H NMR shifts of different annulenes were measured and the systems evaluated, if 4n or 4n+2 π-electrons were present. The hydrogen atoms inside the polyene ring with 4n+2 π-electrons exhibit as decreased shielding, a downfield shift, while the outer ones are shielded, exhibiting an upfield shift. The below depicted [18]-annulene is an example for this type of compounds (Figure 3). For systems with 4n π-electrons, the shieldings were found to be vice versa.[13b, 15]

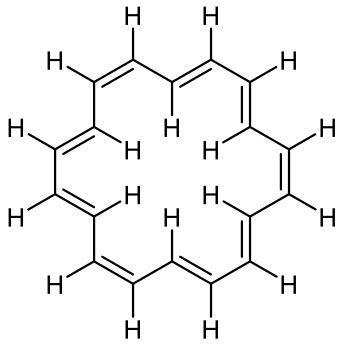

Figure 3. [18]-Annulene, the inner hydrogens are highly shielded with a ^{1}H NMR shift of -1.9 ppm, the outer ones are highly deshielded, exhibiting a ^{1}H NMR shift of 8.2 ppm.[15]

As the computational possibilities increased exponentially after World War II, quantum chemistry flourished. The molecular orbitals were calculated and their energy levels quantified. NMR shifts were not only be computed, but the ring current itself quantified, correlating to aromatic character. Starting from the magnetic susceptibility parameter Λ, ring currents were computed, culminating in the NICS parameter, the Nucleus-Independent Chemical Shift.[17] NICS was an attempt by Schleyer to quantify aromaticity independent from ring size, inclusion of non-carbon atoms into rings and charge etc. (Figure 4). First, the position inside the middle of the ring plane was used for ring current probing, abbreviated as NICS(0).

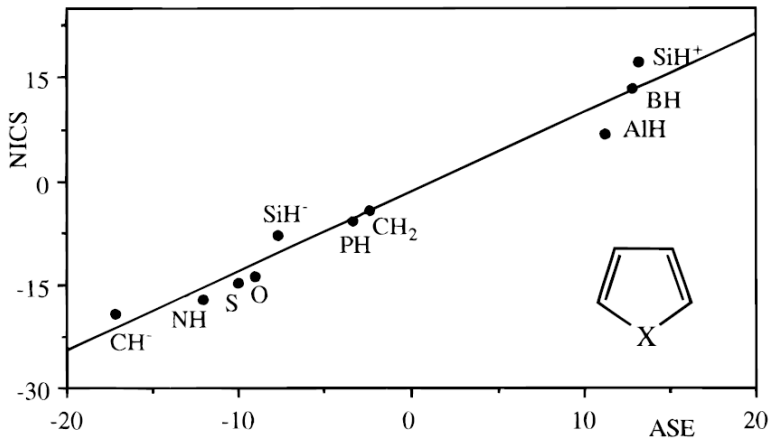

Figure 4. Schleyer's Plot of NICS values (ppm) against ASEs (aromatic stabilization energy) (kcal/mol) for a set of five-membered heterocycles C_4H_4X (cc= 0.966).[17]

The concept was quickly expanded, as different positions of the NICS probe were evaluated (Figure 5), only the π-component of the shift considered, and much more.[18] An outstanding variety of NICS parameters came into being, often paired with the question, which one should be used, and which is best.[19]

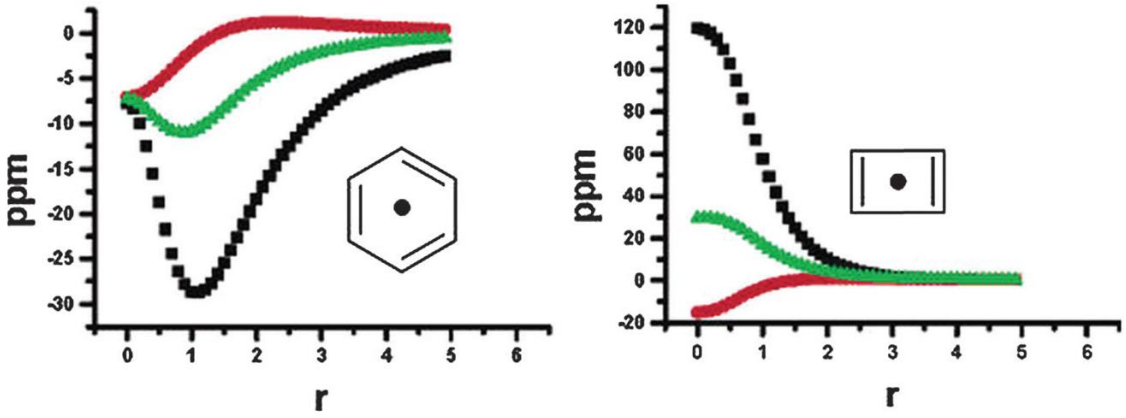

Figure 5. In-plane (red), out-of-plane (black) and isotropic (green) NICS values for benzene (left) and cyclobutadiene (right) as a function of distance.[20]

Aromaticity was a term reserved for benzene-like compounds, at least so in the beginning. With increasing synthetic, analytical and computational methods, compounds like the square planar Al_4^{2-} anion,[21] borazine[22] and cyanuric acid[23] were predicted to be (slightly) aromatic

and concepts like Möbius[24] and Spherical[25] aromaticity were investigated. The cyclic compound S_2N_2 first proposed to be aromatic, later not aromatic,[26] then again confirmed to be aromatic, despite present diradical character.[27] Structural criteria like bond length equivalence, energetic criteria like hydrogenation energies or magnetic criteria such as NICS, the term aromaticity expanded far from where it was at the beginning[28] – a simple matter of odor.[29]

Aromaticity and superacid chemistry, these topics are closely related and have quite a history. Superacids are per definition acids stronger than 100% sulfuric acid.[30] Due to the leveling effect of water, the employed compounds must be absolutely water-free.[31] Acid strength is quantified by the Hammett acidity function H_0 (see Equations 1 and 2).[32]

$$(1)\quad H_0 = -\log a_{H^+} \cdot \frac{f_B}{f_{BH^+}} = -\log K_{BH^+} + \log \frac{c_B}{c_{BH^+}}$$

With (2) $$B + H^+ \rightleftharpoons BH^+$$

While Gillespie defined the term superacid, G. O. Olah is perhaps the one chemist with the greatest impact in superacidic chemistry, earning him the nobel prize in 1994.[33] Several reactions, for example the Friedel-Crafts alkylation or the electrophilic aromatic substitution, require highly acidic conditions to function. The latter takes place via an arenium ion, a protonated benzene derivative, a non-aromatic Wheland-intermediate. Olah's work includes a huge variety of aromatic compounds, which are protonated in superacidic media. His NMR spectroscopic studies, mostly at low temperatures, enabled the characterization of various aromatic, non-aromatic and even some antiaromatic compounds. Notable amongst others are his works on protonated (substituted) benzenes,[34] protonated squaric acid (which becomes aromatic upon protonation)[35] or the 2-norbornyl cation.[36]

2. Objectives

Extensive studies on the behavior of benzene in superacidic media do exist, also most simple aromatic compounds were already investigated in various superacids. These systems are large enough to readily stabilize one or two positive charges. One aim of this thesis is to protonate slightly larger systems in superacidic media, so that tri- or even tetracations could be prepared.

The protonation of the three isomers of tricarboxybenzene will be investigated to analyze the influence of the substitution pattern of the species on the protonation sequence and the subsequent change in aromatic character (Scheme 1). The importance of the respective protonated functional group, which is attached to the aromatic core, will also be evaluated by reacting 1,3,5-tricyano- and 1,3,5-triaminobenzene in superacidic media. Finally, the protonation of 1,2,4,5-tetracarboxybenzene is ultimately attempted to test the influence of the amount of positive charge on the aromatic character.

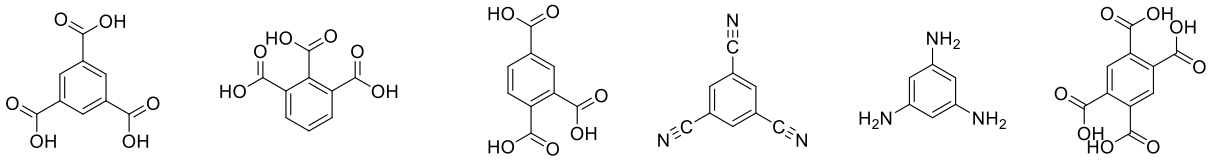

Scheme 1. Lewis structures of (from left to right) trimesic acid, hemimellitic acid, trimellitic acid, 1,3,5-tricyanobenzene, 1,3,5-triaminobenzene and pyromellitic acid.

The most basic centers of the compounds from the first block are expected to be at the attached functional groups. This is not certain for the next group of species. The three isomers of trihydroxybenzene and their methyl ethers were reacted by Olah in superacidic media.[34] The target of this thesis will be to extend Olah's ^{1}H NMR data, foremost attempt to isolate these cations and compare the analytical results to those from the first group of compounds (Scheme 2). The site of protonation, be it at the oxygen or at the ring, is of special interest, as it should greatly influence aromatic character.

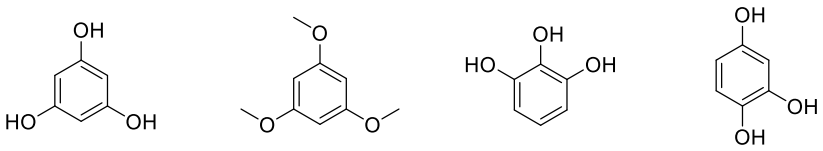

Scheme 2. Lewis structures of (from left to right) phloroglucinol, phloroglucinol-trimethylether, pyrogallol and hydroxyhydrochinon.

So far, only pure carbon-containing, six-cycle rings are listed. Aromaticity is not limited to benzene and its derivatives, but to far more species. Cyanuric acid and urazole are N-heterocyclic compounds, which exhibit both carbonyl and N-H moieties as possible sites for protonation (Scheme 3). Cyanuric acid is a debatable compound regarding aromaticity,[23] while urazole is aromatic. Additionally, diaminomaleonitrile will be investigated in superacidic media, as the possibility of cyclization and consequently aromatization should be evaluated.

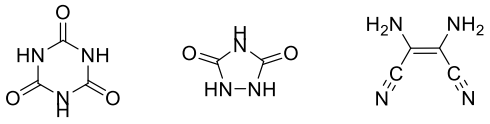

Scheme 3. Lewis structures of cyanuric acid (left), urazole (middle) and diaminomaleonitrile (right).

3. Results

The molecules were mainly protonated in the superacidic systems HF/SbF_5 and HF/AsF_5. If beneficial or necessary, weaker superacidic systems like HF/GeF_4 or HF/BF_3 were also employed. Prepared salts were isolated and by means of NMR and vibrational spectroscopy as well as single crystal X-ray diffraction characterized. Quantum-chemical calculations of the found products enabled assessment of aromatic character, foremost by NICS(0) computations. The results for each group of investigated species are summarized in the following.

3.1 Tricarboxybenzenes

All three isomers of tricarboxybenzene were mono-, di- and even triprotonated in HF/SbF_5. Triprotonations were also observed when using HF/AsF_5, except for 1,2,3-tricarboxybenzene as starting material, were only diprotonation was possible. The mono- and diprotonated species of 1,2,3- and 1,2,4-tricarboxybenzene were isolated and selected salts crystallographically characterized. The triprotonation of 1,3,5-tricarboxybenzene is visualized in Equation 3, the formed salts were stable at room temperature.

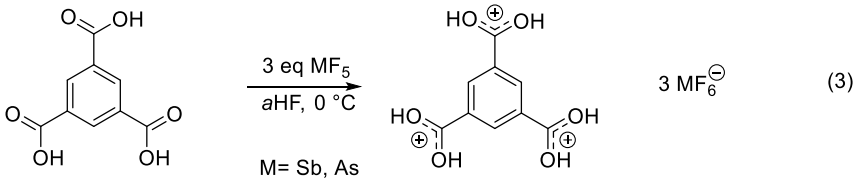

(3)

The hexafluoridoantimonate of triprotonated 1,3,5-tricarboxybenzene was redissolved in *a*HF and NMR spectroscopically characterized. ^{13}C NMR data showed the deshielding of the carboxonium and C-H arylic carbons are deshielded by triprotonation, while the tertiary arylic carbons are shielded. The trication was also successfully crystallized as [1,3,5-$C_6H_3(COOH_2)_3$][$(SbF_6)_3$] · 3HF (Figure 6). Most notable is the slight decrease in bond length of the CC single bonds by triprotonation.

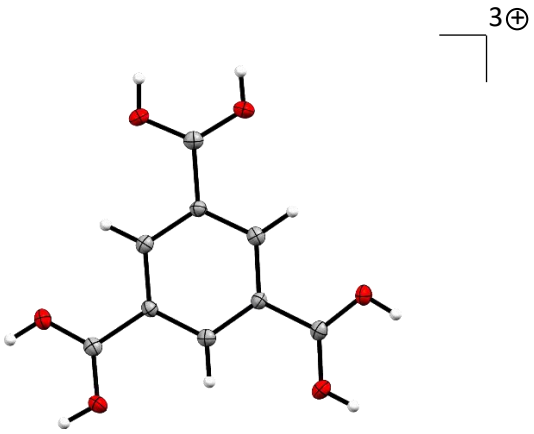

Figure 6. Formula unit of [1,3,5-$C_6H_3(COOH_2)_3$][$(SbF_6)_3$] · 3HF, view along *c*, displacement ellipsoids at 50% probability, closest HF and SbF_6^- molecules are shown.

1,2,3-Tricarboxybenzene was triprotonated by employing HF/SbF_5. First protonation occurs at the carboxy group in 2-position. Second and third protonation then take place at the other two carboxy groups (Equation 4). The formed salts are stable at room temperature.

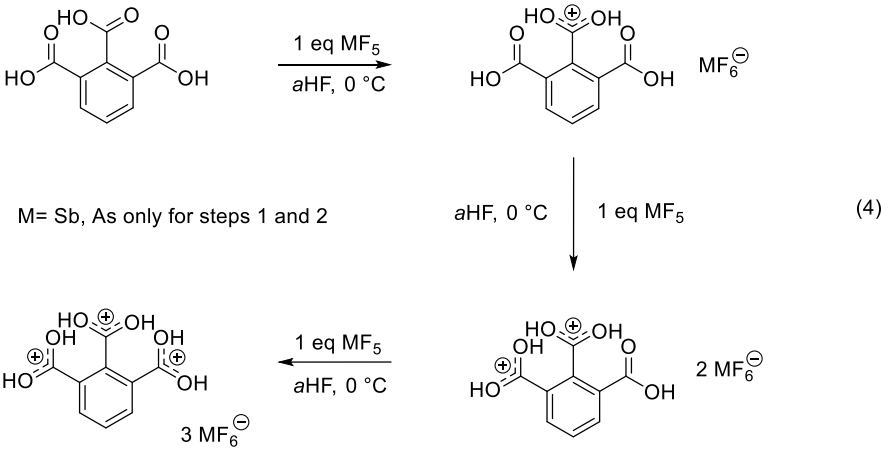

The mono- and tricationic species were also isolated as [1,2,3-$C_6H_3(COOH)_2(COOH_2)$][SbF_6] · 3HF and [1,2,3-$C_6H_3(COOH_2)_3$][$(SbF_6)_3$] (Figure 7). A slight decrease in bond length by protonation is observed in the triprotonated species for one CC single bond.

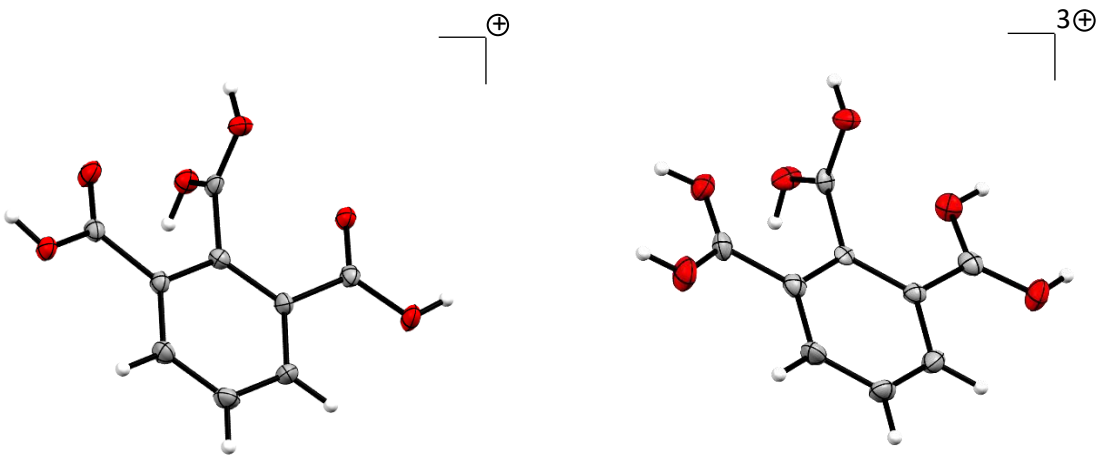

Figure 7. Hydrogen bonding between cations of $[1,2,3\text{-}C_6H_3(COOH_2)(COOH)_2][SbF_6] \cdot 3HF$, view along *a* (left) and formula unit of $[1,2,3\text{-}C_6H_3(COOH_2)][(SbF_6)_3]$, view along *c* (right), displacement ellipsoids at 50% probability.

The monoprotonation of 1,2,4-Tricarboxybenzenes leads to an intramolecular hemiprotonation, as the proton is located between the two oxygens of the carboxy groups in positions 1 and 2 (Equation 5). Second protonation thus occurs at the carboxy group in position 4, while triprotonation breaks the hemiprotonation and leads to the found trication. The latter was the only species, which was only stable up to 0 °C.

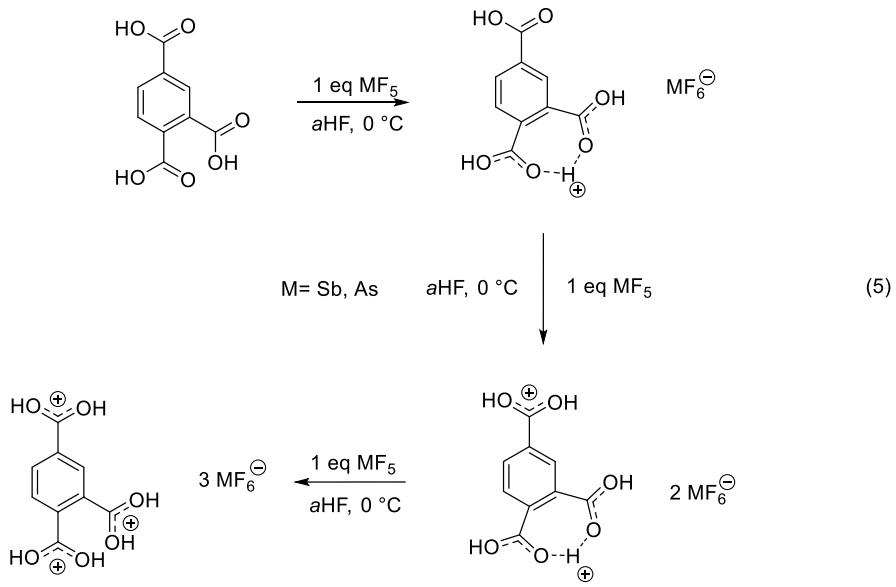

The mono- and triprotonated species of 1,2,4-tricarboxybenzene were crystallized as [1,2,4-$C_6H_3(COOH)_2(COOH)_2(H)][AsF_6]$·HF and [1,2,4-$C_6H_3(COOH_2)_3][(SbF_6)_2(Sb_2F_{11})]$ (Figure 8).

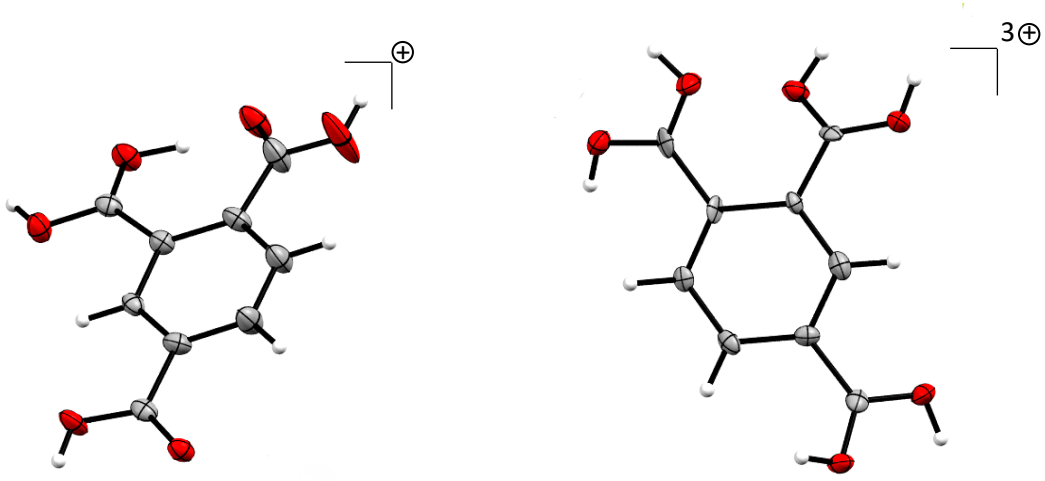

Figure 8. Formula unit of [1,2,4-$C_6H_3(COOH)(COOH)_2(H)][AsF_6]$ · HF, view along *b* (left) and formula unit of [1,2,4-$C_6H_3(COOH_2)_3][(Sb_2F_{11})(SbF_6)_2]$, view along *c* (right), displacement ellipsoids at 50% probability.

The shielding and deshielding of ^{13}C resonances are easily observable for all three isomers. For all three isomers all carboxy carbons and C-H aromatic carbons are deshielded upon triprotonation compared to the neutral starting material, while the tertiary arylic carbons are shielded. This correlates to the calculated NPA charges, which show an increase of the positive charge at the deshielded carbons and a decrease of positive charge at the shielded carbons. The C-H aromatic carbons donate electron density to the tertiary aromatic carbons, so that the positive charges are better stabilized.

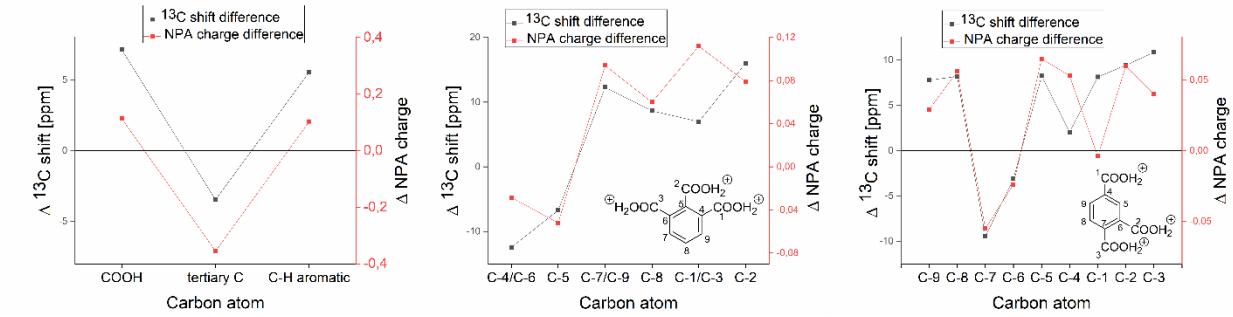

Figure 9. Plot of the difference of the NPA charges[a] of the carbon atoms and ^{13}C NMR shifts of 1,3,5-tricarboxybenzene vs its triprotonated species (left), 1,2,3-tricarboxybenzene vs. its triprotonated species (middle) and 1,2,4-tricarboxybenzene vs its triprotonated species] (right). [a] DFT, B3LYP/6-311G++(3d2f, 3p2d).

The NICS(0) of each species was calculated and is depicted in Figure 10. The differences between the three isomers can ultimately be narrowed down to their ability to stabilize the positive charges by the aromatic ring.

The 1,3,5-isomer can stabilize the positive charge the best by resonance stabilization (Scheme 4, left) as all three carboxy/carboxonium groups are in *meta* position to each other. As the CC single bonds are slightly shortened, the right resonance structure is of importantance. The triprotonation leads to an increase in NICS(0) compared to mono- and diprotonated species, while still an overall decrease compared to the starting material occurs. The depicted resonance is not possible for the other isomers to such extent. The 1,2,4-isomer has only a slight decrease in NICS(0) by monoprotonation due to one positive charge being stabilized by two carboxy groups. The diprotonation enables that stabilization by resonance. A stepwise decrease in aromatic character occurs for the 1,2,3-isomer, as electron density is donated via a hyperconjugative effect from the unprotonated carboxy group(s) to the protonated one(s) (Scheme 4, right). The aromatic core itself still donates electron density to the carboxonium groups in positions 1 and 3, so that this hyperconjugation is present in the triprotonated species of 1,2,3-tricarboxybenzene.

The sterics of the carboxy or carboxonium group highly influence NICS(0). If the group is planar regarding the aromatic core, a greater influence on the ring current is detected as when the group is tilted against the ring plane. This may be explained by the interaction of the lone pairs of the oxygen atoms with the π-electrons of the aromatic ring. As the quantum chemical calculations have correctly predicted the conformations of the cations in the crystal

structures, a simple solid-state effect such as preferred hydrogen bonding may be ruled out. In fact, each isomers preferred conformation is explained by the computations.

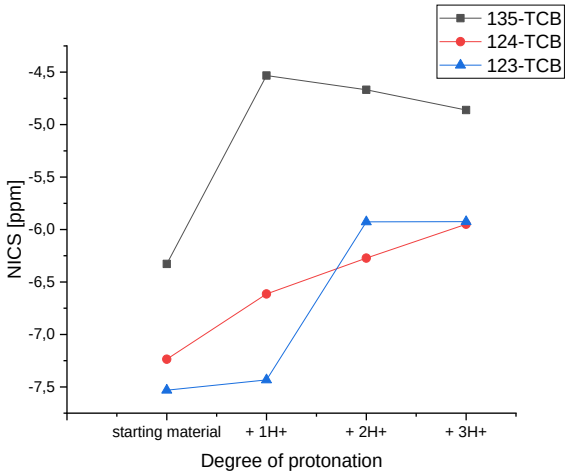

Figure 10. Plot of the NICS(0) values of 1,3,5-tricarboxybenzene (135-TCB), 1,2,4-tricarboxybenzene (124-TCB), 1,2,3-tricarboxybenzene (123-TCB) and their protonated derivatives. [a] DFT, B3LYP/6-311G++(3d2f, 3p2d).

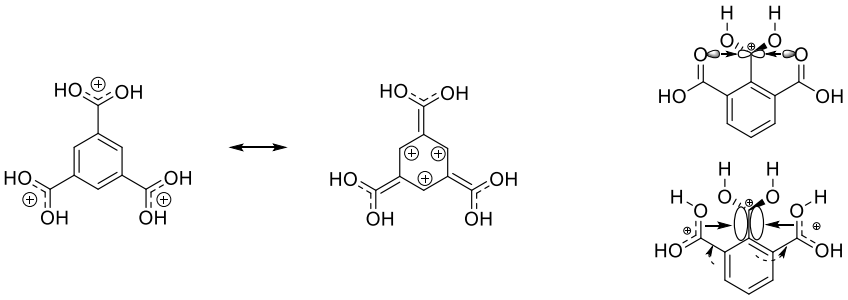

Scheme 4. Two resonance structures for triprotonated 1,3,5-tricarboxybenzene (left) and the stabilizing hyperconjugative effect in mono- and triprotonated 1,2,3-tricarboxybenzene (right).

3.2 1,3,5-Tricyano- and 1,3,5-Triaminobenzene

1,3,5-Tricyano- and 1,3,5-triaminobenzene were investigated under superacidic conditions to examine the influence of the functional group attached to the aromatic core on aromaticity. The results are compared to the previously described protonation of 1,3,5-tricarboxybenzene.

1,3,5-Tricyanobenzene is triprotonated in HF/SbF_5 and HF/AsF_5 and forms the trinitrilium species (Equation 6). By employing a mixture of $CH_3F/SbF_5/SO_2$ or $CH_3F/AsF_5/SO_2$ also the

respective *N*-methyl trication was prepared (Equation 7). 1,3,5-triaminobenzene was purchased as a hydrochloride. Triprotonation, formation of a triammonium species, occurred directly in pure HF, no addition of any Lewis acid was required. Reacting with HF/BF_3 or HF/SbF_5 enabled isolation and characterization of the triprotonated species (Equation 8), but no quadruple protonation was possible even when using higher equivalents of Lewis acid. All here shown salts were stable at room temperature.

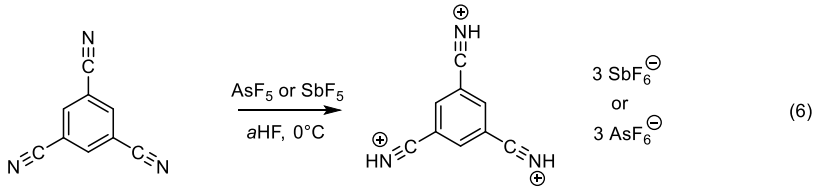

(6)

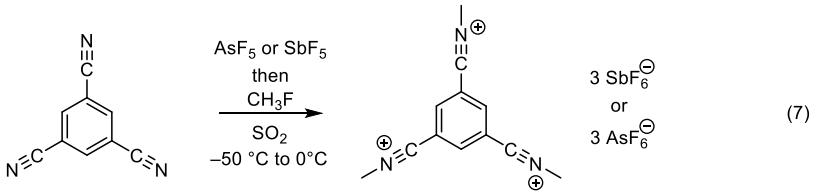

(7)

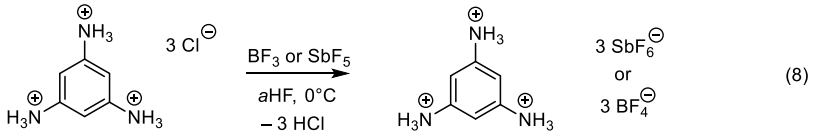

(8)

The triamino species has been examined under weaker acidic conditions. The monoprotonated compound is in an equilibrium between monoammonium and arenium species at moderately acidic conditions with a pH value of 5.5.[37] The ammonium species is found at lower temperatures, while the arenium species is more stable at higher temperatures.[38] With decreasing pH value, only the di- and triammonium species are present. This prompted us to test if a triammonium arenium tetracation was formed. Although the presence of a tetracation was not found, the triammonium species was isolated and crystallographically characterized for the first time. The trinitrilium and triammonium trications as found in the crystal structures are depicted in Figure 11.

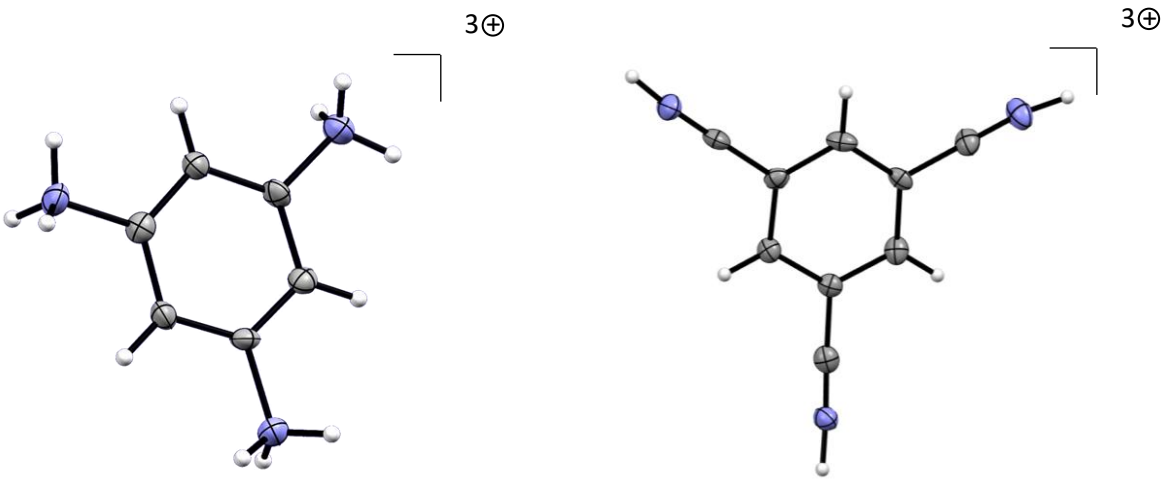

Figure 11. The cations [1,3,5-$C_6H_3(NH_3)_3$], view along *b* (left) and [1,3,5-$C_6H_3(CNH)_3$], view along *a* (right), displacement ellipsoids at 50% probability.

The NICS(0) of all evaluated species was calculated and is displayed in Figure 11. The amino species shows a significant increase in aromaticity by protonation, while the nitriles` NICS(0) is mostly unaffected, decreasing by 0.5 ppm due to protonation. The NICS(0) of 1,3,5-tricarboxybenzene decreases by 1.4 ppm for comparison. The nitrilium species may exhibit the in Scheme 4, left displayed resonance stabilization by a far smaller degree. While the triamino species has a lone pair at each nitrogen, the ammonium species does not. This lone pair influences and inhibits the ring current, leading to a more positive NICS(0) as compared to the triammonium species.

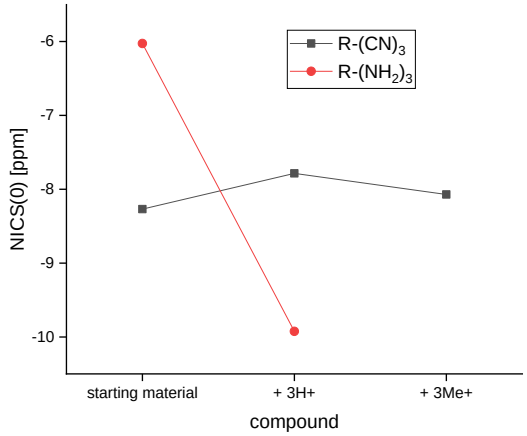

Figure 12. Plot of the NICS(0)[a] values of 1,3,5-triamino- and 1,3,5-tricyanobenzene and their triprotonated derivatives as well as the N-methyl trinitrilium species. [a] DFT, B3LYP/6-311G++(3d2f, 3p2d).

3.3 1,2,4,5-Tetracarboxybenzene

All of the previously described molecules form upon protonation trications at most. Starting from 1,2,4,5-tetracarboxybenzene, both HF/SbF_5 and HF/AsF_5 are strong enough to form a room temperature stable tetracation (Equation 9).

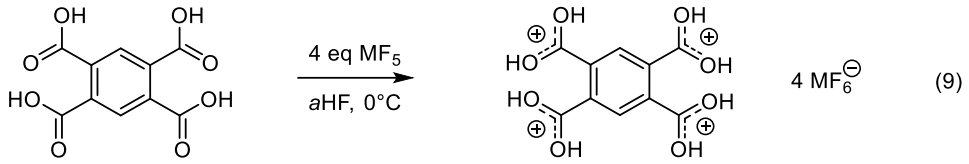

(9)

The salt was crystallized as $[C_6H_2(COOH_2)_4][(SbF_6)_4] \cdot HF$, the formula unit is depicted in Figure 13. A decrease in CC bond length by tetraprotonation was found for the CC single bonds, which has also been observed for 1,3,5-tricarboxybenzene. Some double bond character is thus present, meaning some resonance stabilization from the aromatic core to the carboxonium groups occurs.

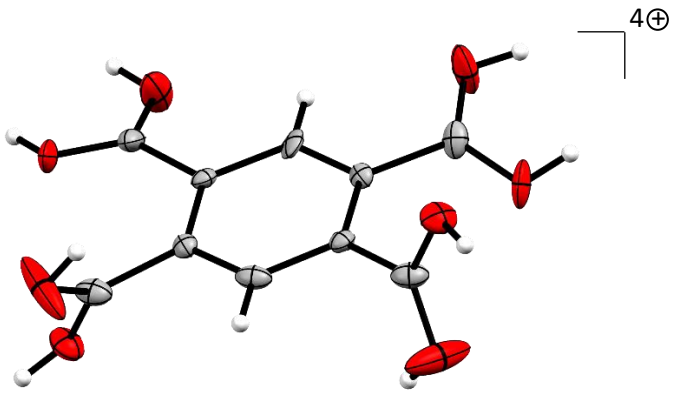

Figure 13. Formula unit of $[C_6H_2(COOH_2)_4][(SbF_6)_4] \cdot HF$, view along *a,* displacement ellipsoids at 50% probability.

While in the prepared tricarboxonium species the tertiary arylic carbons are still shielded, the sheer amount of positive charge in the tetracation leads to a deshielding of all carbon resonances. NPA charges were calculated for the starting material and the tetracation, showing that the carboxy carbon atoms got more positive than the oxygen atoms by

protonation. More of a carbocation than oxonium species is thus present. A tetracation of this small molar mass has not been synthesized yet (65 g/mol per charge).

The difference in NICS(0) amounts to 0.55 ppm, the tetracation being less aromatic than the neutral compound. This is still less than computed for the tricarboxy species, but in the same range as the tricyano species. As depicted in Scheme 5, only two carbon atoms in the ring can stabilize the positive charge at any time, in triprotonated 1,3,5-tricarboxybenzene three ring carbons can hold a positive charge at the same time. Inhibition of the ring current is thus smaller for the tetracation compared to 1,3,5-tricarboxonium benzene.

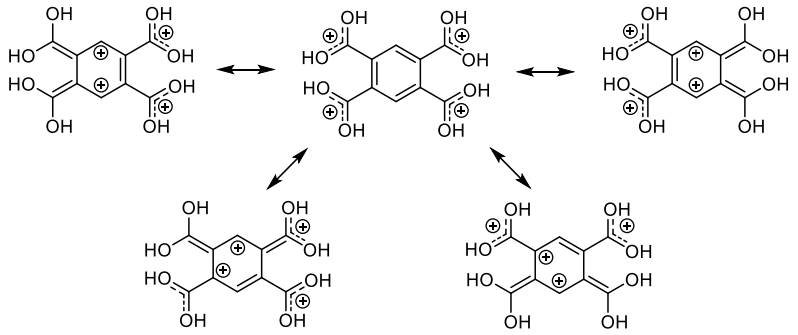

Scheme 5. Selected resonance structures for tetraprotonated 1,2,4,5-tetracarboxybenzene.

3.4 Trihydroxybenzenes and 1,3,5-Trimethoxybenzene

Protonation of all previously discussed compounds has always occurred at the respective attached functional groups. While all three or even four functional groups were successfully protonated, the aromatic core did not retain enough basicity to be also protonated. The trihydroxy- and trimethoxybenzenes have previously been protonated in solution.[34, 39] Some quantum chemical calculations regarding protonation of selected trihydroxybenzenes do also exist.[40] While reports show that the first protonation always occurs at a ring carbon, second protonation occurs at a specific ring carbon or at an oxygen atom, depending on the substitution pattern.[34] As no solid state characterization has been achieved so far, our goal was to isolate the protonated species and compare their characteristics, especially their aromaticity, to the other here reported species.

The protonation of the three isomers of trihydroxybenzene as well as that of 1,3,5-trimethoxybenzene were carried out as depicted in Equations 10-13. All four neutral starting materials were monoprotonated in *a*HF without addition of any Lewis acid, at a ring carbon. Diprotonation of the four discussed species was only possible using the superacidic systems HF/SbF_5 or HF/AsF_5.

1,3,5-trihydroxybenzene is mono- and diprotonated as visualized in Equation 10, leading to a room temperature stable arenium cation. The second protonation occurs at another ring carbon in *meta* position to the methylene group, a cyclohexenyl carboxonium dication is formed, which was found to be stable at 0°C.

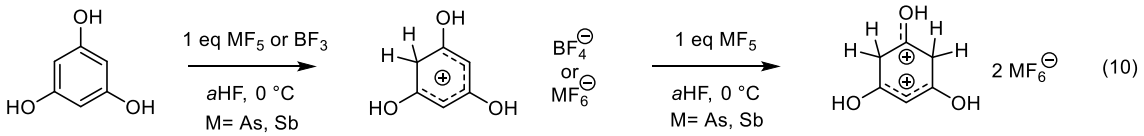

(10)

1,3,5-trimethoxybenzene reacts in a similar fashion to the trihydroxy derivative (Equation 11), exhibiting the same basic positions. While the monoprotonated species was also stable at room temperature, the dication decomposed in solution already above −40°C.

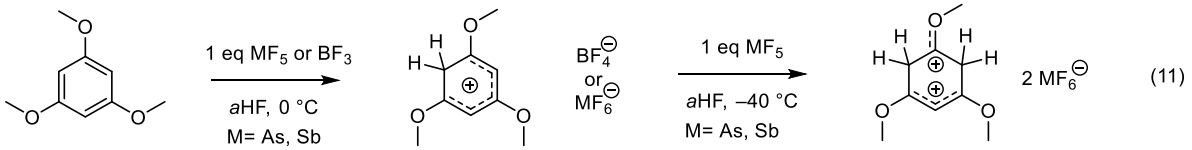

(11)

1,2,3-trihydroxybenzene was monoprotonated at the ring carbon at position 4 (Equation 12). The diprotonation was only achieved at temperatures below −60°C. The second protonation occurred at the hydroxy oxygen in *meta* position to the methylene group, resulting in the formation of an arenium oxonium dication.

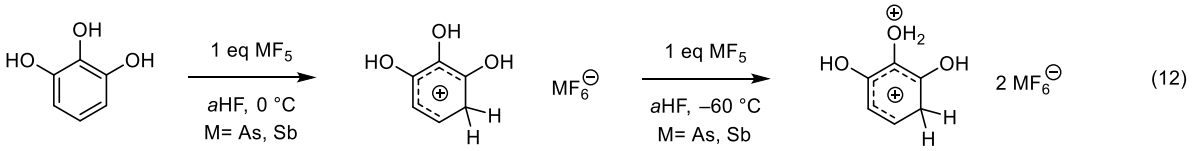

(12)

1,2,4-trihydroxybenzene was monoprotonated at a ring carbon in position 5 (Equation 13), diprotonation occurred at the oxygen of the hydroxy group in position 1, in *meta* position to the methylene group. The formed arenium oxonium dication decomposed above −40°C.

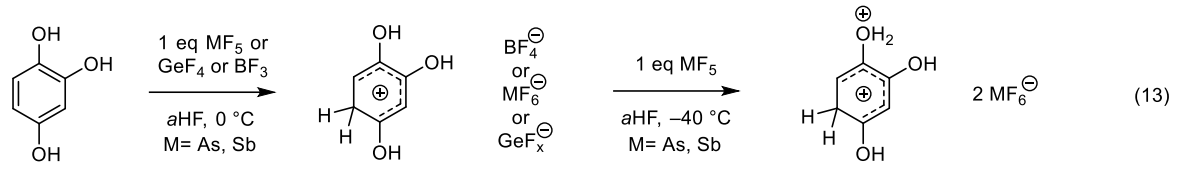

(13)

The exact crystallographic characterization of the simplest arenium cation, the benzenium cation $C_6H_7^+$, has only been achieved in 2007.[41] While other arenium ions have been investigated by single crystal X-ray diffraction,[42] not much crystallographic data exists regarding arenium ions with hetero atom containing functional groups. All shown mono- and dications were successfully crystallized and characterized. The cations are depicted in Figure 14 and Figure 15. Noteworthy is that mono- and diprotonated 1,2,3-trihydroxybenzene crystallized together in one salt.

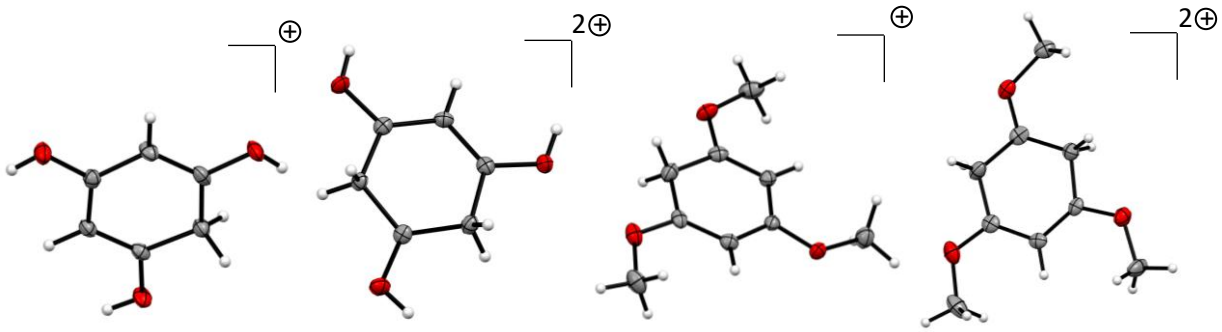

Figure 14. From left to right: [1,3,5-$C_6H_4(OH)_3$], view along *b*, [1,3,5-$C_6H_5(OH)_3$], view along *b*, [1,3,5-$C_6H_4(OCH_3)_3$], view along *b*, [1,3,5-$C_6H_5(OCH_3)_3$], view along *c*, displacement ellipsoids at 50% probability.

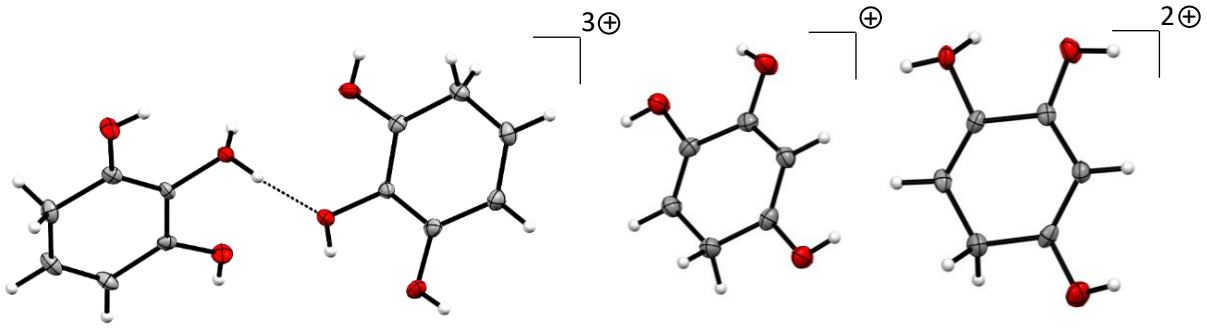

Figure 15. From left to right: [1,2,3-$C_6H_4(OH)_3$][1,2,3-$C_6H_4(OH)_2(OH_2)$] with the strong hydrogen bond marked between mono- and dication, view along *b*, [1,2,4-$C_6H_4(OH)_3$], view along *a* and [1,2,4-$C_6H_4(OH)_2(OH_2)$], view along *a*, displacement ellipsoids at 50% probability.

All arenium monocations exhibit a typical cyclohexadienyl structure (Scheme 6). The localization of the double bonds in the 1,3,5-substitued arenium ions is better described by the structure with the double bonds parallel to each other and the positive charge at the carbon in *para* position to the methylene group. The crystallographic findings are supported by ^{13}C NMR spectroscopic data of the arenium ions, as the *para* carbon gets deshielded around 45% more compared to the ones in *meta* position to the methylene group. Also, NPA computations show a larger increase in positive charge of the *para* carbon compared to the *meta* ones. A similar observation is made for the 1,2,3- and 1,2,4-pattern arenium ions.

These findings are mirrored again by the crystallographic data, as for the 1,2,3-pattern arenium ion the middle structure has the least importance and for the 1,2,4-pattern the right one.

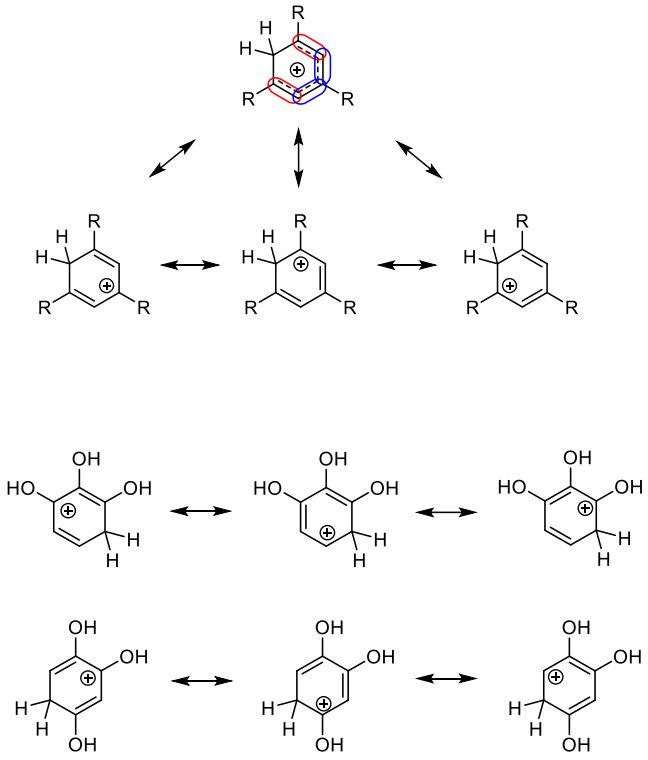

Scheme 6. Top: Resonance stabilization for the 1,3,5-substitution pattern arenium ions, red: “short” bonds, blue: “long” bonds; Bottom: Resonance stabilization for the 1,2,3- (upper scheme) and 1,2,4-substitution pattern (lower scheme) arenium ions.

The described dications can be separated into two categories: Second protonation occurs at a carbon or at an oxygen atom. Both 1,3,5-substitued species fall into the first category, the 1,2,3- and 1,2,4-substitued ones into the second. The latter can be easily described as arenium oxonium dications, as all analytic data show a minimal difference between respective mono- and dications. The only significant difference is the elongation of the CO bond of the oxonium group. Diprotonated 1,3,5-trihydroxy- and methoxybenzene are of a different sort. As protonation occurs at the ring, the arenium character is destroyed and the cyclohexadienyl character is no longer present. NPA charges and ^{13}C NMR data show for the carbonyl moiety between the methylene groups a massive deshielding to above 230 ppm, which is in the same range compared to the carbonyl carbon of protonated acetone. The CO bond lengths are also within deviations similar. On the other side of the dication one double bond is left inside the ring, which stabilizes another positive charge in conjunction with the remaining hydroxy

groups. The term cyclohexenyl carboxonium dication may be most adequate for these two species.

The difference between the two groups is ultimately visualized by Mapped Electrostatic Potentials (MEPs) (Figure 16). The highest concentration of positive charge of the cyclohexenyl carboxonium dications is at the carboxonium carbons. The aromatic ring of the arenium oxonium dications shows roughly the same electron density, the (second) positive charge is heavily concentrated on the oxonium oxygen.

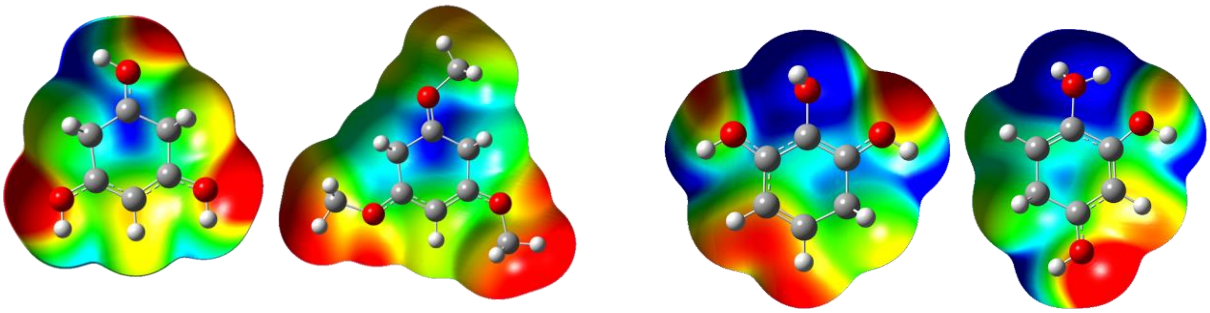

Figure 16. From left to right: Molecular 0.0004 bohr^{-3} 3D isosurfaces with MEP of [1,3,5-$C_6H_5(OH)_3$] (0.27 a.u. (red) to 0.36 a.u. (blue)), [1,3,5-$C_6H_5(OCH_3)_3$] (0.22 a.u. (red) to 0.32 a.u. (blue)), [1,2,3-$C_6H_4(OH)_2(OH_2)$] (0.26 a.u. (red) to 0.32 a.u. (blue)) and [1,2,4-$C_6H_4(OH)_2(OH_2)$] (0.26 a.u. (red) to 0.32 a.u. (blue)), calculated on B3LYP/6–311g++(3df,3pd) level of theory.

While all starting materials are quite aromatic, the arenium ions are (per definition) non-aromatic, their NICS(0) is close to zero (Figure 17). The difference in NICS(0) between mono- and diprotonated 1,2,3- and 1,2,4-trihydroxybenzene is small, as the arenium character is not influenced by the oxonium group. The cyclohexenyl carboxonium dications exhibit an even higher NICS(0), which is positive, trending towards antiaromatic character.

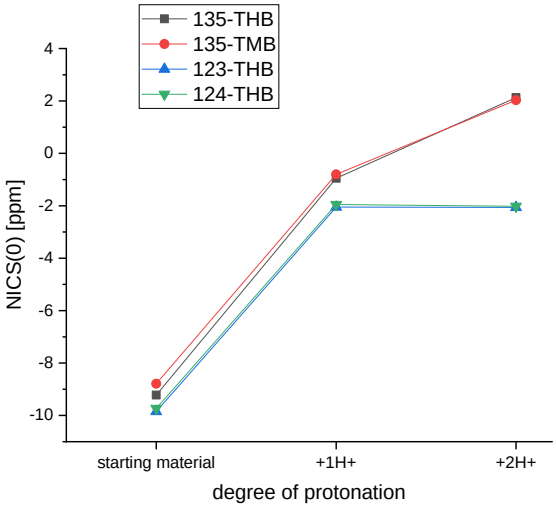

Figure 17. NICS(0) values of in this chapter discussed species (THB = trihydroxybenzene; TMB = Trimethoxybenzene), calculated on DFT, B3LYP/6-311G++(3d2f, 3p2d).

The protonation sequence of the trihydroxybenzenes is highly dependent on substitution pattern. The cyclohexenyl carboxonium salts are even stable up to 0°C, the arenium oxonium ones decompose at much lower temperatures due to oxonium character. The difference in stability between diprotonated 1,3,5-trimethoxy- and trihydroxybenzene is explained by the varying contribution of the hydroxy- or methoxy oxygen atoms in stabilizing the positive charge.

3.5 Cyanuric acid and Urazole

All neutral compounds, which were discussed in the previous chapters, were undeniably aromatic. All were benzene derivatives, in which protonation occurred either at the attached functional group or at the aromatic ring. The first showed rather small yet detectable changes in aromatic character, while the latter underwent an expected change from aromatic to non-aromatic, at least by monoprotonation.

But can it be turned around? Starting from non-aromatic compounds, perhaps even non-cyclic, can aromaticity be created by superacids?

Cyanuric acid itself is a disputed compound regarding aromaticity. The neutral compound is at best slightly aromatic, as calculated by NICS(0) and other methods. Keto-enol tautomerism heavily favors the keto species, although the enol one is certainly aromatic.[23] A trication, where each carbonyl moiety has been protonated, is theoretically much more aromatic. Each lone pair of the nitrogen stabilizes the positive charge by resonance, which in turn leads to an aromatic triazine derivative (Scheme 7). Protonation ultimately enables the keto-enol tautomerism, as triprotonation makes proton migration obsolete, reducing it to a question of resonance.

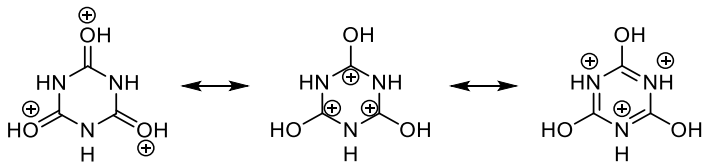

Scheme 7. Resonance structures for triprotonated cyanuric acid.

Mono- and diprotonation of cyanuric acid was achieved as shown in Equations 14 and 15, the basic site being the carbonyl oxygens in each case. Triprotonation was not observed even with large excess of Lewis acid.

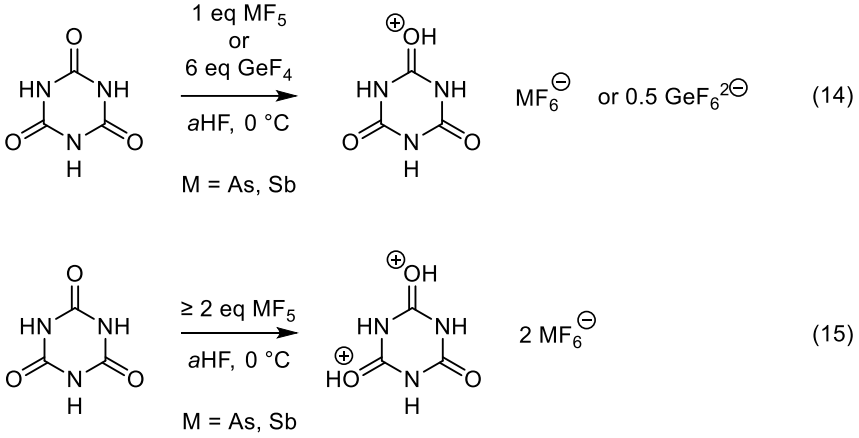

Bond length equalization and same size of angles inside the ring are criteria for aromaticity. Cyanuric acid itself is no perfect hexagon, the bonds inside the ring are not equisized and the angles differ from 120° as experimentally found by X-ray diffraction (Figure 18). The monoprotonated and diprotonated species show a significant bond equalization inside the ring, but only directly at the COH^+ moieties. The adjacent bonds, namely the CN bonds, become equisized within standard deviations. The other CN bonds, located at the unprotonated carbonyl group, are increasingly elongated by each protonation. The protonated species become more distorted. The remaining CO group is then simply not basic enough, as seen by the short CO distances and supported by calculated NPA charges, to allow triprotonation.

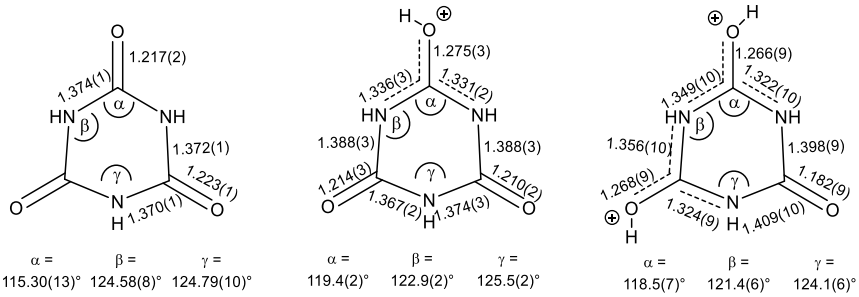

Figure 18. Selected bond lengths [Å] and angles of cyanuric acid[43] as well as its mono- and diprotonated species.

When formally removing either a nitrogen or a carbon from cyanuric acid known five-membered rings remain. The first is known as parabanic acid, the latter as urazole. Parabanic acid has been investigated in superacidic media.[44] The question of enabled resonance and

ultimately aromaticity was not so much of a question for this compound. With two adjacent carbonyl groups, missing the NH group with its free electron pair, resonance stabilization over the whole ring is not enabled. Urazole on the other hand is aromatic as computed by NICS(0) value, but the bonds within the ring are not equisized and bond angles differ from ideal 108°. Like with cyanuric acid, protonation enables resonance stabilization, but now only diprotonation is required for a complete bond conjugation over the whole ring. The mono- and diprotonation was achieved in various superacidic media (Equations 16 and 17). The formed salts were stable up to room temperature. The remaining carbonyl moiety of monoprotonated urazole is more basic, as it is diprotonated by HF/GeF_4, while cyanuric acid is only monoprotonated.

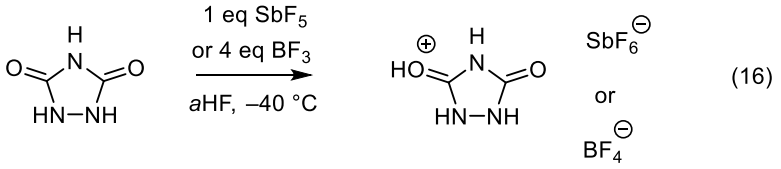

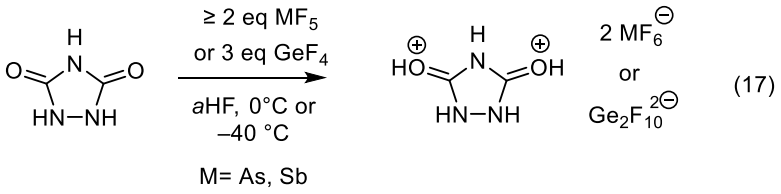

Monoprotonation of urazole leads to the same bond length decrease inside the ring as in cyanuric acid, but no elongation occurs at the unprotonated CO moiety. In fact, most bonds are shortened (Figure 19). Diprotonation results in further decrease in bond lengths, the angles are within standard deviation 108°. Urazole becomes more aromatic by mono- and diprotonation when considering bond lengths and angles.

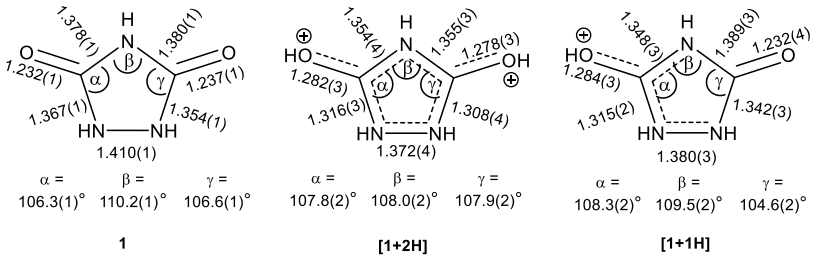

Figure 19. Selected bond lengths [Å] and angles of urazole[45] as well as its mono- and diprotonated species.

While cyanuric and parabanic acid are not aromatic, urazole is aromatic, which is confirmed by NICS(0) (Figure 20). Only the diprotonated species of parabanic acid and the triprotonated one of cyanuric acid become significantly more aromatic. Urazole shows a steady decrease in NICS(0), meaning increasing aromaticity.

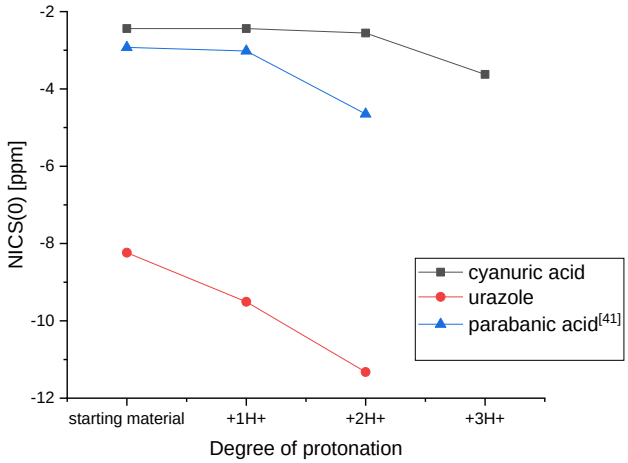

Figure 20. NICS(0) of urazole, parabanic[41] and cyanuric acid as well as their protonated derivatives, calculated on DFT, B3LYP/6-311G++(3d2f, 3p2d).

3.6 Diaminomaleonitrile

All previously shown species were cyclic compounds from the beginning. Aromaticity is linked to rings, historically as for the mystery of benzene but also stated by concepts like NICS. More recent theories like Möbius or spherical aromaticity are disputable, this is also the case for Y-aromaticity.[46] Some molecules, amongst others the tricyano- and trinitromethanid anions,[47] the butadienyl cation[48] or the guadinium dication,[49] but also (protonated) cyanuric acid should possess that characteristic. If a Y-shaped system is flat and it has a π-system with 4n+2 electrons cross-conjugated via an atom, one may speak of Y-aromaticity (Figure 21). The ring current via NICS is then measured above the center atom of that compound.

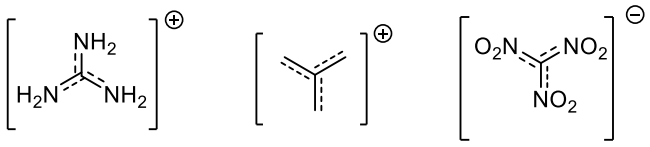

Figure 21. Lewis structures of the guadinium cation (left), 2-butene cation (middle) and trinitromethanide anion (right).

Diaminomaleonitrile (abbreviated as DAMN) is another candidate for Y-aromaticity. Protonation was carried out in HF/SbF_5 and HF/AsF_5. Monoprotonated DAMN is formed when one or two equivalents of Lewis acid are used, resulting in the formation of an ammonium cation (Equation 18). When at least four equivalents of Lewis acid are used, the diprotonated species, an ammonium nitrilium dication, is formed (Equation 19).

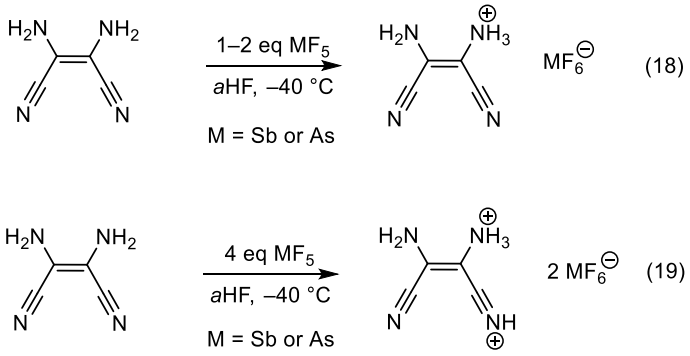

Diaminomaleonitrile, the tetramer of hydrogen cyanide, is structurally closely related to cyanamide. Cyanamide is protonated at the nitrile and not at the amino group, but DAMN is first protonated at an amino group. Quantum-chemical calculations expect it to be vice versa, which indicates a solid-state interaction as a stabilizing effect.

Monoprotonation of DAMN elongates the C-$N(H)_3$ bond but shortens the C-$N(H)_2$ bond. The trend is amplified by diprotonation, the C-$N(H)_2$ bond is in length between CN single and double bond. Also, the C-C(NH) bond is shortened, coming closer to a CC double bond.

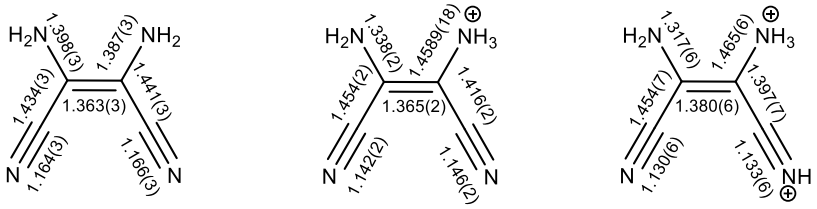

Figure 22. Bond lengths [Å] and angles of DAMN[50] as well as its mono- and diprotonated species.

To explain the crystallographically found bond lengths, especially of the dication, NRT calculations were employed to visualize resonance stabilization and charge localization. The results for the diprotonated species are illustrated in Scheme 8, left. The most important resonance structure is a trication anion, a zwitterionic species, which is also described as an ammonium iminium nitrilium trication carbanion. The simple ammonium iminium dication is slightly less important. Two resonance structures with heterocumulenic character at the CCNH moiety are also computed. Two 3-center-4-electron bonds are observed, one at the CCN(H_2) moiety, the other one at the CCN(H) moiety. The stabilization is visualized by MEP (Scheme 8, right), which shows a green colored band denoting similar electron density, a more positive electrostatic potential is detected at the ammonium group and a more negative one at the nitrile group.

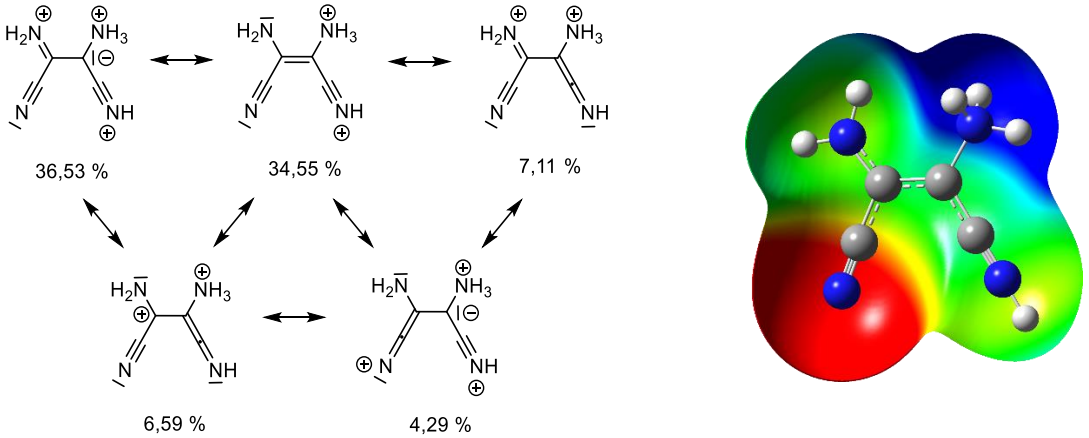

Scheme 8. Most important resonance structures of diprotonated DAMN with weighting (left), Molecular 0.0004 bohr^{-3} 3D isosurface with MEP of [C_2(CN)(CNH)NH_2NH_3] (0.24 a.u. (red) to 0.36 (blue)) (right).

These resonance structures may be essential for the next observations. When keeping DAMN in a mixture of HF/SbF_5, the latter in large excess, no trication is found, but a tetracation is

obtained (Figure 23). Dimerization of two dications under hydrogen cyanide formation takes place, which results in the formation of an aromatic pyrazole tetracation. Dimerization of DAMN, although under different conditions and other products, is known and involved in theories about nucleosynthesis in space. Considering bond lengths and NPA charges, two positive charges are mostly located at the iminium moieties, while the other two are present at the nitrilium groups.

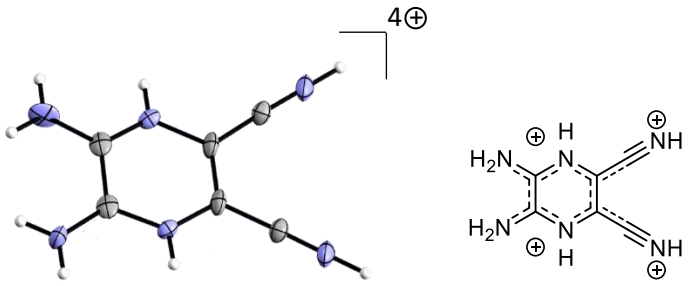

Figure 23. $[C_2(NH_2)_2(NH)_2C_2(CNH)_2]$, displacement ellipsoids at 50% probability (left), Lewis structure on the right.

4. Conclusion and Summary

The triprotonation of tricarboxy-, tricyano- and triaminobenzene as well as the tetraprotonation of tetracarboxybenzene were achieved in superacidic media. The tri- and tetracationic species were prepared, isolated and characterized by vibrational and NMR spectroscopy and single crystal X-ray diffraction. Most isolated salts were stable at room temperature. Protonation sequence and substitution pattern influence aromatic character. Overall, it is decreased for all mentioned species except triaminobenzene, which shows a significant increase in aromaticity upon triprotonation.

The mono- and diprotonation of the three isomers of trihydroxybenzene and 1,3,5-trimethoxybenzene were accomplished in superacids. The arenium monocations were isolated and characterization confirmed the cyclohexadienyl structure. Diprotonation results in the formation of cyclohexenyl carboxonium dications in case of 1,3,5-trihydroxy and 1,3,5-trimethoxybenzene, cyclohexadienyl character is lost and aromaticity is further decreased, trending towards antiaromaticity. Diprotonated 1,2,3- and 1,2,4-trihydroxybenzene retain their arenium character, they are as non-aromatic as their monoprotonated derivatives. The second positive charge is localized at the oxonium oxygen atom, this also results in a lower thermal stability of these two species compared to the cyclohexenyl carboxonium dications.

Mono- and diprotonated of cyanuric acid was achieved using superacidic media. Expected resonance stabilization was observed in the ring in proximity to the protonated carbonyl groups. Still, the positive charges were not stabilized over the whole ring, bond length equalization of all CN bonds was not observed, distortion increased by protonation. Triprotonation of cyanuric acid, which would have led to an aromatic species, is not possible due to lack of basicity of the dication.

Urazole was reacted under similar conditions as cyanuric acid, protonation occurring at the carbonyl groups. The mono- and diprotonated species showed an overall decrease in bond lengths in the ring, which indicates resonance stabilization over the whole ring. Aromaticity as computed by NICS(0) significantly increased.

Diaminomaleonitrile is first protonated at an amino and second at a nitrile group in superacidic systems. The formed diprotonated species was shown to be no simple dication, but rather an

ammonium iminium nitrilium trication carbanion with heterocumulenic character. While retaining an unprotonated basic nitrile group, triprotonation was not possible. Instead, dimerization of two dications resulted in the formation of an aromatic pyrazolium tetracation.

5. Citations

[1] A. W. Hofmann, *Proc. R. Soc. Lond.* **1857**, *8*, 1-3.
[2] A. J. Rocke, *Angew. Chem. Int. Ed.* **2015**, *54*, 46-50.
[3] A. Kekulé, *Bull. Soc. Chim. Fr.* **1865**, *3*, 98-110.
[4] A. Kekulé, *Liebigs Ann.* **1866**, *137*, 129-196.
[5] G. Schultz, *Chem. Ber.* **1890**, *23*, 1265-1312.
[6] R. Hoffmann, *R. Am. Sci* **2015**, *103*, 18-22.
[7] J. Thiele, *Liebigs Ann.* **1899**, *306*, 87-142.
[8] L. Pauling, J. Sherman, *J. Chem. Phys.* **1933**, *1*, 679-686.
[9] L. Pauling, J. Sherman, *J. Chem. Phys.* **1933**, *1*, 606-617.
[10] L. Pauling, *J. Am. Chem. Soc.* **1931**, *53*, 1367-1400.
[11] E. G. Cox, *Nature* **1928**, *122*, 401-401.
[12] [a] E. Hückel, *Z. Phys* **1931**, *70*, 204-286; [b] E. Hückel, *Z. Phys.* **1931**, *72*, 310-337; [c] E. Hückel, *Z. Phys.* **1932**, *76*, 628-648.
[13] [a] W. Von E. Doering, F. L. Detert, *J. Am. Chem. Soc.* **1951**, *73*, 876-877; [b] W. Von E. Doering, L. H. Knox, *J. Am. Chem. Soc.* **1954**, *76*, 3203-3206.
[14] F. London, *J. Phys. Radium* **1937**, *8*, 397-409.
[15] J. A. Pople, K. G. Untch, *J. Am. Chem. Soc.* **1966**, *88*, 4811-4815.
[16] C. J. Giunta, V. V. Mainz, in *Pioneers of Magnetic Resonance, Vol. 1349*, American Chemical Society, **2020**, pp. 3-20.
[17] P. v. R. Schleyer, C. Maerker, A. Dransfeld, H. Jiao, N. J. R. Van Eikema Hommes, *J. Am. Chem. Soc.* **1996**, *118*, 6317-6318.
[18] E. Paenurk, R. Gershoni-Poranne, *Phys. Chem. Chem. Phys* **2022**, *24*, 8631-8644.
[19] A. Stanger, *Eur. J. Org. Chem.* **2020**, *2020*, 3120-3127.
[20] R. Gershoni-Poranne, A. Stanger, *Chem. Soc. Rev.* **2015**, *44*, 6597-6615.
[21] M. Solà, *Nat. Chem.* **2022**, *14*, 585-590.
[22] R. Islas, E. Chamorro, J. Robles, T. Heine, J. C. Santos, G. Merino, *Struct. Chem.* **2007**, *18*, 833-839.
[23] L. Pérez-Manríquez, A. Cabrera, L. E. Sansores, R. Salcedo, *J. Mol. Model.* **2011**, *17*, 1311-1315.
[24] Z. S. Yoon, A. Osuka, D. Kim, *Nat. Chem.* **2009**, *1*, 113-122.
[25] M. Bühl, A. Hirsch, *Chem. Rev.* **2001**, *101*, 1153-1184.
[26] Y. Jung, T. Heine, P. l. v. R. Schleyer, M. Head-Gordon, *J. Am. Chem. Soc.* **2004**, *126*, 3132-3138.
[27] B. Braïda, A. Lo, P. C. Hiberty, *ChemPhysChem* **2012**, *13*, 811-819.
[28] A. Stanger, *Chem. Commun.* **2009**, 1939.
[29] K. Krämer, *Chem. World* **2021**.
[30] R. J. Gillespie, T. E. Peel, in *Adv. Phys. Org. Chem, Vol. 9* (Ed.: V. Gold), Academic Press, **1971**, pp. 1-24.
[31] G. A. Olah, G. K. S. Prakash, J. Sommer, A. Molnar, *Superacid Chemistry* **2009**, *Wiley, Hoboken, NJ*, 1-34.
[32] [a] L. P. Hammett, A. J. Deyrup, *J. Am. Chem. Soc.* **1932**, *54*, 2721-2739; [b] R. J. Gillespie, J. Liang, *J. Am. Chem. Soc.* **1988**, *110*, 6053-6057.
[33] G. A. Olah, *nobel lecture* **1994**.
[34] G. A. Olah, Y. K. Mo, *J. Am. Chem. Soc.* **1972**, *94*, 5341-5349.
[35] G. A. Olah, J. Bausch, G. Rasul, H. George, G. K. S. Prakash, *J. Am. Chem. Soc.* **1993**, *115*, 8060-8065.
[36] M. Saunders, P. v. R. Schleyer, G. A. Olah, *J. Am. Chem. Soc.* **1964**, *86*, 5680-5681.
[37] T. Yamaoka, H. Hosoya, S. Nagakura, *Tetrahedron* **1968**, *24*, 6203-6213.
[38] T. Yamaoka, H. Hosoya, S. Nagakura, *Tetrahedron* **1970**, *26*, 4125-4130.

[39] A. J. Kresge, H. J. Chen, L. E. Hakka, J. E. Kouba, *J. Am. Chem. Soc.* **1971**, *93*, 6174-6181.
[40] C. M. Mayhan, H. Kumari, J. M. Maddalena, G. N. Borgmeyer, C. A. Deakyne, *J. Coord. Chem.* **2021**, *74*, 61-73.
[41] F. Scholz, D. Himmel, L. Eisele, W. Unkrig, I. Krossing, *Angew. Chem. Int. Ed.* **2014**, *53*, 1689-1692.
[42] C. A. Reed, K.-C. Kim, E. S. Stoyanov, D. Stasko, F. S. Tham, L. J. Mueller, P. D. W. Boyd, *J. Am. Chem. Soc.* **2003**, *125*, 1796-1804.
[43] G. C. Verschoor, E. Keulen, *Acta Cryst. B* **1971**, *27*, 134-145.
[44] S. Beck, M. Raljic, C. Jessen, A. J. Kornath, *Eur. J. Org. Chem.* **2020**, *2020*, 4521-4527.
[45] F. Belaj, *Acta Cryst. C* **1992**, *48*, 1088-1090.
[46] P. Gund, *J. Chem. Educ.* **1972**, *49*, 100.
[47] J. Cioslowski, S. T. Mixon, E. D. Fleischmann, *J. Am. Chem. Soc.* **1991**, *113*, 4751-4755.
[48] A. Dworkin, R. Naumann, C. Seigfred, J. M. Karty, Y. K. Mo, *J. Org. Chem* **2005**, *70*, 7605-7616.
[49] Y. Morgenstern, F. Zischka, A. Kornath, *Chem. Eur. J.* **2018**, *24*, 17311-17317.
[50] B. R. Penfold, W. Lipscomb, *Acta Cryst. B* **1961**, *14*, 589-597.

6. Appendix

The following appendix contains a list of publications and conference contributions, the manuscripts and drafts which are to be published in the context of this dissertation. All published manuscripts have been peer-reviewed and published in scientific journals. The Supporting Information for each paper is named after the title of the paper and found on an attached Compact Disc.

6.1 List of Publications, Drafts and Conference Contributions

6.1.1 Publications

1. A. Nitzer, M. Regnat, C. Jessen, A. J. Kornath, *Third Time is a Charm – Protonating Tricarboxybenzenes*, *Eur. J. Org. Chem.* **2022**, *2022*, *5*, e202101488.
2. A. Nitzer, R. Hübsch, C. Jessen, A. J. Kornath, *Two Roomtemperature-stable Trications – Triprotonated Triamino- and Tricyanobenzene*, *ChemistryOpen* **2022**, *11*, *5*, e202200049.
3. M. C. Bayer, C. Kremser, C. Jessen, A. Nitzer, A. J. Kornath, *Strengthening of the C−F Bond in Fumaryl Fluoride with Superacids*, *Chem. Eur. J.* **2022**, *28*, *18*, e202104422.
4. M. C. Bayer, N. Greither, C. Jessen, A. Nitzer, A. J. Kornath, *Intermediates in Friedel-Crafts Acylation of Fumaryl Halides, Eur. J. Inorg. Chem.* **2022**, e202200391.
5. M. C. Bayer, N. Greither, V. Bockmair, A. Nitzer, A. J. Kornath, *Stabilizing the C=N Double Bond Character in Fumaramide with the Aid of Superacids*, *Eur. J. Inorg. Chem.* **2022**, e202200501.

6.1.2 Drafts

1. A. Nitzer, C. Jessen, A. J. Kornath, *A small room temperature stable tetracation*.
2. A. Nitzer, C. Jessen, R. Haiges, K. O. Christe, A. J. Kornath, *Preparation of a room temperature stable cyclohexenyl carboxonium dication*.
3. A. Nitzer, C. Jessen, M. Cornelsen, R. Haiges, K. O. Christe, A. J. Kornath, *Arenium, oxononium and arenium oxonium cations – Protonation of 1,2,3- and 1,2,4-trihydroxybenzene*.
4. A. Nitzer, C. Jessen, A. J. Kornath, *Increasing aromaticity by protonation*.
5. A. Nitzer, C. Jessen, A. J. Kornath, *N, C, O – distribution of charge in protonated urazole*.
6. A. Nitzer, P. Manhart, C. Jessen, A. J. Kornath, *Diaminomaleonitrile – mono-, di- …and tetraprotonation?*.

6.1.3 Conference contributions

1. Oral presentation, *Methylierungen ausgewählter Nitrile*, A. Nitzer, T . Saal, A. Kornath, K. O. Christe, R. Haiges, 18. Deutscher Fluortag, Schmitten, Germany.
2. Oral presentation, *Aromatic trications*, A. Nitzer, A. J. Kornath, 20th European Symposium on Fluorine Chemistry, Berlin, Germany.

Third time is a charm – protonating tricarboxybenzenes

Alexander Nitzer, Martin Regnat, Christoph Jessen, Andreas J. Kornath[a]*

[a] A. Nitzer, M. Regnat, C. Jessen, Prof. Dr. A. Kornath
Department of Chemistry and Pharmacy
LMU Munich
Butenandtstrasse 5–13, 81377 Munich, Germany
E-mail: alexander.nitzer@cup.uni-muenchen.de, martin.regnat@campus.lmu.de, christoph.jessen@cup.uni-muenchen.de, akoch@cup.uni-muenchen.de

Supporting information for this article is given via a link at the end of the document.

Abstract: Triprotonation of the three constitution isomers of tricarboxybenzene was accomplished. Furthermore, the preparation of selected mono- and dications showed the sequence of protonation steps. The cations were mostly isolated as [SbF_6] and [AsF_6] species, which were characterized by Raman and NMR spectroscopy as well as X-ray structure determination. To further elucidate the experimental results, quantum chemical calculations are employed, especially in regard to charge distribution with NPA charges and aromaticity by NICS(0) values. Thermal decomposition of the compounds was investigated in order to explore the possibility of acyl cation formation. The influence of the aromatic system, substitution pattern and anomeric effect concerning the properties of the respective compounds was thus explained.

Introduction

Olah and White[1] prepared protonated carbonic acid and various other hydroxycarbenium ions,[1-2] which were extensively studied by low temperature NMR spectroscopy. Furthermore, the correlation between π-electron densities and ^{13}C chemical shifts was investigated, performing rudimentary quantum chemical calculations to describe experimental findings. Early works were initiated amongst others by Spiesecke and Schneider,[3] who described the substituent effects in monosubstitued benzenes on ^{13}C and ^{1}H NMR shifts, relating measured values to electronegativity or Hammet constants. Farnum[4] later described general relations between NMR data and charge density. Although a correlation of electron density to NMR shielding is present, a more complex description by paramagnetic and diamagnetic shielding for NMR shifts as correction is needed. In this work, early correlations regarding aromaticity are made, as the ring current is a criterion of that exceptional state. Olah and co-workers[5] prepared various antiaromatic 9-fluoroenyl cations, evaluating the obtained NMR data and employing quantum chemical calculations to explain their results. Although no direct correlation between the antiaromatic nature and NMR data was found, Schleyer continued working on this topic and introduced the Nucleus-Independent Chemical Shift (NICS). NICS is a suitable scale for aromaticity[6], relating aromatic character, observed for example by reactivity, to quantum chemical calculations. Combined with magnetic susceptibility exaltations data computed via an increment scheme, an appropriate scale for aromaticity is obtained. Apart from the NICS(0) value, commonly abbreviated as NICS, which measures the ring current in the plane of an aromatic systems other probing positions, for example above the investigated system, can be evaluated.[7]

Apart from smaller, aliphatic hydroxycarbenium ions, protonation of benzoic acid with FSO_3H/SbF_5 was achieved by Birchall and Gillespie[8] in 1965. The presence of an $=OH^+$ group was confirmed by ^{1}H NMR spectroscopy, clearly observable by integration. Olah and Westerman have reported the ^{13}C NMR data of protonated mono- and dicarboxylic acid esters, where they correlate the deshielding of certain ^{13}C resonance with substituent effects in other hydrogen carbons.[9] They also report the diprotonation of oxalic acid in this study, generally emphasizing the utility of ^{13}C over ^{1}H NMR shifts for structural determination. The contribution of mesomeric structures is related to shielding or deshielding of specific ^{13}C resonances of the cation. It was only in 1977 that Bruck and Rabinovitz[10] reported the protonation of benzene dicarboxylic acids in magic acid-SO_2. Diprotonation of the three constitution isomers is achieved at low temperatures. Depending on the substitution pattern, the dicarboxonium ions undergo decomposition upon warming up, forming carboxonium acylium dications.

Interestingly, the behavior of tricarboxybenzenes in superacidic media has not been investigated so far. Apart from the simple question, if those systems are basic enough to achieve triprotonation, possible formation of acylium ions was considered, as well if any selectivity regarding site and sequence of protonation and acylium formation is given.

Herein we report the triprotonation of all three constitution isomers of tricarboxybenzene, elucidating on the sequence of protonation and discussing the particular effect on the aromaticity of the systems.

Results and Discussion

Triprotonation of 1,3,5-tricarboxybenzene was achieved in the superacidic systems HF/SbF_5 and HF/AsF_5. The starting material began dissolving at –20 °C, achieving a complete solution at 0 °C. Removal of the solvent at –78 °C led to the formation of colorless solids, respectively (Equation 1).

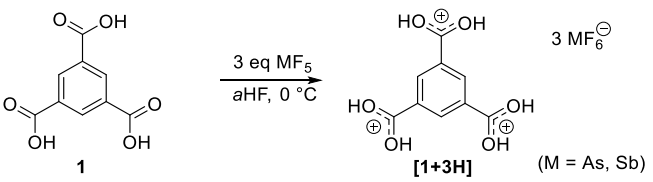

Equation 1. Protonation of 1,3,5-tricarboxybenzene.

Using single crystal X-ray diffraction analysis **[1+3H]**[$(SbF_6)_3$]·3HF could be identified. Raman spectroscopy showed only marginal thermal decomposition at room temperature over several hours. Upon decomposition, no formation of acylium ions was observed, but that of diprotonated and monoprotonated species, e.g. carboxonium salts.

In a similar fashion, protonation of 1,2,3-tricarboxybenzene was carried out. Mono-, di- and triprotonation were achieved by using the respective stoichiometry of antimony pentafluoride in *a*HF. Excess amounts of arsenic pentafluoride in *a*HF at most enabled diprotonation, showing the boundaries of the acidity of HF/AsF_5 (Equation 2).

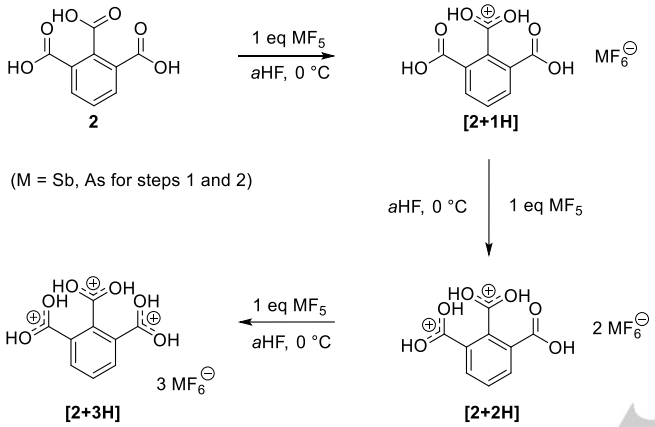

Equation 2. Protonation of 1,2,3-tricarboxybenzene.

NMR spectroscopy confirmed the sequence shown in Equation 2, in case of the trication, 2D NMR spectra enabled a complete assignment of chemical shifts. Unequivocal proof was accomplished by single crystal X-ray diffraction with the determination of **[2+1H]**[SbF_6]·HF and **[2+3H]**[$(SbF_6)_3$] as the monoprotonated and triprotonated species, showing the first site of protonation to be the carboxy group in position 2. While the respective mono- and diprotonated salts were stable at room temperature over several hours, the tricationic species decomposed within minutes at room temperature into the partially protonated species.

Likewise, protonation of 1,2,4-tricarboxybenzene was investigated. Notably, the usage of one equivalent of Lewis acid results in an intramolecular hemiprotonation, with the proton being located between the carboxy groups in positions 1 and 2. The system HF/BF_3 is acidic enough to form the monocation, while HF/GeF_4 at most leads to the dication. This diprotonation occurs at the carboxy group in position 4. Similar to 1,2,3-tricarboxybenzene, HF/AsF_5 is not acidic enough to break the intramolecular hemiprotonation, which is required to form the trication (Equation 3).

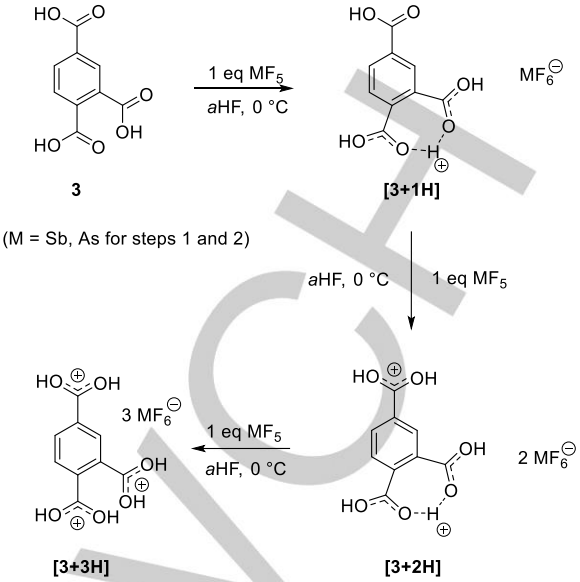

Equation 3. Protonation of 1,2,4-tricarboxybenzene.

Single crystal X-ray diffraction confirmed the sequence shown in Equation 3, identifying **[3+1H]**[AsF_6]·HF as the monoprotonated and **[3+3H]**[$(Sb_2F_{11})(SbF_6)_2$] as the triprotonated species. Salts containing the mono- and diprotonated species were stable at room temperature, while the tricationic salts decomposed within minutes into the partially protonated species, thus being the most unstable tricationic species compared to the other two isomers.

First and foremost, the crystallographic data enabled clear identification of site of protonation, but also effects of protonation on the bond lengths of all types of bonds. The complete list of crystallographic details can be found in the Supporting Information (Chapter 3).

In **[1+3H]**[$(SbF_6)_3$]·3HF, in contrast to the starting material,[11] the C-O bonds are with 1.270(4) and 1.272(3) Å (Figure 24) equally long, ranging between a C-O single and double bond, which is typical for carboxonium ions.[12] The C-C bond between the carboxonium and tertiary arylic carbon is slightly shortened by around 0.025 Å due to the protonation, while no detectable change of the aromatic CC bond lengths occurs. The carboxonium groups are slightly tilted against the ring by 6.4(4)°.

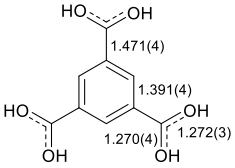

Figure 24. Bond distances of **[1+3H]** in Å.

The bond lengths of mono- and triprotonated 1,2,3-tricarboxybenzene are summarized in Figure 25. In **[2+1H]**[SbF_6]·HF, the unprotonated carboxy groups in positions 1 and 3 are only slightly tilted against the ring plane by –8.8(3)° and –10.2(3)° respectively, and the carboxonium group in position 2 is

oriented perpendicular to the ring.
Strong hydrogen bonds between the carboxy groups connect the cations in a zig-zag fashion, forming chains, while the anion and co-crystallized HF interlink the cations via the carboxonium groups, bridging the cation chains vertically.

In **[2+3H]**[$(SbF_6)_3$], the torsions of the carboxonium groups are quite similar to the monoprotonated salt and the starting material.[13] No contacts between the cations exist, as they are fully enclosed by anions. When comparing the trication, monocation and starting material, apart from the obvious change of the CO bond lengths, no significant changes in bond lengths are observed (Figure 25).

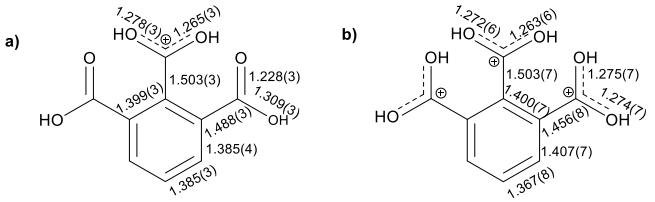

Figure 25. Selected bond distances of a) **[2+1H]** and b) **[2+3H]** in Å.

In **[3+1H]**[AsF_6]·HF, all carboxy groups are only slightly tilted against the plane, with the group in position 4 being twisted by –4.9(5)° and the groups in position 1 and 2 by –10.9(5)° and 10.3(5)° respectively. The bridging nature of the proton between the two carboxy oxygens is reflected by the equisized C-O bond distances of the carboxy groups in positions 1 and 2 (Figure 26).

In **[3+3H]**[$(Sb_2F_{11})(SbF_6)_2$], all carboxonium groups are twisted against the plane, in positions 1 and 2 by respectively –41(1)° and –32(1)° and in position 4 by –17(1)°. Throughout the different protonation levels, bond distances do not change drastically (Figure 26).

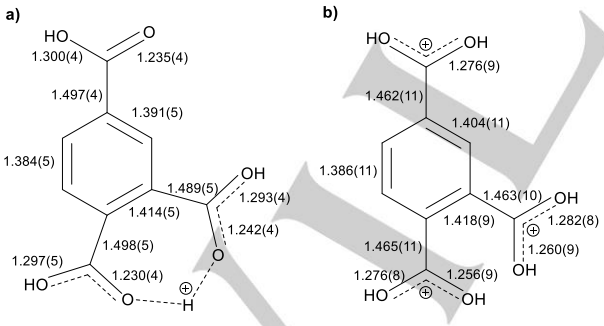

Figure 26. Selected bond distances of a) **[3+1H]** and b) **[3+3H]** in Å.

Comparing all three isomers, the level of protonation has no detectable effect on the CC bond lengths inside the ring. Apart from the carboxonium character of the [$COOH_2$] moiety, a sometimes detectable decrease in the bond length of $C_{carboxonium}$-$C_{aromatic}$ is observed. While the torsion angles of the [$COOH_{(2)}$] moieties of the 1,3,5- and 1,2,3-isomer do not drastically change, the 1,2,4-isomer undergoes variable geometries.

The protonation of the tricarboxybenzenes can also be traced by NMR spectroscopy, especially ^{13}C NMR data. The complete list of NMR data can be found in the Supporting Information (Chapter 4). Using ^1H NMR, the presence of $C(OH)_2^+$ groups is shown for all trications, which can be attributed to the aromatic hydrogens by integration, thus confirming triprotonation (see Table 1). The ^1H NMR spectrum of **[1+3H]** displays the carboxonium resonance at 13.06 ppm and the aromatic protons at 9.00 ppm. Three signals are also found in the ^{13}C NMR spectrum. For **[3+3H]**, the $C(OH)_2^+$ groups adjacent to each other are magnetically equivalent, occuring at 9.48 ppm, while the group in position 4 exhibits an even more deshielded signal at 12.91 ppm. The ^{13}C NMR spectrum also features three distinct signals in the expected regions. **[2+3H]** shows only one signal for the $C(OH)_2^+$ groups at 9.86 ppm in the ^1H NMR spectrum, while the ^{13}C NMR spectrum exhibits two resonances, at 176.50 ppm for the position 1 and 3 carbons and another resonance at 185.53 ppm for the position 2 carbon.

Table 1. ^1H and ^{13}C NMR shifts of triprotonated tricarboxybenzenes. [a], [b], [c]

	[1+3H] 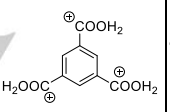	**[2+3H]** 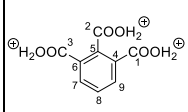	**[3+3H]** 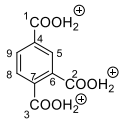
δ (^1H) ($COOH_2$)	13.06	9.86	12.91 (Pos. 4) 9.48 (Pos. 1, 2)
δ (^1H) (aromatic)	9.00	8.66 (H-7/H-9) 8.01 (H-8)	8.50 (H-5) 8.30 (H-9) 7.79 (H-8)
δ (^{13}C) (carboxylic)	178.14	185.53 (C-2) 176.50 (C-1/C-3)	182.43 (C-3) 178.34 (C-1) 178.17 (C-2)
δ (^{13}C) (C-H aromatic)	135.54	143.58 (C-7/C-9) 137.11 (C-8)	141.72 (C-9) 136.32 (C-5) 133.67 (C-8)
δ (^{13}C) (tertiary, arylic)	133.07	129.52 (C-5) 122.77 (C-4/C-6)	132.17 (C-4) 129.45 (C-6) 123.52 (C-7)

[a] all shifts in ppm. [b] measured at 0°C in *a*HF with acetone-d_6 as external reference. [c] [Sb_xF_y] as anions.

Generally, upon protonation, the sequence of carbon signals for all three isomers is quite similar. All carboxylic and C-H aromatic carbons are deshielded, which mostly increases with the level of protonation (see Figure 27 and Figure 28), while the tertiary arylic carbons are shielded. For **1** the carboxylic carbons shifts are deshielded by 7 ppm due to protonation. The C-H aromatic

carbon resonances are shifted downfield by 6 ppm, the tertiary arylic carbon resonances upfield by 3 ppm.

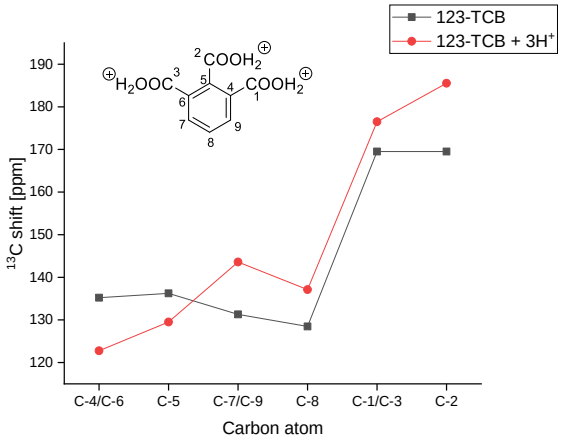

Figure 27. Plot of ^{13}C NMR shifts of 1,2,3-tricarboxybenzene (**2**) in DMSO-d_6 and of **[2+3H]** in *a*HF.

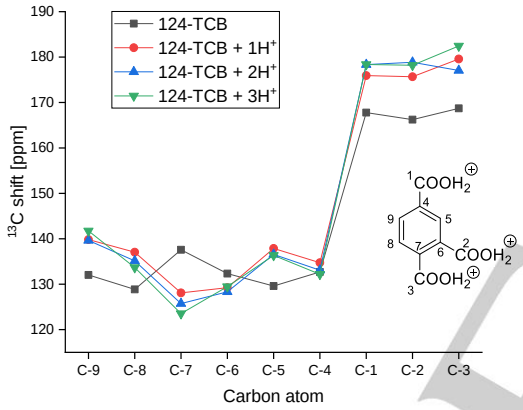

Figure 28. Plot of ^{13}C NMR shifts of 1,2,4-tricarboxybenzene (**3**) in DMSO-d_6 and of **[3+1H]**, **[3+2H]** and **[3+3H]** in *a*HF.

The ^{13}C spectra of the respective trications therefore show an ordered structure with the distinct sequence of carboxylic, C-H aromatic and tertiary arylic carbon signals (from low to high field), irrespective of the substitution pattern.

To evaluate NMR shifts and the charge localization and to quantify the aromatic character to some extent, quantum chemical calculations are performed. The full list of calculations is given in the Supporting Information (Chapter 5). For all isomers and the respective protonation levels, optimization and frequency calculations were conducted on the DFT, B3LYP/6-311G++(3d2f, 3p2d) level of theory. Furthermore, NICS(0) values of the previously optimized species were calculated on the same level. As stated before, correlations between ^{13}C NMR data and charge density can be applied for structural analyses,[4, 9] so NPA charges of the various species were calculated. Okazaki and Laali[14] investigated pyrene and its protonation/oxidation cations by using DFT, GIAO and NICS calculations, which showed a correlation between ^{13}C NMR shifts, calculated and measured, as well as the NPA charges. NICS values were calculated to examine aromaticity of the respective compounds.

For all tricarboxybenzenes, differences in NPA charges correlate to the differences in ^{13}C NMR shifts of the respective carbon atom after protonation. The electron density of all tertiary arylic carbons is increased, while that of all other carbons decreases, which influences the diamagnetic parameter, leading to the shielding and deshielding of the respective atoms (see Figure 29).

As NICS(0) calculations also give ^{13}C NMR shielding data, they were evaluated besides mentioned NPA charges. A complete list of calculated and measured ^{13}C NMR resonances for **1**, **2**, **3** and their triprotonated species is given in the Supporting Information (Chapter 5.11). For **1** and **[1+3H]**, the resonances are predicted with a deviation of 5 ppm, only the C-H aromatic carbons in **[1+3H]** are predicted to be even more deshielded by 15 ppm compared to the experimentally observed difference of 6 ppm. For the other two isomers, the trends of shielded and deshielded carbons by triprotonation are satisfactorily expected in any case, although the relative values are in some cases over- or underestimated. While the carboxylic or carboxonium carbon resonances are accurately computed for all isomers, the discrepancy between measured and computed shifts for the aromatic carbon resonances is the most significant for **[3+3H]**, but still adequately representing experimental observations.

A study by Vazquez also compared measured NMR shift to calculated ones with a comparable DFT method.[15] For the investigated pyramidal alkenes the computed ^{13}C NMR resonances are in good agreement with experimental data, although an under- or overestimation of certain shifts, similar to our work, was found. Regarding employed solvents, *a*HF and CD_3OD are protic and highly polar solvents, DMSO-d_6 is still polar, but aprotic and therefore the correct prediction of trends is particularly worth mentioning. As three positive charges are brought into each (aromatic) system, the NMR shifts together with NPA charges do predict and support experimental results. As either a magnetic or electrostatic probe, they give a good depiction of charge distribution and stabilization.

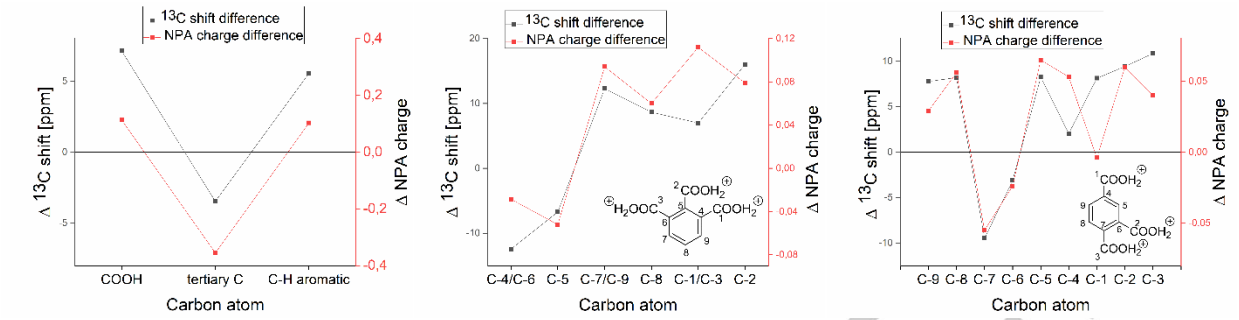

Figure 29. Plot of the difference of the NPA charges[a] of the carbon atoms and ^{13}C NMR shifts of **1** vs **[1+3H]** (left), **2** vs **[2+3H]** (middle) and **3** vs **[3+3H]** (right). [a] DFT, B3LYP/6-311G++(3d2f, 3p2d).

All in all, NICS(0) values decrease by protonation (see Figure 30), although all here examined systems do not become non-aromatic, as protonation never occurs at the ring. Thus the calculable effect is rather small, but still significant enough to be observed.

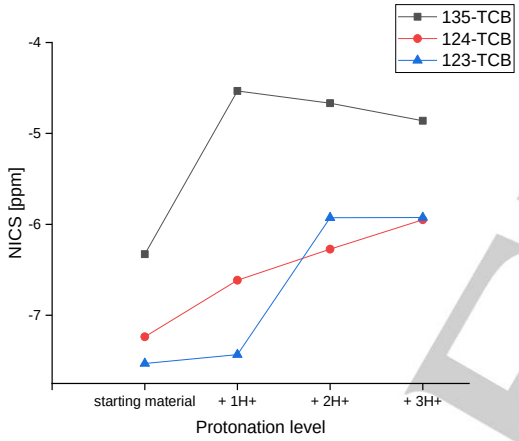

Figure 30. Plot of the NICS(0) values of 1,3,5-tricarboxybenzene (135-TCB), 1,2,4-tricarboxybenzene (124-TCB), 123-tricarboxybenzene (123-TCB) and their protonated derivatives. [a] DFT, GIAO-B3LYP/6-311G++(3d2f, 3p2d)

For the trications, several resonance structures may be drawn. Exemplary, in Scheme 9 two structures of **[1+3H]** are depicted. While in the left one the positive charges are located at the carboxonium groups, in the right one they are inside of the ring. The latter structure is obviously not of great importance as proximity of charges and non-aromatic character of the ring are highly unfavourable. That the right structure is still not to be excluded fully, is indicated by experimental data, as explained by ^{13}C shifts or even crystallographically found bond lengths. As NICS(0) quantifies ring current, the contribution of the right structure should decrease ring current, leading to a more positive value of NICS(0). The depicted resonance is for **[2+3H]** and **[3+3H]** only possible for two carboxonium groups, which are directed in *meta* position to each other. Naturally, stability of an aromatic compound does not depend on NICS(0), a quantum chemically calculated parameter. In case of the protonation of the tricarboxybenzenes, NICS(0) shows an explainable correlation with stability of the trications. Also NPA charges, as a more direct parameter compared to the before mentioned magnetic indicators, show the charge distribution occurring, as amongst other effects the C-H aromatic carbons become more positive.

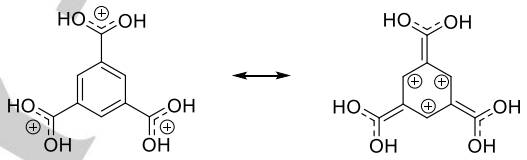

Scheme 9. Selected resonance structures of **[1+3H]**.

For the protonation of 1,3,5-tricarboxybenzene, the NICS(0) values first show a decrease in aromaticity for the monoprotonation with the shift being less negative, while di- and triprotonation again slightly increase the aromaticity of the system. The [$COOH_{(2)}$] groups are slightly twisted in **1** and its protonated derivatives, optimizing the overlap of the p-orbitals of the oxygens with the π-system of the ring, making **[1+3H]** the most stable of the here shown trications. In the 1,2,3-isomer, the carboxy groups in positions 1 and 3 are only slightly twisted against the ring for optimal overlap with the π-system, quite similar to the 1,3,5-isomer, while the carboxy group in position 2 is more tilted against the plane. Monoprotonation shows only a minor decrease in aromaticity, indicating a rather small contribution of the π-system, which suggests a rather isolated carboxonium ion.

As the configuration of the [$COOH_{(2)}$] moieties are found by X-ray characterization and quantum chemical calculation, solid state effects are deemed negligible for the consideration. In fact, NBO calculations indicate a stabilization by the carboxy groups in positions 1 and 3 specifically by the respective lone pair of the carbonyl oxygens via hyperconjugation to the empty p-orbital of carboxonium carbon in position 2 by 72.4 kcal/mol in total (see Figure 31).

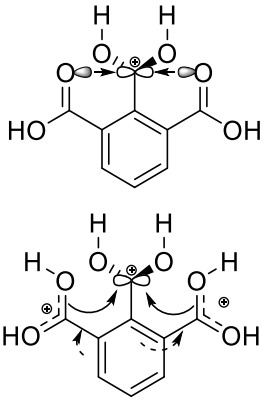

Figure 31. Stabilization of **[2+1H]** and **[2+3H]**.

A first protonation at position 2 is rather counterintuitive, as carboxy groups are commonly known to be *meta* directors, indicating an initial protonation at position 1. Diprotonation requires a twisting of all groups, leading to a disruption of the π-system, while triprotonation again results in a conformation similar to the monoprotonated species. Here, the stabilizing effect of the oxygen lone pairs as depicted in Figure 31 is no longer possible due to the carboxonium nature. Nevertheless, NBO calculations detect a donation of approximately 2–3 kcal/mol from the C-O bonds in positions 1 and 3 to the anti-bonding CO orbitals in position 2. In turn, electron density is donated to the carboxonium groups from the aromatic system (see Figure 31). Protonation of 1,2,4-tricarboxybenzene shows an almost linear decrease in aromaticity, indicating a consistent increase in π-donation from the ring. NBO calculations detect no stabilizing effect as observed with **[2+1H]** and **[2+3H]**, indicating that the conformation of the adjacent carboxonium groups in **[3+3H]** is predominantly caused by charge and steric nature. NBO calculations were further examined to quantify second order perturbations, exemplary donations from the bonding orbitals of the C-H bonds into the antibonding orbitals of C(aromatic)-C(carboxonium) bonds were compared. While these donations amount for **[1+3H]** to 4.39 kcal/mol, for **[2+3H]** it is 3.42 kcal/mol and only 2.93 kcal/mol for **[3+3H]**. The stabilization by the aromatic system is most significant for the **[1+3H]** isomer.

Conclusion

In conclusion, triprotonated tricarboxybenzenes are small and surprisingly stable species, stabilized by the aromatic π-system and/or hyperconjugation, which highly depends on the respective substitution pattern. Triprotonated 1,3,5-tricarboxybenzene is the most stable isomer as the aromatic system can overlap most easily, with triprotonated 1,2,3-tricarboxybenzene being second most stable and triprotonated 1,2,4-tricarboxybenzene the least stable. Electron donation, i.e. migration of charge density is calculated and can be measured, especially by ^{13}C NMR spectroscopy, showing the donating effect of the aromatic system. Experimental NMR values fit astonishingly well to calculated data, especially the change in NPA charge. Aromaticity decreases as indicated by NICS(0) values, depending on the substitution pattern. Decomposition does not lead to acylium ions, but partially protonated cations.

Experimental Procedures

Caution! Avoid contact with any of these compounds. Hydrolysis might form HF, which burns skin and causes irreparable damage.

Apparatus and Materials

Standard Schlenk technique with a stainless steel vacuum line was used to perform all reactions. All reactions in superacidic media were carried out in FEP/PFA reactors closed with a stainless steelvalve. HF was dried with F_2 prior to use. Raman spectra were recorded on a Bruker MultiRAM FT-Raman spectrometer with Nd:YAG laser excitation (λ = 1064 nm). For Raman measurements, samples of products were transferred into a cooled glass cell, which were evacuated afterwards. The educts were transferred into NMR tubes and measured at room temperature. NMR spectra were recorded on either on a Jeol ECX400 NMR or a Bruker AV400 NMR instrument. The spectrometer were externally referenced to $CFCl_3$ for ^{19}F and to tetramethylsilane for ^{1}H and ^{13}C NMR spectra. The spectra were recorded inside 4 mm FEP NMR tube inliners. Acetone-d_6 was employed for external shimming when aHF was used as solvent for the respective compounds. The educts were measured in 9 mm glass NMR tubes. The NMR samples were prepared by re-dissolving the respective protonated tricarboxybenzene at the designated measuring temperature in *a*HF and transferring the solution into a 4 mm FEP NMR tube inliner. The inliner was then frozen and flame sealed. The low-temperature X-ray diffraction was performed with an Oxford X-Calibur3 equipped with a Kappa CCD detector, operating with Mo-K_α radiation (λ = 0.71073 Å) and a Spellman generator (voltage 50 kV, current 40 mA).

Deposition Numbers 2049675 for **[1+3H]**[$(SbF_6)_3$]·3HF, 2049673 for **[2+1H]**[SbF_6]·HF, 2049672 for **[2+3H]**[$(SbF_6)_3$], 204976 for **[3+1H]**[AsF_6]·HF and 2049674 for **[3+3H]**[$(Sb_2F_{11})(SbF_6)_2$] contain the supplementary crystallographic data for this paper. These data are provided free of charge by the joint Cambridge Crystallographic Data Centre and Fachinformationszentrum Karlsruhe Access Structures service www.ccdc.cam.ac.uk/structures.

General Procedure

In a typical experiment, the lewis acid and *a*HF were condensed into a FEP reactor at –196 °C. The mixture was reacted at –40 °C for 15 minutes and frozen to –196 °C. The respective tricarboxybenzene (~0.1–0.8 mmol) is added under constant N_2-flow. The complete mixture was reacted at before mentioned temperature. The solution was cooled down to –78 °C and the solvent was removed *in vacuo*. Some material of the obtained colorless salts was used for Raman spectroscopy, the rest was redissolved in *a*HF. A part of the solution was transferred into a FEP NMR tube, the rest was used to crystallize crystals suitable for single crystal X-ray diffraction.
For all experimental details, see the Supporting Information.

Acknowledgements

We are grateful to the Department of Chemistry and Pharmacy of the Ludwig Maximilians University of Munich, the Deutsche Forschungsgemeinschaft (DFG) and the F-Select GmbH for their financial support.

Keywords: Aromaticity • Carboxonium ions • Protonation • Superacids • Tricarboxybenzenes

[1] G. A. Olah, A. M. White, *J. Am. Chem. Soc.* **1968**, *90*, 1884-1889.
[2] G. A. Olah, A. M. White, *J. Am. Chem. Soc.* **1967**, *89*, 3591-3594.
[3] H. Spiesecke, W. G. Schneider, *J. Chem. Phys.* **1961**, *35*, 731-738.
[4] D. G. Farnum in *Advances in Physical Organic Chemistry Vol. 11*, **1975**, 123-175.
[5] G. A. Olah, G. K. S. Prakash, G. Liang, P. W. Westerman, K. Kunde, J. Chandrasekhar, P. V. R. Schleyer, *J. Am. Chem. Soc.* **1980**, *102*, 4485-4492.
[6] P. V. R. Schleyer, C. Maerker, A. Dransfeld, H. Jiao, N. J. R. Van Eikema Hommes, *J. Am. Chem. Soc.* **1996**, *118*, 6317-6318.
[7] H. Fallah-Bagher-Shaidaei, C. S. Wannere, C. Corminboeuf, R. Puchta, P. V. R. Schleyer, *Org. Lett.* **2006**, *8*, 863-866.
[8] T. Birchall, R. J. Gillespie, *Can. J. Chem.* **1965**, *43*, 1045-1051.
[9] G. A. Olah, P. W. Westerman, *J. Org. Chem.* **1973**, *38*, 1986-1992.
[10] D. Bruck, M. Rabionvitz, *J. Am. Chem. Soc.* **1977**, *99*, 240-241.
[11] Z.-Z. Fan, X.-H. Li, G.-P. Wang, *Acta Crystallogr. E* **2005**, *61*, 1607-1608.
[12] M. Schickinger, T. Saal, F. Zischka, J. Axhausen, K. Stierstorfer, Y. Morgenstern, A. J. Kornath, *ChemistrySelect* **2018**, *3*, 12396-12404.
[13] F. Takusagawa, A. Shimada, *Bull. Chem. Soc. Jpn.* **1973**, *46*, 2998-3004.
[14] T. Okazaki, K. K. Laali, *Org. Biomol. Chem.* **2004**, *2*, 2214-2219.
[15] S. Vázquez, *J. Chem. Soc., Perkin Trans. 2* **2002**, 2100-2103.

Entry for the Table of Contents

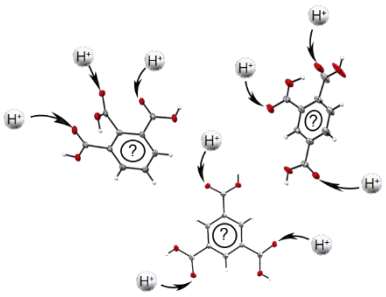

Tricarboxybenzenes were (tri-)protonated, resulting in the formation of astonishingly stable species. The different isomers are stabilized by mesomerism and hyperconjugation depending on the substitution pattern. These effects are observable by X-ray diffraction and NMR spectroscopy and also computable by NPA and NICS calculations, enabling qualitative and quantitative statements.

RESEARCH ARTICLE

Two room-temperature stable trications – Triprotonated triamino- and tricyanobenzene

Alexander Nitzer, Robert Hübsch, Christoph Jessen, Andreas J. Kornath*[a]

[a] A. Nitzer, R. Hübsch, C. Jessen, Prof. Dr. A. Kornath
Department of Chemistry and Pharmacy
LMU Munich
Butenandtstrasse 5–13, 81377 Munich, Germany
E-mail: alexander.nitzer@cup.uni-muenchen.de, r.huebsch@campus.lmu.de, christoph.jessen@cup.uni-muenchen.de, akoch@cup.uni-muenchen.de

Supporting information for this article is given via a link at the end of the document.

Abstract: Protonation of 1,3,5-tricyano- and 1,3,5-triaminobenzene was achieved in various superacidic media, resulting in the formation of the respective trinitrilium and triammonium species. Furthermore, the respective *N*-methyl nitrilium species was synthesized by methylation. Characterization was performed by NMR and vibrational spectroscopy followed by single crystal X-ray diffraction analyses of selected species. Fourfold protonation of the amine, which would have led to the triammonium arenium species could not be achieved. Quantum chemical calculations are employed to enable full vibrational assignment as well to quantify charge localization.

Introduction

Apart from various carbonium and oxonium cations, numerous studies discuss the protonation of nitrogen-containing species. Evidently, an enormous variety of ammonium ions are known. Iminium or diazonium cations commonly appear in organic syntheses, most often as intermediates. Even more exotic cations like protonated hydrazoic acid[1] or the N_5^+ ion[2] do exist.

Out of all aromatic nitrogen-containing species the protonation of pyridine is most obvious, with it being a key compound in organic chemistry. Protonation of various nitriles,[3] for example of benzonitrile and terepthalonitrile, was easily achieved and led to the respective nitrilium species.[4] With the protonation of 1,3,5-tricarboxybenzene,[5] we wanted to investigate the protonation of other 1,3,5-substitued benzenes, but with nitrogen containing functional groups (Figure 32).

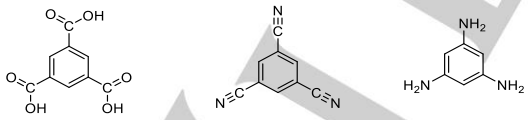

Figure 32. Structures (left to right) of 1,3,5-tricarboxybenzene, 1,3,5-tricyanobenzene and 1,3,5-triaminobenzene.

1,3,5-triaminobenzene is fascinating, as its monoprotonation results in a temperature-dependent equilibrium (Scheme 10). The σ-complex (arenium ion) is energetically favoured and the mono ammonium species is entropically favoured.[6]

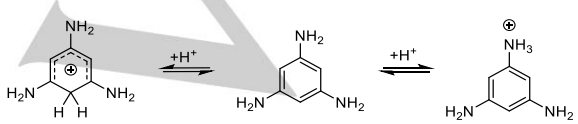

Scheme 10. Equilibrium of monoprotonated 1,3,5-triaminobenzene.

As the basic amine moieties should be readily protonated in superacidic media, we intended to investigate, whether it would be still possible to also protonate the aromatic ring. Benzene itself can be protonated in sufficient superacidic media,[7] so 1,3,5-triaminobenzene is a candidate for a fourfold protonation. 1,3,5-tricyanobenzene has a basic site at each nitrile group, where protonation should occur first. After triprotonation enough basicity in the ring could remain to enable fourfold protonation.

Results and Discussion

1,3,5-tricyanobenzene is readily protonated at 0 °C in the superacidic media HF/SbF_5 and HF/AsF_5 (Scheme 11).

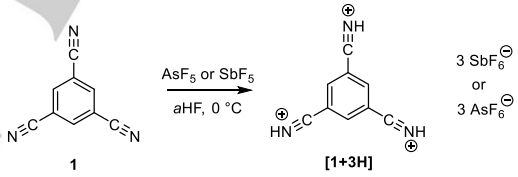

Scheme 11. Protonation of 1,3,5-tricyanobenzene.

The starting material was dissolved at only about 0 °C in *a*HF (anhydrous hydrogen fluoride) and reacted with the respective superacidic mixtures, resulting in the immediate formation of yellow to colorless solids. Precipitating already at –20 °C, the salts were characterized after removal of the solvent at –78 °C.

As methylation of nitriles[8] is easily possible by means of using the system CH_3F-SO_2-MF_5 (M=Sb, As),[9] we intended to investigate the differences in electronic properties of the protonated and methylated derivative.

Methylation of 1,3,5-tricyanobenzene was achieved by adding methyl fluoride to frozen antimony or arsenic pentafluoride and reacting the mixture at –50 °C in sulfur dioxide (Scheme 12). After freezing the solution to –196 °C, 1,3,5-tricyanobenzene was added and the solution was allowed to warm to 0 °C. The *in situ* formed $[SO_2CH_3][MF_6]$ (M = Sb or As) acts as methylating agent,[9] which reacts with the nitrile. A simultaneous dissolution and homogenization with the nitrile at 0 °C allowed for the formation of the *N*-methyl nitrilium salts. Cooling of the reaction mixture leads to the precipitation of the yellowish salts at –40 °C, which are then characterized after removing the solvent at –60 °C.

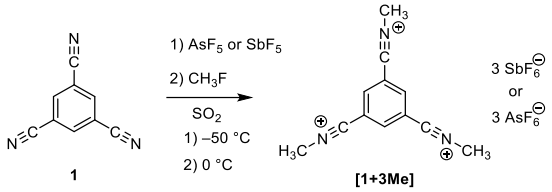

Scheme 12. Methylation of 1,3,5-tricyanobenzene.

The room temperature stable salts of both **[1+3H]** and **[1+3Me]** were first characterized by Raman spectroscopy. A slight blue-shift of the C≡N stretching vibration is the first indication of protonation and an even larger blue-shift a proof of methylation, without considering the vibrations assigned to the anions. Furthermore, **[1+3H]**[$(SbF_6)_3$] was re-dissolved in anhydrous hydrogen fluoride at 0 °C and **[1+3Me]**[$(SbF_6)_3$] in sulfur dioxide at –20 °C, respectively, followed by an NMR spectroscopic examination. For unequivocal proof, crystallization enabled isolation of **[1+3H]**[$(Sb_2F_{11})_2(SbF_6)$] · 3HF as determined by single crystal X-ray diffraction analysis. The results will be discussed further below.

1,3,5-triaminobenzene hydrochloride was reacted with HF/BF_3 and HF/SbF_5 respectively with the starting material already dissolving at –40 °C. Removal of the solvent yielded colorless solids for characterization (Scheme 13).

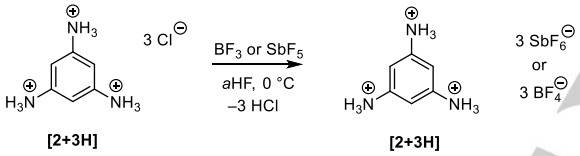

Scheme 13. Isolation of triprotonated 1,3,5-triaminobenzene.

The room temperature stable [$(SbF_6)_3$], [$(BF_4)_3$] species and the starting material were compared by vibrational spectroscopy, showing similarity of the three compounds up to the fingerprint region. Futhermore, comparison of ^{14}N NMR data of the starting material in D_2O and of **[2+3H]**[$(SbF_6)_3$] in *a*HF revealed the same cationic species. Crystallization of the triammonium species in the system HF/SbF_5 yielded **[2+3H]**[$(SbF_6)_3$] · HF as determined by single crystal X-ray diffraction analysis. The data will be discussed at a later point. No crystal structure of **2** or **[2+3H]** has been reported so far. Even with tenfold stoichiometric amount of SbF_5, no fourfold protonation was achieved, only polyfluoridoantimonates could be observed.

X-ray Crystal Structures: By recrystallization from *a*HF crystals of both cationic species were grown, which were suitable for single crystal X-ray diffraction. The complete list of bond lengths and additional crystallographic details can be found in the Supporting Information (Chapter 3).

[1+3H][$(Sb_2F_{11})_2(SbF_6)$] · 3HF crystallizes in the triclinic space group *P*–1 (*Z* = 2) (Figure 33). The C≡N distances amount to 1.125(7), 1.135(7) and 1.141(7) Å, similar to those of the starting material and comparable to other nitrilium ions.[4] The C-C bonds adjacent to the CN groups measure 1.424(8), 1.426(8) and 1.442(7) Å and are thus of similar length compared to 1,3,5-tricyanobenzene.[10] A shortening of these bonds, as it was observed by protonation of 1,3,5-tricarboxybenzene, where the C-C bonds adjacent to the [$COOH_2$] moiety were slightly shortened, is not observed for the nitrilium derivative. The aromatic C-C bonds do not change in length by protonation, measuring 1.382(7) to 1.399(7).

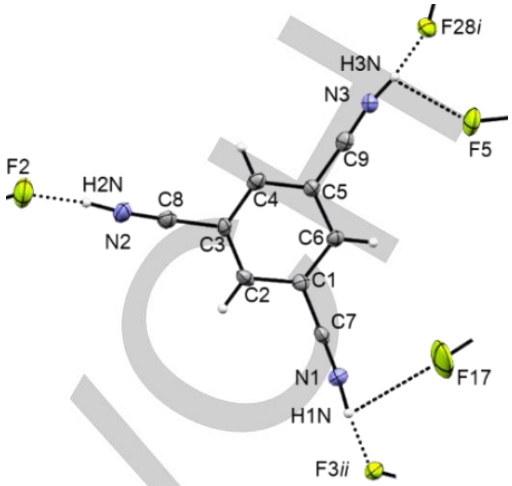

Figure 33. Section of the crystal structure of **[1+3H]**[$(Sb_2F_{11})_2(SbF_6)$] · 3HF, view along *a*, displacement ellipsoids at 50% probability, *i* = x, –1+y, 1+z, *ii* = 1–x, 1–y, –z.

Triprotonated 1,3,5-triaminobenzene, **[2+3H]**[$(SbF_6)_3$] · HF crystallizes in the monoclinic space group $P2_1/n$ (*Z* = 4) (Figure 34). The CN bonds measure 1.484(9), 1.480(8) and 1.459(8) Å and are in the range of typical C–N single bonds.[11] In the crystal structure of protonated 2,4,6-tri-*tert*-butylaniline (TBA)[12] a C-N distance of 1.473(5) Å was found, a similar length as in the here presented ammonium species. The crystal structure of aniline hydrobromide measured at 70°C exhibits a C-N bond distance of 1.47 Å.[13] In the respective hydrochloride compound, a C-N bond length of 1.35 Å is present, a significant decrease in length compared to the afore mentioned species.[14] The authors note that in various other ammonium species, be it aromatic, aliphatic or heterocyclic, a similar observation of a short C-N distance was made.[14] Thus a significant influence of the counterion is observed, whilst the amount of charge on the cation is not of importance. The temperature has also only a marginal influence on the C-N bond length.

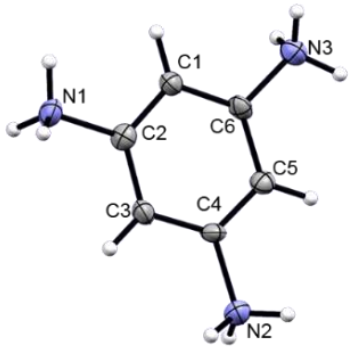

Figure 34. Cation from the asymmetric unit of **[2+3H]**[$(SbF_6)_3$] · HF, view along *a*, displacement ellipsoids at 50% probability.

NMR spectroscopy: The complete list of NMR spectroscopic data is given in the Supporting Information (Chapter 4). Sulfur dioxide was used as the solvent for NMR spectroscopical analyses of **1** and **[1+3Me]** at 26 °C and –20 °C respectively, while **[1+3H]** was characterized at 0°C in *a*HF. An overview of chemical shifts is given in Table 2. Aromatic protons

slightly shift depending on solvent and temperature. Still, a moderate deshielding of these resonances from starting material to nitrilium ion is observed. The NH protons display narrow signals for **[1+3H]** at 9.84 ppm, while the methyl protons are observed at 5.44 ppm for **[1+3Me]**. Solvent effects and temperature do not play a major role for ^{13}C NMR shifts. Only upon protonation and methylation ^{13}C resonances shift significantly. The C-H aromatic carbons are shifted downfield, while the **C**-CN carbons and nitrilium carbons are shifted upfield. The *N*-methyl nitrilium species displays the methyl group at 34.0 ppm. The change from nitrile to nitrilium is detected in the ^{14}N NMR spectrum as the nitrogen resonance shifts downfield.

Table 2. ^{1}H, ^{13}C and ^{14}N NMR shifts of **1**, **[1+3H]** and **[1+3Me]**. [a]

	1[b]	**[1+3H]**[c]	**[1+3Me]**[d]
δ ^{1}H (C-**H**)	8.72	9.03	10.49
δ ^{1}H (CN**H**$^{+}$)		9.84	
δ ^{1}H (N–**C**H$_3$)			5.44
δ ^{13}C (**C**-H)	141.1	150.4	150.1
δ ^{13}C (**C**–CN)	113.8	109.1	111.3
δ ^{13}C (**C**≡N)	111.2	100.1	100.9
δ ^{13}C (N–**C**H$_3$)			34.0
δ ^{14}N	–238.8	–214.7	–215.1

[a] all shifts in ppm. [b] in SO_2 at 26 °C. [c] in *a*HF at 0 °C. [d] in SO_2 at –20 °C.

NMR spectroscopy of 1,3,5-triaminobenzene hydrochloride in D_2O and in *a*HF showed the presence of the ammonium species to be prevalent, as the presence of a ND_3^+ group is detected in the ^{14}N NMR spectrum (Figure 35, see SI Chapter 4.5 for detailed explanation). The described equilibrium between arenium and mono ammonium species[6] was also detected. Besides the two aromatic signals in the ^{13}C NMR spectrum other signals, the strongest at 29.7 ppm and 158.3 ppm, are observed (Figure 35). The amount of hydrochloric acid in D_2O thus acidifies the NMR sample sufficiently to induce the equilibrium. For the sample in *a*HF, only two signals in the ^{13}C NMR spectrum are detected (Table 3). The triammonium species thus can be assumed to be present in the solution, as a mono- or diammonium species would exhibit more resonances. An equilibrium between arenium and ammonium ion is no longer possible, when at least diprotonation, in any case triprotonation of **2** is achieved. A fourfold protonation must thus also be excluded.

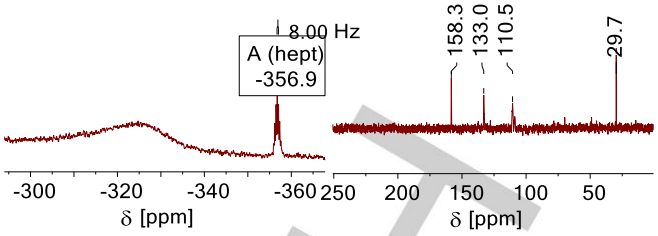

Figure 35. ^{14}N NMR (left) and ^{13}C NMR (right) of **[2+3H]**[Cl_3] in D_2O, shifts in ppm.

Table 3. ^{1}H, ^{13}C and ^{14}N NMR shifts of **[2+3H]**. [a]

	[2+3H][Cl_3] in D_2O[b]	**[2+3H]**[(SbF_6)$_3$] in *a*HF[d]
δ ^{1}H (C-**H**)	7.03	7.55
δ ^{13}C (**C**-H)	110.5	122.0
δ ^{13}C (**C**-NH_3)	133.0	132.1
δ ^{14}N	–356.9	–333.5

[a] all shifts in ppm, measured at 25 or 26 °C.

Vibrational spectroscopy: Protonation or methylation of **1** is detectable by IR and Raman spectroscopy. For clarity only selected frequencies of cations from respective hexafluoridoantimonates are depicted in Table 4. Most obvious are the respective blue-shifts of the C≡N stretching vibration of 31 cm^{-1} (IR) and 64 cm^{-1} (Raman) upon protonation and of 148 cm^{-1} (IR) and 157 cm^{-1} (Raman) upon methylation. The ring breathing mode at 974 cm^{-1} in **1** only shifts slightly by protonation or methylation. The intensity of the respective line however is intensified, especially by protonation. For **[1+3H]**, the NH stretching vibrations occur as a broad band at 3437 cm^{-1} in the IR. The C–N stretching vibration of **[1+3Me]** is observed at 910 cm^{-1} (IR) and 905 cm^{-1} (Raman), furthermore the deformation of the methyl group appears at 1429 cm^{-1} in the IR spectrum. The complete list of vibrational data is provided in the Supporting Information (Chapter 2).

Table 4. Selected experimental vibrational frequencies [cm^{-1}] of **1**, **[1+3H]** and **[1+3Me]**; assignments based on calculated vibrational frequencies [cm^{-1}]. [a]

Assignment	**1**	**[1+3H]**[(SbF_6)$_3$]	**[1+3Me]**[(SbF_6)$_3$]
ν (C≡N)	2249 (m) / 2248 (100)	2280 (m) / 2312 (70)	2397 (m) / 2405 (100)
ring breathing (only Raman)	974 (3)	1000 (72)	998 (16)
ν (NH) (only IR)		3437 (m, broad)	
δ (CH_3) (only IR)			1429 (m)
ν (C–N)			910 (m) / 905 (11)

[a] Calculated on B3LYP/6–311g++(3d2f,3p2d) level of theory, IR intensities in km/mol, Raman intensities in Å^4/u; abbreviations for IR intensities: m – medium.

For triprotonated 1,3,5-triaminobenzene selected vibrations are listed in Table 5, showing the similarity of hydrochloride compound compared to **[2+3H]**[$(BF_4)_3$] and **[2+3H]**[$(SbF_6)_3$]. The ring breathing mode appears at the same wavenumber for the hydrochloride as well as for the [SbF_6] and [BF_4] salt. Furthermore, the deformation vibration of the NH_3 group appears for all three salts at a similar position in the IR spectra, i.e. at around
1650 cm^{-1}. A deformation mode of a NH_2 group would appear at a lower wavenumber, thus excluding the presence of an unprotonated amino group in any cation.[15]

Table 5. Selected experimental vibrational frequencies [cm^{-1}] of **[2+3H]** with respective anions, assignments based on respective calculated vibrational frequencies [cm^{-1}]. [a]

Assignment	**[2+3H]**[$(Cl)_3$]	**[2+3H]**[$(SbF_6)_3$]	**[2+3H]**[$(BF_4)_3$]
ring breathing (only Raman)	1007 (100)	1008 (56)	1008 (100)
δ (NH_3) (only Raman)	1635 (25)	1651 (23)	1649 (51)
ρ (NH_3) (only IR)		1028 (vs)	1028 (m)

[a] Calculated on B3LYP/6–311g++(3d2f,3p2d) level of theory, IR intensities in km/mol, Raman intensities in $Å^4/u$; abbreviations for IR intensities: vs – very strong, m – medium.

Quantum chemical calculations: For **1**, **[1+3H]** and **[1+3Me]** as well as **2** and **[2+3H**] quantum chemical calculations are employed using DFT on the B3LYP/6–311G++(3d2f, 3p2d) level of theory. Gausview 6.0 was used for visualization, Gaussian16 for calculations.[16] Vibrational frequencies were computed after the optimization, selected observed and calculated vibrations of 1,3,5-tricyanobenzene as well as its triprotonated and trimethylated derivatives are listed in Table 6. DFT in general, hybrid functionals especially, are suitable for prediction of vibrational frequencies.[17] The C≡N stretching vibration is calculated to be at higher wavenumbers, which is explainable by the gas-phase-optimization of the computed molecule, leading to overall higher calculated wavenumbers. The two predicted modes are too close together to be observed individually. The blueshift of the C≡N stretching is also expected by the employed calculations, although the overestimation of the vibration(s) becomes smaller. The two modes which are predicted diverge compared to **1**, which is observable by the broadening of the assigned Raman line. The shift of the C≡N stretching mode by methylation is almost exactly calculated, the two calculated modes being only 1 and 4 cm^{-1} blueshifted compared to the observed one. The ring breathing mode of **1** is overestimated by the DFT method, in **[1+3H]** and **[1+3Me]** the difference is smaller. The calculations expect a slight redshift of the mode, while a slight blueshift is observed. The calculation expects the C–N stretching vibration in the methylated compound to appear by almost 50 cm^{-1} lower. This discrepancy may be due to a stabilizing effect occurring between the methyl group and the nitrogen, more on that matter will be elaborated when discussing NPA charges.

Table 6. Selected experimental and *[calculated]* Raman frequencies [cm^{-1}] of **1**, **[1+3H]** and **[1+3Me]**. [a]

Assignment	**1**	**[1+3H]**[$(SbF_6)_3$]	**[1+3Me]**[$(SbF_6)_3$]
ν (C≡N)	2248 (100) *[2280 (877)]* *[2278 (586)]*	2312 (70) *[2331 (767)]* *[2326 (638)]*	2405 (100) *[2409 (2759)]* *[2406 (2129)]*
ring breathing	974 (3) *[1017 (76)]*	1000 (72) *[1003 (70)]*	998 (16) *[1008 (87)]*
ν (C–N)			905 (11) *[847 (137)]*

[a] Calculated on B3LYP/6–311g++(3d2f,3p2d) level of theory, Raman intensities in $Å^4/u$, observed intensities scaled to 100.

The ring breathing mode of **[2+3H]** is observed at 1007 cm^{-1} in the hydrochloride, at 1008 cm^{-1} in the hexafluoridoantimonate and tetrafluoridoborate and predicted at 1021 cm^{-1}, fitting closely to the experimental data.

The computed bond distances for **1**, **[1+3H]** and **[2+3H]** mostly agree with the measured ones. Selected distances are listed in Table 7. The gas-phase optimization leads to similar bond lengths of each type of bond, for example all CN bonds being predicted to be equally long. The measured bond lengths in the cations are under influence of various solid-state effects such as hydrogen bonding. A (slight) deviation from the computed lengths can thus be explained. Nevertheless, most experimentally observed bond distances do fit to the calculated lengths, in both cationic species they are at most slightly overestimated. Only for **1**, where not hydrogen bonding, but π-π interactions are mainly contributing to the packing, the difference between calculation and observation is apparent. The C≡N and CC (ring) bond lengths are slightly overestimated even when considering standard deviations of measured lengths, the C–C(N) distance is predicted to be longer.

Table 7. Selected observed and *[calculated]* bond lengths (Å) of **1**, **[1+3H]** and **[2+3H]**. [a]

Bond	**1**	**[1+3H]**	Bond	**[2+3H]**
d (C≡N)	1.135(3) *[1.166]*	1.135(7) *[1.148]*		
d (C–CN)	1.444(3) *[1.432]*	1.426(8) *[1.436]*	d (C–N)	1.480(8) *[1.502]*
d (CC) (ring)	1.387(3) *[1.404]*	1.390(6) *[1.410]*	d (CC) (ring)	1.375(7) *[1.400]*

[a] Calculated on B3LYP/6–311g++(3d2f,3p2d) level of theory, calculated bond lengths rounded to the third decimal place.

To locate charges and to comprehend the stabilization of the cations, NPA charges were calculated on the described level of theory. 1,3,5-tricyanobenzene easily forms the respective (tri-)nitrilium species, either by protonation or methylation (Scheme 14).

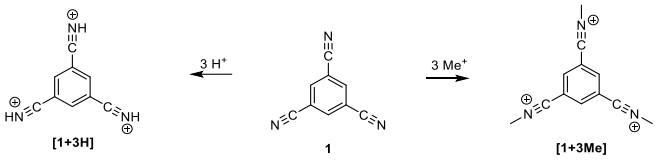

Scheme 14. Synthesized nitrilium species derived from 1,3,5-tricyanobenzene.

As computed by the NPA calculations, the positive charge, emerging either by methylation or protonation, is mostly located at the nitrilium carbon (Figure 36). The NPA charge of that carbon increases from 0.263 in **1** to 0.582 in **[1+3Me]** and 0.628 in **[1+3H]**. The *N*-methyl nitrilium species exhibits a larger stabilization of the positive charge on the nitrogen compared to the protonated derivative. The nitrogens` NPA charge increases from –0.258 in **1** to –0.114 in **[1+3Me]**, whereas in **[1+3H]** it even slightly decreases to –0.272. The participation of the aromatic carbons is small but present, with the C-H aromatic carbons losing electron density, the arylic carbons connected to the nitrilium groups gaining it. Lopez and co-workers[18] studied protonation of various nitriles by theoretical calculations. They showed that depending on which group is attached to the nitrile/nitrilium species, σ-electron density (alkyl group) or π-electron density (aryl group) is provided to the nitrile carbon. When analyzing NPA charges of **1**, **[1+3H]** and **[1+3Me]**, this σ-electron donation is observable. So, the underestimation of the observed C–N stretching vibration in the methylated compound may also be explained.

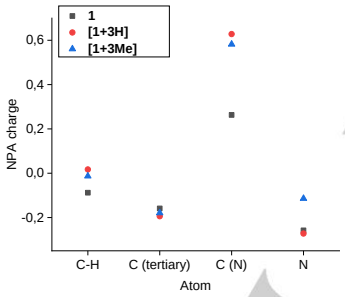

Figure 36. Plot of the NPA charges[a] of the non-hydrogen atoms of **1**, **[1+3H]** and **[1+3Me]**. [a] DFT, B3LYP/6-311G++(3d2f, 3p2d).

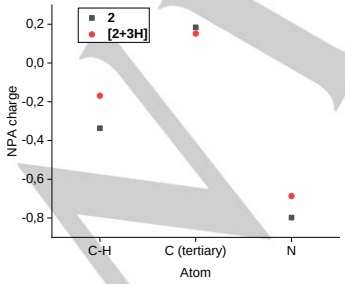

Figure 37. Plot of the NPA charges[a] of the non-hydrogen atoms of **2** and **[2+3H]**. [a] DFT, B3LYP/6-311G++(3d2f, 3p2d).

Protonation of 1,3,5-triaminobenzene shows a similar change of NPA charges in the aromatic system as calculated for 1,3,5-tricyanobenzene (Figure 37). As the protonated site is directly connected to the ring, thus "lacking" a carbon compared to **1**, the positive charge is located on the sp^3 hybridized nitrogen. Still, the C-H aromatic carbons show a larger increase in NPA charge compared to **[1+3H]**.

^{13}C NMR shieldings were calculated for here discussed species using the GIAO method[19] on B3LYP/6–311G++(3d2f, 3p2d) level of theory. A comparable method was used by Vazquez to compute ^{13}C chemical shifts, which were in good agreement with experimental data.[20] The observed NMR shifts as well as the calculated ones are listed in Table 7. The before mentioned charge stabilization occurring in **[1+3H]** and **[1+3Me]** is also expected by the computed values. The greatest deviation from calculated shieldings is found for the aromatic carbons in **[1+3H]**, the calculations expecting a further deshielded value, by 8 ppm from the observed one.

Table 8. Selected measured and *[calculated]* ^{13}C NMR shieldings [ppm] of **1**, **[1+3H]**, **[1+3Me]** and **[2+3H]**. [a]

Atom	**1** in SO_2 @RT	**[1+3H]** in HF @0°C (Δ to **1**)	**[1+3Me]** in SO_2 @–20°C (Δ to **1**)	Atom	**[2+3H]** in *a*HF @RT
CN	111.2 *[118]*	100.1 (–11.1) *[100]*	100.90 (–10.3) *[102]*		
CCN	113.8 *[117]*	109.1 (–4.7) *[109]*	111.3 (–2.5) *[112]*	**C**N	132.1 *[134]*
C-H	141.1 *[141]*	150.4 (+9.3) *[158]*	150.1 (+9.0) *[153]*	**C**-H	122.0 *[128]*
N-**C**H_3			34.0 *[35]*		

[a] Calculated on B3LYP/6–311g++(3d2f,3p2d) level of theory with GIAO method, calculated ^{13}C shielding with TMS as reference, shielding rounded to a full number.

The $C(OH)_2^+$ moiety of the previously reported triprotonated 1,3,5-tricarboxybenzene seems to interact with the aromatic ring to a greater extent compared to the CNH^+ moiety of **[1+3H]**. The C-C bond between the protonated group and the aromatic ring in triprotonated 1,3,5-tricarboxybenzene decreases slightly in length compared to the starting material. This observation is not made for 1,3,5-tricyanobenzene (bonds depicted in blue boxes, Figure 38). The sp hybridized CN carbon has more s-orbital character compared to the sp^2 hybridized COOH carbon, leading to a short C-C(N) bond, which is already present in **1**. A slight increase in CC bond strength occurs in the nitrilium species, found by Raman spectroscopy. The stretching mode of the C-C bond blue-shifts from 1285 cm^{-1} in **1** to 1293 cm^{-1} in **[1+3H]** and to 1311 cm^{-1} in **[1+3Me]**.

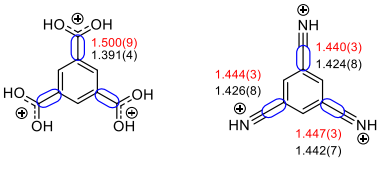

Figure 38. Triprotonated 1,3,5-tricarboxybenzene (left)[5] and 1,3,5-tricyanobenzene (right) with selected bond lengths (Å) of the neutral compound (red) and triprotonated species (black).

The formation of a triammonium arenium ion of **2** could not be achieved. The stability of the ammonium species would suggest sufficient remaining basicity of the benzene moiety. Still, too much charge seems to be concentrated on one cation, ruling out fourfold protonation.

Conclusion

For the first time synthesis of room temperature stable *N*-H and *N*-methyl trinitrilium salts of 1,3,5-tricyanobenzene together with the isolation of novel 1,3,5-triammonium benzene salts was achieved. The triprotonated nitrile has the positive charges located mainly on the nitrilium carbons, while the methylated species transfers more of the positive charge on the nitrogens due to σ-electron donation. The influence on the C-H aromatic carbons is considerable for both nitrilium species, in case of the triammonium species, these carbons are charged in the same magnitude as the nitrogens. Comparison with the previously reported protonation of 1,3,5-tricarboxybenzene shows, that the delocalization of positive charge highly depends on the functional group attached to the ring. A carboxonium group is better stabilized by the aromatic system than a nitrilium group.

Experimental Procedures

Caution! Avoid contact with any of these compounds. Hydrolysis might form HF, which burns skin and causes irreparable damage.

Apparatus and Materials

Standard Schlenk technique with a stainless steel vacuum line was used to perform all reactions. All reactions in superacidic media were carried out in FEP/PFA reactors closed with a stainless steelvalve. HF was dried with F_2 prior to use. Raman spectra were recorded on a Bruker MultiRAM FT-Raman spectrometer with Nd:YAG laser excitation (λ = 1064 nm). For Raman measurements, samples of products were transferred into a cooled glass cell, which were evacuated afterwards. The starting materials were transferred into NMR tubes and measured at room temperature. IR spectra were recorded with a Vertex-80V FT-IR spectrometer. Samples were placed on a CsBr single-crystal plate within a cell, which was cooled for the compounds not stable at room temperature. NMR spectra were recorded on a Jeol ECX400 NMR instrument. The spectrometer was externally referenced to $CFCl_3$ for ^{19}F, CH_3NO_2 for ^{14}N and to tetramethylsilane for ^{1}H and ^{13}C NMR spectra. The spectra were recorded inside 4 mm FEP NMR tube inliners. Acetone-d_6 was employed for external shimming when *a*HF or SO_2 were used as solvents for the respective compounds. The starting materials were measured in 9 mm glass NMR tubes. The NMR samples were prepared by (re-)dissolving the respective protonated or methylated compound at the designated measuring temperature in *a*HF or SO_2 and transferring the solution into a 4 mm FEP NMR tube inliner. The inliner was then frozen and flame sealed. The low-temperature X-ray diffraction was performed with an Oxford X-Calibur3 equipped with a Kappa CCD detector, operating with Mo-K_α radiation (λ = 0.71073 Å) and a Spellman generator (voltage 50 kV, current 40 mA).

Deposition Numbers 2085061 for **[1+3H]**[$(Sb_2F_{11})(SbF_6)_2$]·3HF and 2085062 for **[2+3H]**[$(Sb_2F_{11})(SbF_6)_2$]·HF contain the supplementary crystallographic data for this paper. These data are provided free of charge by the joint Cambridge Crystallographic Data Centre and Fachinformationszentrum Karlsruhe Access Structures service www.ccdc.cam.ac.uk/structures.

General Computational Procedures

Quantum-chemical calculations were done using Gaussian16 with the integrated NBO 3.0 package. GaussView 6.0 was used for visualization. All structures were computed on DFT, B3LYP/6-311G++(3d2f, 3p2d) level of theory. First, each structure was optimized. Computation of frequencies or of NMR shieldings was done after optimization, the latter using the GIAO method. NPA charges were calculated using the integrated NBO 3.0 software on described level of theory. For more details see the Supporting Information.

General Procedure

In a typical experiment for protonation, the lewis acid and *a*HF were condensed into a FEP reactor at –196 °C. The mixture was reacted at –40 °C for 15 minutes and frozen to –196 °C. The 1,3,5-triamino- or 1,3,5-tricyanobenzene (~0.2–0.5 mmol) was added under constant N_2-flow. The complete mixture was reacted at before mentioned temperature. The solution was cooled down to –78 °C and the solvent was removed *in vacuo*. Some material of the obtained colorless salts was used for Raman spectroscopy, the rest was redissolved in *a*HF. A part of the solution was transferred into a FEP NMR tube, the rest was used to grow crystals suitable for single crystal X-ray diffraction.
In a typical experiment for methylation, the lewis acid, methyl fluoride and SO_2 were condensed into a FEP reactor at –196 °C. The mixture was reacted at –50 °C for 15 min and frozen to –196 °C. 1,3,5-tricyanobenzene (~0.2–0.5 mmol) was added under constant N_2-flow. The complete mixture was reacted at 0 °C. The solution was cooled down to –60 °C and the solvent was removed *in vacuo*. Some material of the obtained colorless salts was used for Raman spectroscopy, the rest was redissolved in SO_2 for NMR spectroscopy.
For all experimental details, see the Supporting Information.

Acknowledgements

We are grateful to the Department of Chemistry and Pharmacy of the Ludwig Maximilians University of Munich, the Deutsche Forschungsgemeinschaft (DFG) and the F-Select GmbH for their financial support.

Keywords: Spectroscopy • Superacid • Triaminobenzene • Trication • Tricyanobenzene

[1] K. O. Christe, W. W. Wilson, D. A. Dixon, S. I. Khan, R. Bau, T. Metzenthin, R. Lu, *J. Am. Chem. Soc.* **1993**, *115*, 1836-1842.

[2] K. O. Christe, W. W. Wilson, J. A. Sheehy, J. A. Boatz, *Angew. Chem. Int. Ed.* **1999**, *38*, 2004-2009.
[3] G. A. Olah, T. E. Kiovsky, *J. Am. Chem. Soc.* **1968**, *90*, 4666-4671.
[4] R. Haiges, A. F. Baxter, N. R. Goetz, J. A. Axhausen, T. Soltner, A. Kornath, K. O. Christe, *Dalton Trans.* **2016**, *45*, 8494-8499.
[5] A. Nitzer, M. Regnat, C. Jessen, A. Kornath, Eur. J. Org. Chem 2022, e202101488.
[6] [a] T. Yamaoka, H. Hosoya, S. Nagakura, *Tetrahedron* **1968**, *24*, 6203–6213; [b] T. Yamaoka, H. Hosoya, S. Nagakura, *Tetrahedron* **1970**, *26*, 4125-4230.
[7] [a] C. A. Reed, K.-C. Kim E. S. Stoyanov, D. Stasko, F. S. Tham, L. J. Mueller, P. D. W. Boyd, *J. Am. Chem. Soc.* **2003**, *125*, 1796-1804; [b] F. Scholz, D. Himmel, L. Eisele, W. Unkrig, I. Krossing, *Angew. Chem. Int. Ed.* **2014**, *53*, 1689-1692.
[8] A. Nitzer, *master thesis*, LMU Munich (DE), **2018**.
[9] G. A. Olah, J. R. DeMember, R. H. Schlosberg, *J. Am. Chem. Soc.* **1969**, *91*, 2112-2113.
[10] D. S. Reddy, K. Panneerselvam, G. R. Desiraju, H. L. Carrell, C. J. Carell, *Acta Cryst. C* **1995**, *51*, 2352-2354.
[11] A. F. Hollleman, E. Wiberg, N. Wiberg, *Lehrbuch der Anorganischen Chemie*, Walter de Gryuter & Co., Berlin, New York, **2007**.
[12] M. R. Talipov, J. S. Hewage, S. V. Lindeman, J. R. Gardinier, R. Rathore, *Angew. Chem. Int. Ed.* **2014**, *53*, 938-942.
[13] I. Nitta, T. Watanabe, I. Taguchi, *Bull. Chem. Soc. Jpn.* **1961**, *34*, 1405-1410.
[14] C. J. Brown, *Acta Cryst. C* **1949**, *2*, 228-232.
[15] D. Cook, *Can. J. Chem.* **1964**, *42*, 2292-2299.
[16] *Gaussian 16, Revision A.03*, M. J. Frisch, G. W. Trucks, H. B. Schlegel, G. E. Scuseria, M. A. Robb, J. R. Cheeseman, G. Scalmani, V. Barone, G. A. Petersson, H. Nakatsuji, X. Li, M. Caricato, A. V. Marenich, J. Bloino, B. G. Janesko, R. Gomperts, B. Mennucci, H. P. Hratchian, J. V. Ortiz, A. F. Izmaylov, J. L. Sonnenberg, D. Williams-Young, F. Ding, F. Lipparini, F. Egidi, J. Goings, B. Peng, A. Petrone, T. Henderson, D. Ranasinghe, V. G. Zakrzewski, J. Gao, N. Rega, G. Zheng, W. Liang, M. Hada, M. Ehara, K. Toyota, R. Fukuda, J. Hasegawa, M. Ishida, T. Nakajima, Y. Honda, O. Kitao, H. Nakai, T. Vreven, K. Throssell, J. A. Montgomery, Jr., J. E. Peralta, F. Ogliaro, M. J. Bearpark, J. J. Heyd, E. N. Brothers, K. N. Kudin, V. N. Staroverov, T. A. Keith, R. Kobayashi, J. Normand, K. Raghavachari, A. P. Rendell, J. C. Burant, S. S. Iyengar, J. Tomasi, M. Cossi, J. M. Millam, M. Klene, C. Adamo, R. Cammi, J. W. Ochterski, R. L. Martin, K. Morokuma, O. Farkas, J. B. Foresman, and D. J. Fox, Gaussian, Inc., Wallingford CT, **2016**.
[17] M. W. Wong, Chem. Phys. Lett. **1996**, *256*, 391–399.
[18] J. L. López, A. M. Graña, R. A. Mosquera, *J. Phys. Chem. A* **2009**, *113*, 2652-2657.
[19] R. Ditchfield, Mol. Phys. **1974**, *27*, *4*, 789–807.
[20] S. Vázquez, *J. Chem. Soc., Perkin Trans. 2* **2002**, 2100–2103.

Entry for the Table of Contents

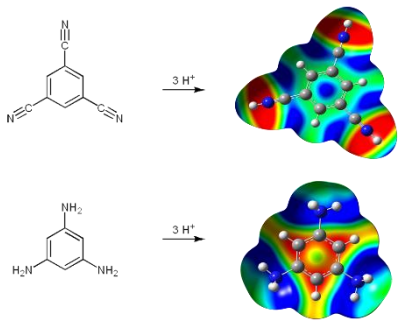

Triprotonation of 1,3,5-tricyanobenzene and 1,3,5-triaminobenzene was achieved in (super)acidic media. The nitrile species was also successfully trimethylated. Characterization and comparison between the three trications are made by vibrational and NMR spectroscopy as well as single crystal X-ray diffraction. The influence of protonation or methylation on the systems is evaluated and compared to predictions made by quantum-chemical calculations.

RESEARCH ARTICLE

A small room temperature stable tetracation

Alexander Nitzer, Christoph Jessen and Andreas J. Kornath*[a]

[a] A. Nitzer, C. Jessen, Prof. Dr. A. Kornath
Department of Chemistry and Pharmacy
LMU Munich
Butenandtstrasse 5–13, 81377 Munich, Germany
E-mail: alexander.nitzer@cup.uni-muenchen.de, christoph.jessen@cup.uni-muenchen.de, akoch@cup.uni-muenchen.de

Supporting information for this article is given via a link at the end of the document.

Abstract: 1,2,4,5-tetracarboxybenzene was tetraprotonated in the superacidic media HF/SbF_5 and HF/AsF_5. Room temperature stable salts were formed and characterized by vibrational and NMR spectroscopy. Crystals of the hexafluoridoantimonate were prepared and enabled single-crystal X-ray structure determination. NPA charges are calculated to evaluate charge distribution. To ascertain influence of the aromatic ring in stabilizing four positive charges NICS(0) was calculated.

Introduction

Small organic tetracationic species are surprisingly uncommon. A true carbocationic species is the easily accessible, but rather bulky, tetraazuliporphyrin tetracation **A** (Figure **39**).[1] The hexafluorobenzene tetracation is produced by femtosecond laser pulses, but exists only for femtoseconds.[2] Superacid chemistry as established by Olah did little work in this area. Only in 1995 the synthesis and NMR spectroscopic properties of the 1,3,5,7-adamantanetetrakis(α, α-diphenylmethyl)tetrayl tetracation **B** were reported.[3]

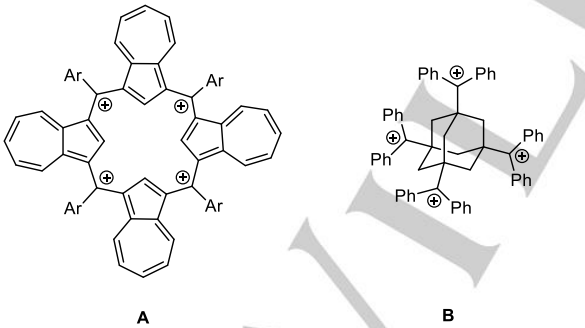

A B

Figure 39. Left: The tetraazuliporphyrin tetracation (**A**) depicted in its most contributing mesomeric structure[1]; Right: The 1,3,5,7-adamantanetetrakis(α, α-diphenylmethyl)tetrayl tetracation (**B**).[3]

Nitrogen containing tetracations are more commonly known. The tris(cyclopropenylio)cyclopropenylium salt is the first isolated tetraction. Stabilization occurs by the alkylamino groups and the aromatic core.[4] In 1984, Thomaides and co-workers[5] synthesized **C** (Figure 40) via hexaaminobenzene, although in a mixture together with the neutral compound and radical dication. Quantum chemical calculations were showed a larger contribution of the nitrogens compared to the aromatic core in stabilizing the charge.[6] The compound is more ammonium than carbenium cation. In 2016 nitrogen-containing tetra- and pentacationic species were reported. These polyaromatics were NMR spectroscopically characterized in FSO_3H-SbF_5-SO_2ClF solution, being identified as intermediates in an arylation reaction leading to **D**.[7]

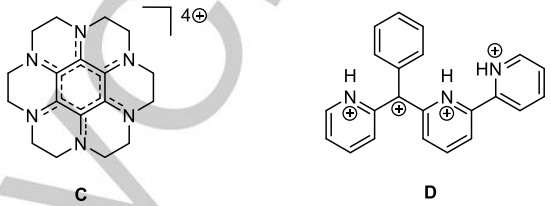

C D

Figure 40. Left: Hexaazaoctadecahydrocoronene tetracation (**C**)[5-6]; Right: One of the tetracations (**D**) observed by Klumpp et al.[7]

The common ground of most reported tetracationic species is that they are stabilized by their size. Also atoms like nitrogen do stabilize the positive charges to a great extent. Often an aromatic system donates electron density for stabilization. Pyromellitic acid (1,2,4,5-tetracarboxybenzene) has essentially all it needs to be a candidate for fourfold protonation, but is much smaller than all reported tetracations.

Results and Discussion

Fourfold protonation of 1,2,4,5-tetracarboxybenzene was achieved in the superacidic media HF/SbF_5 and HF/AsF_5 (Equation 1). After mixing the superacids at 0 °C, the solutions were frozen to –196 °C and 1,2,4,5-tetracarboxybenzene was added under N_2-flow. The mixtures were warmed to 0 °C. Colorless solids immediately precipitated. After removing the solvent at –78 °C characterization was done.

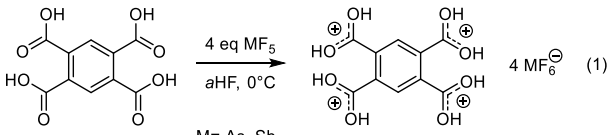

1 [1+4H] (1)

Low-temperature Raman and IR spectroscopy confirmed protonation of **1** by an overall shift of the lines of the C=O and C=C stretching vibrations together with the presences of lines assigned to the respective anions. Redissolving **[1+4H]**[$(SbF_6)_4$] in *a*HF enabled NMR spectroscopy. Upon warming up to 25 °C enough material dissolved to enable ^{13}C besides ^{1}H NMR spectroscopy. Recrystallization from large amounts of *a*HF led to the growth of crystals, which single-crystal X-ray diffraction

identified as **[1+4H]**[$(SbF_6)_4$]·HF. The hexafluoridoantimonate was stable at room temperature for more than one day.

Crystal structure of tetraprotonated pyromellitic acid: [1+4H][$(SbF_6)_4$]·HF crystallizes in the orthorhombic space group $P2_12_12$ (Z = 2). The formula unit contains the cation with four anions as well as two half-occupied, co-crystallized disordered HF molecules. The asymmetric unit contains half of the cation with the crystallographic mirror plane along the C1-C4 axis. As only half of the cation is present in the asymmetric unit, C1 is only half occupied and is placed on a symmetry position. The cation with bond lengths is depicted in Figure 41.

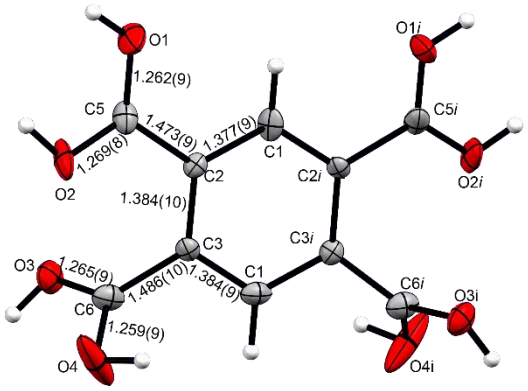

Figure 41. Cation from **[1+4H]**[$(SbF_6)_4$]·HF, view along *b*, displacement ellipsoids at 50% probability. Symmetry code: *i* = –x, –y, –z.

Various crystal structures of 1,2,4,5-tetracarboxybenzene are published. Mostly, it was co-crystallized with other aromatic compounds, forming supramolecular assemblies.[8] In **[1+4H]**[$(SbF_6)_4$]·HF strong hydrogen bonds are found, so comparison with the crystal structure of the dihydrate of **1** is appropriate, as strong hydrogen bonds are observed there too.[9] In that crystal structure also a crystallographic inversion symmetry in the molecule is present. In pyromellitic acid dihydrate the C=O double bonds are 1.2120(18) and 1.2191(18) Å long, the C–O single bonds 1.3033(19) and 1.3113(18) Å. In **[1+4H]** the CO bonds become equivalent in length with distances from 1.259(9) Å to 1.269(9) Å, being in length between CO single and double bond.[10] The adjacent C–C bonds are slightly decreased in length with 1.486(10) and 1.473(9) Å in the tetracation compared to distances of 1.502(2) and 1.500(2) Å in **1**·$2H_2O$. The CC bonds within the ring do not change length upon protonation. One carboxonium group is tilted against the aromatic ring by 15(1)°, the other by 67(1)°. In **1**·$2H_2O$, the carboxy groups are tilted by 71.44(12)° and 19.3(3)°, so in a similar fashion to **[1+4H]**. The complete list of crystallographic data is given in the Supporting Information (Chapter 3).

NMR spectroscopy: Formation of **[1+4H]** is observed by ^{1}H NMR spectroscopy as the resonance of the $C(OH)_2^+$ groups appears at 10.12 ppm. The aromatic protons' signals are covered by the HF signal. In the ^{13}C NMR spectrum all resonances of the carbon atoms are shifted downfield. The carboxonium resonance is shifted the most, by around 11 ppm, the quaternary and even the C-H aromatic signals are shifted by around 4 and 2.5 ppm respectively. The spectra are displayed in the Supporting Information (Chapter 4).

Table 9. ^{1}H and ^{13}C NMR data of (protonated) 1,2,4,5-tetracarboxybenzene.[a]

	1[b]	**[1+4H]**[$(SbF_6)_4$][c]
C-**H**	7.92	
[COO**H$_2$**]$^+$		10.12
COOH	167.39	178.21
C-H	134.70	137.16
C (quarternary)	128.54	132.46

[a] all shifts in ppm, measured at 25 or 26 °C. [b] in DMSO-d_6. [c] in *a*HF.

Vibrational spectroscopy:

Protonation of **1** is observed by Raman spectroscopy (Figure 42). The three intense lines between 1700 and 1550 cm^{-1} are assigned to the C=O and aromatic CC stretching vibrations, selected wavenumbers are listed in Table 10. Upon protonation the C=O stretching vibration is weakened, the aromatic CC stretching vibration strengthened. This is observed as the lines in the range of 1550 cm^{-1} to 1700 cm^{-1} merge closer together in the protonated species. Only by protonation one mode of an aromatic CC stretching vibration is combined with a C=O stretching mode. For the [SbF_6] species, it is detected at 1601 cm^{-1}, for the [AsF_6] species at 1613 cm^{-1}.

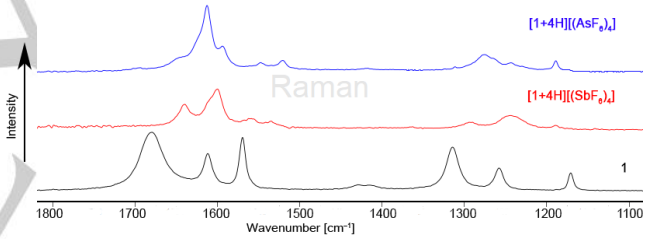

Figure 42. Section of the Raman spectra of **1** and its` protonated derivatives.

Table 10. Selected Raman frequencies of **1** and its protonated derivatives.[a]

	1	**[1+4H]**[$(SbF_6)_4$]	**[1+4H]**[$(AsF_6)_4$]
ν (C=O)	1680 (58)	1561 (8)	1594 (54) 1548 (31)
ν (CC) (ring)	1612 (37)	1640 (13)	1642 (38)
ν (CC) (ring)	1570 (53)		
ν (C=O) + ν (CC) (ring)		1601 (18)	1613 (100)

[a] assignment with calculated frequencies, B3LYP/6–311g++(3d2f, 3p2d) level of theory. Raman intensity in Å^4/u.

Quantum chemical calculations: Structures of **1** and **[1+4H]** were quantum chemically optimized on DFT, B3LYP/6–311g++(3d2f, 3p2d) level of theory. Calculated Raman frequencies enabled assignment of experimentally observed lines. With the optimized structures calculation of NPA charges were performed to localize the positive charges in **[1+4H]**. The positive charge is distributed mainly on the oxygens and the

carbonyl carbons by protonation, the influence on the aromatic carbons is minimal. The NPA charges of the oxygens are increased by 0.123 for the C=O oxygens and by 0.115 for the C–O(H) oxygens. The carbonyl carbons become more positive by 0.138, which fits to the NMR spectroscopically observed deshielding of these carbons. As the carboxy carbons become more positive than the oxygens, **[1+4H]** is more carbocation than oxonium cation.

NPA charges indicate minor distribution of charge to the ring carbons. NICS(0) was computed to investigate if there would be an effect of charge on aromatic character.[11] For 1,2,4,5-tetracarboxybenzene the NICS(0) is –7.37 ppm, that of **[1+4H]** amounts to –6.82 ppm. Protonation thus slightly decreases aromatic character.

Finally the ratio of charge to mass was considered. The charge per mass was calculated for selected tetracations shown in the introduction. For **C** and **D** 81 g/mol per charge and for **E** 92 g/mol for one positive charge are reckoned. The charge per mass for **[1+4H]** is at 65 g/mol for each positive charge, much lower than in any previously reported tetracation.

Conclusion

Pyromellitic acid was tetraprotonated in the superacidic media HF/AsF_5 and HF/SbF_5. The room temperature stable salts were characterized by vibrational and NMR spectroscopy. [1,2,4,5-$C_6H_2(COOH_2)_4$][$(SbF_6)_4$]·HF was obtained by single crystal X-ray diffraction. NPA charges are calculated to quantify charge distribution in the tetracation. The carbocationic character is computed to be even greater than the oxonium character, which is supported by the deshielding of the carbonyl carbon observed by ^{13}C NMR spectroscopy. With a charge to mass ratio of 65 g/mol per positive charge a tetracationic species of smaller size than before known has been synthesized.

Experimental Procedures

Caution! Avoid contact with any of these compounds. Hydrolysis might form HF, which burns skin and causes irreparable damage.

Apparatus and Materials

Standard Schlenk technique with a stainless steel vacuum line was used to perform all reactions. All reactions in superacidic media were carried out in FEP/PFA reactors closed with a stainless steelvalve. HF was dried with F_2 prior to use. Raman spectra were recorded on a Bruker MultiRAM FT-Raman spectrometer with Nd:YAG laser excitation (λ = 1064 nm). For Raman measurements, samples of products were transferred into a cooled glass cell, which were evacuated afterwards. The starting materials were transferred into NMR tubes and measured at room temperature. IR spectra were recorded with a Vertex-80V FT-IR spectrometer. Samples were placed on a CsBr single-crystal plate within a cell, which was cooled for the compounds not stable at room temperature. NMR spectra were recorded on a Bruker AV400 NMR instrument. The spectrometer was externally referenced to $CFCl_3$ for ^{19}F and to tetramethylsilane for ^{1}H and ^{13}C NMR spectra. The spectra were recorded inside 4 mm FEP NMR tube inliners. Acetone-d_6 was employed for external shimming when *a*HF was used as solvent for the respective compounds. The NMR samples were prepared by (re-)dissolving the respective protonated compound at the designated measuring temperature in *a*HF and transferring the solution into a 4 mm FEP NMR tube inliner. The inliner was then frozen and flame sealed. The low-temperature X-ray diffraction was performed with an Oxford X-Calibur3 equipped with a Kappa CCD detector, operating with Mo-K_α radiation (λ = 0.71073 Å) and a Spellman generator (voltage 50 kV, current 40 mA).

Deposition Number 2123213 for **[1+4H]**[$(SbF_6)_4$]·HF contains the supplementary crystallographic data for this paper. This data are provided free of charge by the joint Cambridge Crystallographic Data Centre and Fachinformationszentrum Karlsruhe Access Structures service www.ccdc.cam.ac.uk/structures.

Synthesis of [$C_6H_2(COOH_2)_4$][$(SbF_6)_4$]:

Antimony pentafluoride (255 mg, 1.04 mmol, 10 eq.) and anhydrous HF (ca. 3 mL) were condensed into an FEP reactor at –196 °C. The mixture was homogenized at –20 °C for 15 min. After freezing the solution, pyromellitic acid (26 mg, 0.10 mmol, 1 eq.) was added under nitrogen atmosphere. Followed by removing the nitrogen from the reaction vessel, the mixture was warmed to 0 °C and vigorously mixed, although only minimal dissolving of starting material was observed. The mixture was then cooled down to –78°C, so that excess *a*HF could be removed from the system. [$C_6H_2(COOH_2)_4$][$(SbF_6)_4$] was obtained as a colorless solid, which was stable at room temperature over some hours.

Synthesis of [$C_6H_2(COOH_2)_4$][$(AsF_6)_4$]:

Arsenic pentafluoride (175 mg, 1.03 mmol, 10 eq.) and anhydrous HF (ca. 3 mL) were condensed into an FEP reactor at –196 °C. The mixture was homogenized at –20 °C for 15 min. After freezing the solution, pyromellitic acid (26 mg, 0.10 mmol, 1 eq.) was added under nitrogen atmosphere. Followed by removing the nitrogen from the reaction vessel, the mixture was warmed to 0 °C and vigorously mixed, although only minimal dissolving of starting material was observed. The mixture was then cooled down to –78°C, so that excess *a*HF could be removed from the system. [$C_6H_2(COOH_2)_4$][$(SbF_6)_4$] was obtained as a colorless solid, which was stable at room temperature over some hours.

For all experimental details, see the Supporting Information.

Acknowledgements

We are grateful to the Department of Chemistry and Pharmacy of the Ludwig Maximilians University of Munich, the Deutsche Forschungsgemeinschaft (DFG) and the F-Select GmbH for their financial support

Keywords: Tetracarboxybenzene • Carbocation • Tetracation • Aromaticity • Superacid

[1] N. Sprutta, S. Mackowiak, M. Kocik, L. Szterenberg, T. Lis, L. Latos-Grazynski, *Angew. Chem. Int. Ed.* **2009**, *48*, 3337-3341.

[2] A. Kitashoji, A. Fujihara, T. Yoshikawa, T. Yatsuhashi, *Chem. Lett.* **2019**, *48*, 1472-1475.

[3] N. J. Head, G. K. S. Prakash, A. Bashir-Hashemi, G. A. Olah, *J. Am. Chem. Soc* **1995**, *117*, 12005-12006.

[4] R. Weiss, M. Hertel, H. Wolf, *Angew. Chem. Int. Ed.* **1979**, *18*, 473-474.
[5] R. Breslow, P. Maslak, J. S. Thomaides, *J. Am. Chem. Soc.* **1984**, *106*, 6454-6455.
[6] D. A. Dixon, J. C. Calabrese, R. L. Harlow, J. S. Miller, *Angew. Chem. Int. Ed.* **1989**, *101*, 81-82.
[7] M. Gasonoo, R. R. Naredla, S. O. Nilsson Lill, D. A. Klumpp, *J. Org. Chem.* **2016**, *81*, 11758-11765.
[8] [a] M. Du, Z.-H. Zhang, X.-J. Zhao, *Cryst. Growth Des.* **2005**, *5*, 1247-1254; [b] G. Dutkiewicz, E. Dutkiewicz, M. Kubicki, *Acta Cryst. C* **2018**, *74*, 1420-1426.
[9] S. H. Dale, M. R. J. Elsegood, *Acta Cryst. E* **2003**, *59*, o1087-o1088.
[10] A. F. Holleman, E. Wiberg, N. Wiberg, *Lehrbuch der Anorganischen Chemie*, Walter de Gryuter & Co., Berlin, New York, **2007**.
[11] P. v. R. Schleyer, C. Maerker, A. Dransfeld, H. Jiao, N. J. R. Van Eikema Hommes, *J. Am. Chem. Soc.* **1996**, *118*, 6317-6318.

Entry for the Table of Contents

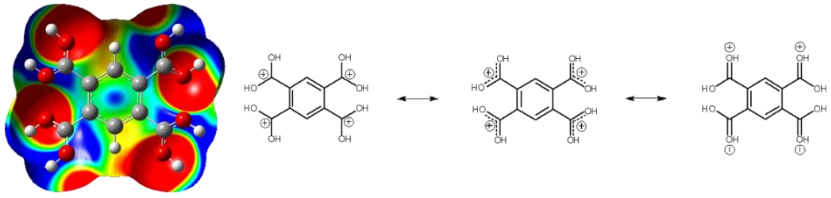

Pyromellitic acid is a candidate for a small tetracation. Fourfold protonation is achieved in the superacidic media HF/SbF_5 and HF/AsF_5. Characterization is done by vibrational and NMR spectroscopy as well as single crystal X-ray diffraction. With the support of NPA and NICS(0) calculations, charge distribution and aromatic character is evaluated.

RESEARCH ARTICLE

Preparation of a room temperature stable cyclohexenyl carboxonium dication

A. Nitzer,[a] C. Jessen,[a] R. Haiges,[b] K. O. Christe[b] and A. J. Kornath[a]

[a] A. Nitzer, M. Cornelsen, C. Jessen, Prof. Dr. A. Kornath
Department of Chemistry and Pharmacy
LMU Munich
Butenandtstrasse 5-13, 81377 Munich, Germany
E-mail: alexander.nitzer@cup.uni-muenchen.de, malte.cornelsen@cup.uni-muenchen.de, christoph.jessen@cup.uni-muenchen.de, akoch@cup.uni-muenchen.de

[b] Prof. Dr. R. Haiges, Prof. Dr. K. O. Christe
Loker Hydrocarbon Research Facility
University of Southern California
837 Bloom Walk, Los Angeles CA 90089-1661, USA
E-mail: haiges@usc.edu, kchriste@usc.edu

Supporting information for this article is given via a link at the end of the document.

Abstract: 1,3,5-trihydroxy and 1,3,5-trimethoxybenzene were mono- and diprotonated in the superacidic media HF/SbF_5, HF/AsF_5 and HF/BF_3. Monoprotonation results in the formation of arenium ions, as protonation occurs at a carbon atom of the ring. Diprotonation at another carbon atom leads to cyclohexenyl carboxonium dications. In case of the hydroxyl derivative, the hexafluoridoantimonate and arsenate are room temperature stable salts. Calculated NPA charges and Mapped Electrostatic Potentials show the carbocationic character present in these dications. NICS(0) was computed to evaluate (non)-aromatic nature of these species.

Electrophilic aromatic substitution is a key reaction in organic chemistry, be it on laboratory or industrial scale, tought during the first organic lecture to every chemistry student. The reaction proceeds via the Wheland intermediate (Figure 43), a non-aromatic species. Abstraction of a proton restores aromaticity.

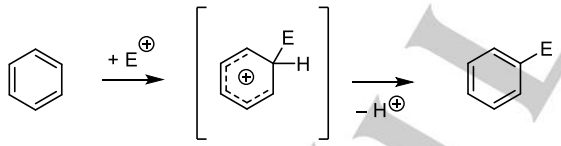

Figure 43. Electrophilic substitution of benzene via the Wheland intermediate.

While usually not isolated in synthesis, the carbocationic intermediate, also known as σ-complex or arenium-ion, become easily accessible by superacidic chemistry, enabling characterization in solution or even as solid compounds. Benzene, the as such most typical aromatic compound, can be protonated in superacidic media, the benzenenium ion $C_6H_7^+$ was first characterized in solution,[1] later then isolated, with crystal structures reported.[2] The crystallographic data together with quantum chemical calculations show the σ-complex to be the favoured structure as opposed to the π-complex or an intermediate π-σ form.[2b] The resonance structures used to describe the Wheland intermediate do fit the cyclohexadienyl cation, but when attaching various substituents to the ring, not only the position of electrophilic attack becomes interesting, but also the respective valence bond structures of the arenium ions, leading to more energetically stable structures.[3]

A variety of arenium ions was characterized, amongst others of protonated phenols.[4] Phenol itself is protonated at the *para*-position to the hydroxy group, but when the reaction mixture is cooled down to –105 °C, ideally employing stronger superacids, presence of a OH_2^+ can be detected.[5] An equilibrium between *O*- and *C*-protonated species is observed. With increasing electron density of the residues, as well as amount of substituents, protonation of the aromatic ring should occur more easily, if the substituent would not be protonated first. Thus, protonation of the dihydroxybenzenes depends on the substitution pattern, as *C*-protonation occurs for Catechol and Resorcinol, while Hydroquinone is *O*-protonated (

Figure **44**).[5]

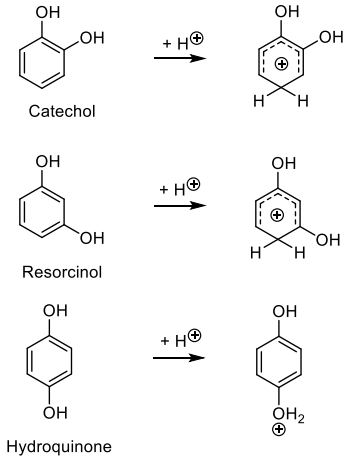

Figure 44. Protonation of dihydroxybenzenes.

Studies in solution have been so far carried out for the trihydroxybenzenes, including methoxy derivatives.[6] Also, kinetic studies[7] and quantum chemical calculations[8] have been employed to describe the species, which were found in solution. The 1,3,5-isomer sparked our interest the most, as double *C*-protonation is observed in superacidic media.

Monoprotonation of 1,3,5-trihydroxybenzol (**1**) and 1,3,5-trimethoxybenzene (**2**) is already achieved in pure anhydrous

HF(*a*HF). Lewis acids, namely BF_3, AsF_5 and SbF_5, are used to form stabilizing anions, leading to precipitation of salts (Equation 1). **1** or **2** were added to the frozen superacids under N_2-flow, then the mixtures were warmed to 0 °C, where the starting material completely dissolved. The solvent was then removed at –78 °C, the received salts characterized.

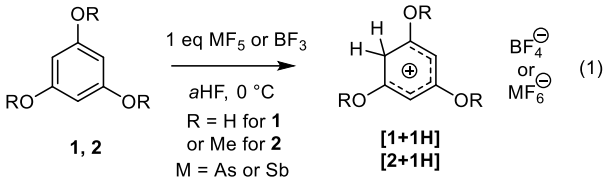

The formed arenium species did not show any kind of decomposition at room temperature. **[1+1H]**[AsF_6] was heated up to 80 °C, no decomposition was observed by Raman spectroscopy. The salts were not highly hygroscopic, so that they could be handled in glassware for a short time.

Diprotonation of **1** and **2** was achieved in the superacidic media HF/AsF_5 and HF/SbF_5 when at least employing two equivalents of lewis acid. While preparation was mostly similar to **[1+1H]** and **[2+1H]**, **[2+2H]** had to be synthesized at –40 °C, as at higher temperatures decomposition occurred.

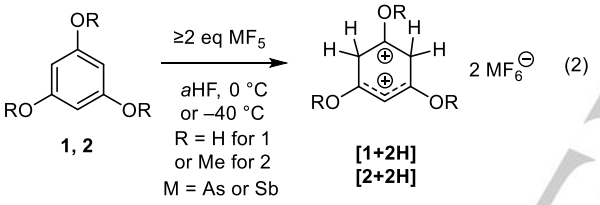

Raman spectroscopy is suitable to characterize the respective salts. Monoprotonation leads in any case to an arenium ion, a non-aromatic ring. The ring breathing vibration is shifted and far less Raman active than in the starting materials.

Selected salts were redissolved in *a*HF and NMR spectroscopy was carried out. With the appearance of the CH_2 group, far more high-field than the CH protons in ^{1}H NMR, the monoprotonated species are distinguished from **1** and **2**. For diprotonated compounds, **[1+2H]** and **[2+2H]** again do exhibit particular NMR shifts, the ring carbon between the CH_2 groups is highly deshielded, comparable to protonated ketones.

Ultimately, of all protonated compounds single crystals suitable for X-ray crystallography could be prepared. Crystals of **[1+1H]**[SbF_6] and **[1+2H]**[$(AsF_6)_2$] were grown by recrystallization from *a*HF. The cations are compared to the crystal structure of **1** based on the most recent report of Görbitz and co-workers from 2008.[9]

Bond lengths of **1**, **[1+1H]** and **[1+2H]** are compared in Figure 45. The CC bonds of **1** are of similar length, between a typical CC single and CC double bond in length.[10] The CO bonds are a bit shorter than standard CO single bonds of 1.43 Å.[10] In **[1+1H]** the CC bonds to the CH_2 group(s) increase in length compared to **1**, trending towards CC single bonds in length. Furthermore, all CO distances in **[1+1H]** are decreased. This trend is amplified in **[1+2H]**, especially for the CO group between the CH_2 groups, which is with 1.255(3) Å closer to a C=O double than a C–O single bond. Also, the CC bonds to the CH_2 groups become slightly more elongated from **[1+1H]** to **[1+2H]**. The trend from aromatic to non-aromatic compound is thus observable by X-ray diffraction.

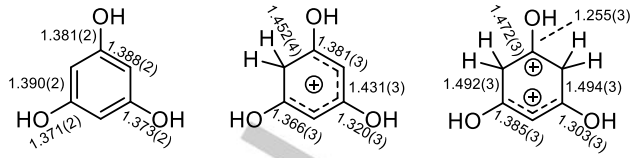

Figure 45. Selected bond lengths of **1**, **[1+1H]** and **[1+2H]**, all lengths in Å.

Crystals of **[2+1H]**[SbF_6] and **[2+2H]**[$(Sb_2F_{11})_2$] were grown by recrystallization from *a*HF. **[2+2H]** decomposed at much lower temperatures compared to **[1+2H]**, as a decomposition product monoprotonated 1-hydroxy-3,5-dimethoxybenzene **[2`+1H]**[SbF_6] was characterized. The methylene group is located in para position to the hydroxy group. Selected bond distances are shown in Figure 46. An entry of **2** was found in the Cambrige Crystallographic Data Center from 2019, which was used for comparison.[11] The bond lengths within the ring do change upon protonation in a similar fashion compared to the hydroxy derivative (Figure 46). The CO bonds to the aromatic ring decrease in length. Similarly to **[1+2H]**, in **[2+2H]** the CO distance of the carbonyl group between the CH_2 groups is drastically shortened with 1.279(9) Å compared to 1.366(3) Å. The CO bonds of the methoxy groups do also become longer by protonation.

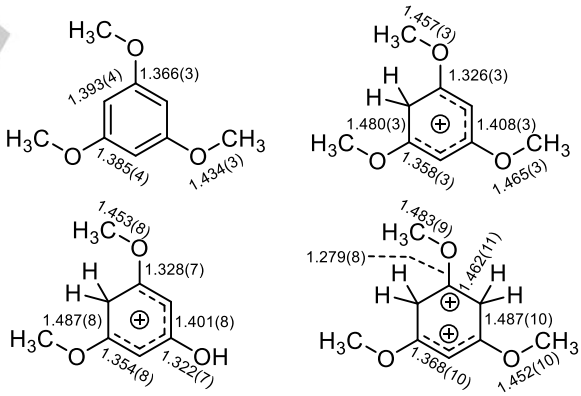

Figure 46. Comparison of bond lengths of **2**, **[2+1H]**, **[2`+1H]** and **[2+2H]**, all lengths in Å.

When comparing all arenium monocations of the 1,3,5-substitution pattern, the similarity in bonding character becomes apparent: The positive charge is largely stabilized by delocalization over the whole ring (Figure 47). The CC bonds apart from the ones to the CH_2 group are being shortened. The decrease is most significant for the bonds marked with the red boxes. The three resonance structures, which are key to the cyclohexadienyl cation, are shown in Figure 47. Double bond character is present for the red marked bonds in two of the three structures. For the other two CC bonds, marked with blue boxes, only in one resonance structure each double bond character is expected. These observations do agree with crystallographic data of the benzenium ion and other arenium ions.[2]

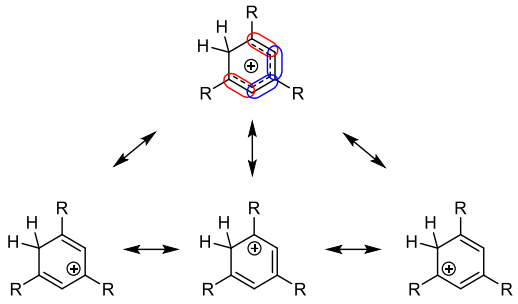

Figure 47. Key cyclohexadienyl resonance structures of in this work prepared arenium monocations of the 1,3,5-subsitution pattern (R = OH, OMe).

While the arenium monocations are planar, the dications **[1+2H]** and **[2+2H]** twist against the ring plane. An idealized structure is depicted in Figure 48. The CO group in between the CH_2 groups exhibits a dihedral angle of 18.3(2)° in **[1+2H]** and 8.1(6)° in **[2+2H]**, twisting out of plane**.** Furthermore, distortion within the ring increases by diprotonation. The bond angles at the CH_2 groups amount to 114.0(2)° and 113.8(2)° in **[1+2H]**, 114.7(6)° and 113.7(6)° in **[2+2H]** (depicted as α and β in Figure 48). The two methylene groups split the ion in two parts, hindering delocalization of bonds.

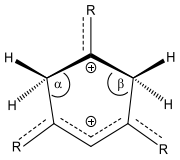

Figure 48. Schematic structure of **[1+2H]** and **[2+2H]** (R = OH, OMe).

Based on the data of Olah,[6a] NMR spectroscopic characterization of here presented species was carried out. As ^{1}H NMR data are consistent with the observations of Olah, we here focus on ^{13}C NMR resonances, as they are not reported until now. An overview of ^{13}C NMR data is given in Table 11.

The presence of the methylene group is detected by ^{13}C NMR as a distinct shift of 35.5 and 37.2 ppm for the monoprotonated compounds. As shown above for example in Figure 47, the positive charge is delocalized over the ring, but only to the *ortho*- and *para*-positions relative to the CH_2-group, not to the *meta*-positions. So the *meta*-carbons only exhibit at best a slight deshielding, the *ortho*- and *para*-carbons are much more deshielded, the *para*-carbons even more than the *ortho*-carbons.

The carbonyl carbon in both diprotonated species, which is located in between the methylene groups (C-1), exhibits a ^{13}C NMR signal at 235.48 ppm for **[1+2H]** and 233.21 ppm for **[2+2H]**, a downfield shift of ca. 50 ppm compared to **[1+1H]** and **[2+1H]**. Those resonances are in the same range compared to protonated alcohols or ketones.[1c] The two methylene groups exhibit their resonances at 43.12 ppm for **[1+2H]**, for **[2+2H]** at 42.29 and 44.39 ppm. The latter shows two resonances due to the methoxy group (C-7) no longer rotating freely around the CO bond, thus resulting in a by ca. 2 ppm more shielded CH_2 group resonance.

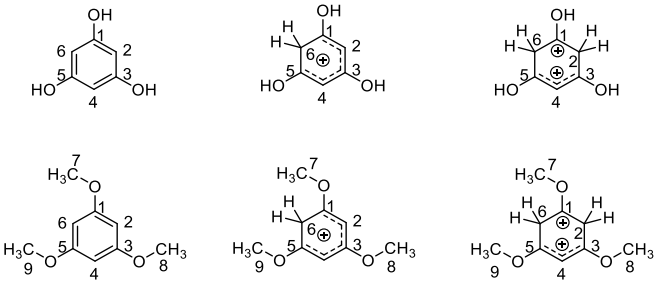

Table 11. ^{13}C NMR shifts of **1**, **2** and their protonated derivatives.[a]

^{13}C	**1**[b]	**[1+1H]**[c]	**[1+2H]**[d]	**2**[e]	**[2+1H]**[f]	**[2+2H]**[g]
C-1	159.0	181.5	235.5	161.7	183.9	233.2
C-3	159.0	191.8	193.7	161.7	193.8	193.0
C-5	159.0	181.5	193.7	161.7	183.9	194.8
C-2	94.2	97.9	43.1	93.1	93.9	44.4
C-4	94.2	97.9	103.9	93.1	93.9	97.5
C-6	94.2	35.5	43.1	93.1	37.2	42.3
C-7				55.5	57.8	72.3
C-8				55.5	59.3	63.5
C-9				55.5	57.8	63.5

[a] All shifts in ppm. [b] In DMSO-d_6 at 26 °C. [c] In *a*HF at 26 °C. [d] In *a*HF as $[SbF_6]$ species at 0 °C. [e] In $CDCl_3$ at 26 °C. [f] In *a*HF as $[BF_4]$ species at 26 °C. [g] In *a*HF as $[Sb_2F_{11}]$ species at –40 °C.

Protonation of **1** and **2** is observed by Raman spectroscopy due to drastic intensity decrease of the ring breathing (Figure 49). The main ring breathing mode of **1** is assigned to the line at 1000 cm^{-1}, another less intensive ring breathing mode appears at 605 cm^{-1} (Table 12). The stronger ring breathing mode becomes less intensive by monoprotonation, appearing at 937 cm^{-1}, the other mode intensifies, appearing at 612 cm^{-1}. In **[1+2H]**, only one ring breathing vibration remains, appearing at 602 cm^{-1}.

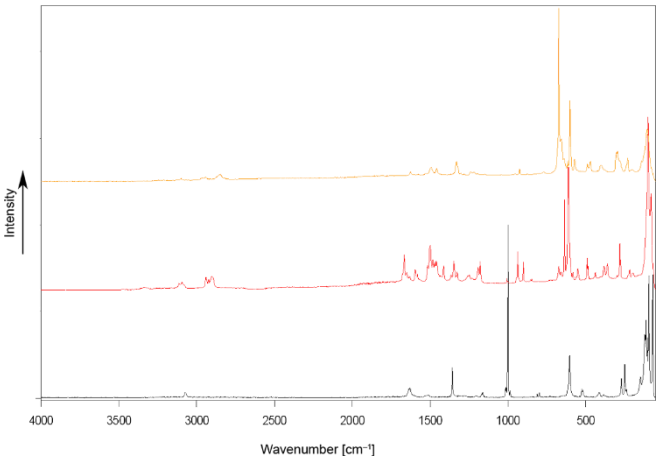

Figure 49. Raman spectra of **1**, **[1+1H]**[SbF_6] and **[1+2H]**[$(SbF_6)_2$].

The strong ring breathing is also observed for **2** at 993 cm^{-1}, a weaker one at 982 cm^{-1}, shifting to 940 and 915 cm^{-1} by monoprotonation and becoming less intensive. In **[2+2H]** it is completely extinguished (Table 12). The CH_2 groups` stretching vibrations are distinguishable from the ones of the CH group(s), appearing at lower energies compared to the CH stretching vibration(s) (Table 12).

Table 12. Selected vibrational frequencies [cm^{-1}] of **1**, **2**, and hexafluoridoantimonates of their mono- and diprotonated derivatives.[a]

	1	**[1+1H]**[SbF_6]	**[1+2H]**[$(SbF_6)_2$]
ring breathing	1000 (100)	937 (22)	
ring breathing	605 (25)	612 (71)	602 (47)
v (CH)	3076 (4) 3068 (3)	3095 (5) 2939 (8)	3099 (2)
v (CH_2)		2923 (6) 2905 (5)	2971 (2) 2943 (3) 2848 (4)
	2	**[2+1H]**[SbF_6]	**[2+2H]**[$(Sb_2F_{11})_2$]
ring breathing	993 (100)	940 (6)	
ring breathing		915 (11)	

[a] Raman intensities in in $Å^4/u$, assignment based on frequencies calculated on B3LYP/6–311g++(3d2f, 3p2d) level of theory.

NICS(0)[12] was calculated for **1**, **2** and their protonated derivatives to quantify aromatic character. Calculations were done employing Gaussian 16 software, GIAO, B3LYP/6–311g++(3d2f,3p2d) level of theory.[13] 1,3,5-trihydroxy- and methoxybenzene naturally exhibit aromatic character, their NICS(0) being negative with –9.22 and –8.79 ppm. Monoprotonation leads to the non-aromatic Wheland-intermediate, the arenium ion. The NICS(0) values are close to zero, for **[1+1H]** it amounts to –0.95 ppm, for **[2+1H]** to –0.80 ppm. Diprotonation leads to a consecutive increase in NICS(0) to 2.13 ppm for **[1+2H]** and 2.03 ppm for **[2+2H]**. That indicates a small anti-aromatic character. All calculations expected planarity to be present at any degree of protonation for the rings. The ring is twisted against the plane as found in the crystal structures in both **[1+2H]** and **[2+2H]**. This may be an attempt by the ring to reduce the small antiaromatic character.

Mapped Electrostatic Potentials and NPA charges were computed to localize electron density and thus positive charge (Figure 50).[13a] The carbonyl carbons between the methylene groups in **[1+2H]** and **[2+2H]** are very positively charged, 0.714 and 0.705 respectively. The deep blue region is concentrated solely on the carbon and not stretching out towards the oxygen, especially for **[1+2H]**. The oxonium character is despite the decreased CO bond lengths smaller than the carbenium character in the dications. The NMR data support the carbenium character of the carbonyl carbon C-1, as for **[1+2H]** and **[2+2H]**, that carbon exhibit the particular ^{13}C resonances above 230 ppm, deshielding corresponding with positive charge. The “lower” part of the dications, containing the single remaining C-H group, is colored in the same yellow-green. This indicates bond conjugation and stabilization of charge over the area.

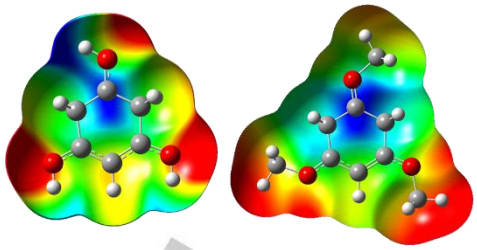

Figure 50. Molecular 0.0004 $bohr^{-3}$ 3D isosurfaces with MEP of **[1+2H]** (0.27 a.u. (red) to 0.36 a.u. (blue)) and **[2+2H]** (0.22 a.u. (red) to 0.32 a.u. (blue)), calculated on B3LYP/6–311g++(3df,3pd) level of theory.

Comparison to protonated ketones, foremost acetone,[14] shows the similarities of the here found carboxonium moiety to that of protonated carbonyls. The CO bonds are within standard deviation of similar length, 1.255(3) Å in **[1+2H]**, 1.279(8) Å in **[2+2H]** compared to 1.271(3) Å in protonated acetone. The reported NPA charge of the carbonyl carbon of acetone is 0.59, increasing up to 0.73 upon protonation, the oxygens` NPA charge slightly increasing from –0.55 to –0.52. For protonation of 1,3,5-trihydroxybenzene, the NPA charge of C-1 increases from 0.32 in **1** to 0.46 in **[1+1H]** to 0.71 in **[1+2H]**. The attached oxygen O-1 from –0.68 to –0.60 in **[1+1H]** to –0.49 in **[1+2H]**. While the oxygen shows more participation at stabilization of the positive charge for 1,3,5-trihydroxybenzene compared to acetone, the overall increase in positive charge is bigger for the carbonyl carbon in **1** compared to acetone.

The second protonation of **1** and **2** splits the species in two halves, one charge located in the carbonyl moiety (“upper half”) and the other in the “lower half”. The latter may be described best as a cyclohexenyl cation, when comparing to suitable literature-known compounds.[15] The term diarenium dication is rather unsuitable, as NICS(0) points towards a further decrease in aromaticity and cyclohexadienyl character is no more present.

The preparation and first-time isolation of mono- and diprotonated 1,3,5-trihydroxy- 1,3,5-trimethoxybenzene was accomplished. The monoprotonated species are arenium ions, which form highly stable salts, decomposing not below 80 °C. The diprotonated compounds are best described as cyclohexenyl carboxonium ions, no literature known compound of this kind is known. In case of **[1+2H]** the prepared salts are stable at room temperature. Aromatic character as calculated by NICS(0) is further decreased compared to the already non-aromatic arenium cations, trending towards antiaromaticity.

Experimental Section

A comprehensive and detailed description of experimental procedures together with spectra, data derived from X-ray diffraction and quantum chemical paramters is given in the Supporting Information. Deposition Numbers 2142688 for **[1+1H]**[SbF_6], 2142687 for **[1+2H]**[$(AsF_6)_2$], 2142689 for **[2+1H]**[SbF_6], 2142691 for **[2+2H]**[$(Sb_2F_{11})_2$] and 2142690 for **[2`+1H]**[SbF_6] contain the supplementary crystallographic data for this paper. These data are provided free of charge by the joint

Cambridge Crystallographic Data Centre and Fachinformationszentrum Karlsruhe Access Structures service www.ccdc.cam.ac.uk/structures.

Acknowledgements

We are grateful to the Department of Chemistry and Pharmacy of the Ludwig Maximilians University of Munich, the Deutsche Forschungsgemeinschaft (DFG) and the F-Select GmbH for their financial support. Furthermore, we like to thank Thomas Saal for extensive support during experimentation at USC Los Angeles.

Keywords: Trihydroxybenzenes • Aromaticity • Superacid • Protonation • Quantum chemical calculations

[1] [a] G. A. Olah, R. H. Schlosberg, R. D. Porter, Y. K. Mo, D. P. Kelly, G. D. Mateescu, *J. Am. Chem. Soc.* **1972**, *94*, 2034-2043; [b] G. A. Olah, R. H. Schlosberg, D. P. Kelly, G. D. Mateescu, *J. Am. Chem. Soc.* **1970**, *92*, 2546-2548; [c] G. A. Olah, J. S. Staral, G. Asencio, G. Liang, D. A. Forsyth, G. D. Mateescu, *J. Am. Chem. Soc.* **1978**, *100*, 6299-6308.

[2] [a] C. A. Reed, K.-C. Kim, E. S. Stoyanov, D. Stasko, F. S. Tham, L. J. Mueller, P. D. W. Boyd, *J. Am. Chem. Soc.* **2003**, *125*, 1796-1804; [b] F. Scholz, D. Himmel, L. Eisele, W. Unkrig, I. Krossing, *Angew. Chem. Int. Ed.* **2014**, *53*, 1689-1692.

[3] M. Hadzic, B. Braïda, F. Volatron, *Org. Lett.* **2011**, *13*, 1960-1963.

[4] [a] T. Birchall, A. N. Bourns, R. J. Gillespie, *Can. J. Chem.* **1964**, *42*, 1433–1439; [b] R. W. Alder, F. J. Taylor, *J. Chem. Soc. B* **1970**, 845–848.

[5] G. A. Olah, Y. K. Mo, *J. Org. Chem.* **1973**, *38*, 353-366.

[6] [a] G. A. Olah, Y. K. Mo, *J. Am. Chem. Soc.* **1972**, *94*, 5341-5349; [b] R. F. Childs, B. D. Paddington, *Can. J. Chem.* **1974**, *52*, 3303–3312; [c] J. C. Jacquesy, J. M. Coustard, M. P. Jouannetaud, *Top. Catal.* **1998**, *6*, 1–7.

[7] [a] A. J. Kresge, G. W. Barry, K. R. Charles, Y. Chiang, *J. Am. Chem. Soc.* **1962**, *84*, 4343–4344; [b] A. J. Kresge, H. J. Chen, L. E. Hakka, J. E. Kouba, *J. Am. Chem. Soc.* **1971**, *93*, 6174-6181.

[8] C. M. Mayhan, H. Kumari, J. M. Maddalena, G. N. Borgmeyer, C. A. Deakyne, *J. Coord. Chem.* **2021**, *74*, 61-73.

[9] C. H. Gorbitz, M. Kaboli, M. L. Read, K. Vestli, *Acta Cryst. E* **2008**, *64*, o2023.

[10] A. F. Holleman, E. Wiberg, N. Wiberg, *Lehrbuch der Anorganischen Chemie*, Walter de Gryuter & Co., Berlin, New York**, 2007**.

[11] F. R. Fronczek, *CSD Communications* **2019**.

[12] P. V. R. Schleyer, C. Maerker, A. Dransfeld, H. Jiao, N. J. R. Van Eikema Hommes, *J. Am. Che. Soc.* **1996**, *118*, 6317-6318.

[13] [a] G. W. T. M. J. Frisch, H. B. Schlegel, G. E. Scuseria, , J. R. C. M. A. Robb, G. Scalmani, V. Barone, B. Mennucci, , H. N. G. A. Petersson, M. Caricato, X. Li, H. P. Hratchian, , J. B. A. F. Izmaylov, G. Zheng, J. L. Sonnenberg, M. Hada, , K. T. M. Ehara, R. Fukuda, J. Hasegawa, M. Ishida, T. Nakajima, , O. K. Y. Honda, H. Nakai, T. Vreven, J. A. Montgomery, Jr., , F. O. J. E. Peralta, M. Bearpark, J. J. Heyd, E. Brothers, , V. N. S. K. N. Kudin, R. Kobayashi, J. Normand, , A. R. K. Raghavachari, J. C. Burant, S. S. Iyengar, J. Tomasi, , N. R. M. Cossi, J. M. Millam, M. Klene, J. E. Knox, J. B. Cross, , C. A. V. Bakken, J. Jaramillo, R. Gomperts, R. E. Stratmann, , A. J. A. O. Yazyev, R. Cammi, C. Pomelli, J. W. Ochterski, , K. M. R. L. Martin, V. G. Zakrzewski, G. A. Voth, , J. J. D. P. Salvador, S. Dapprich, A. D. Daniels, , J. B. F. O. Farkas, J. V. Ortiz, J. Cioslowski, D. J. Fox, *Gaussian, Inc.* **2009**, *Wallingford CT*; [b] G. W. T. M. J. Frisch, H. B. Schlegel, G. E. Scuseria, , J. R. C. M. A. Robb, G. Scalmani, V. Barone, , H. N. G. A. Petersson, X. Li, M. Caricato, A. V. Marenich, , B. G. J. J. Bloino, R. Gomperts, B. Mennucci, H. P. Hratchian, , A. F. I. J. V. Ortiz, J. L. Sonnenberg, D. Williams-Young, , F. L. F. Ding, F. Egidi, J. Goings, B. Peng, A. Petrone, , D. R. T. Henderson, V. G. Zakrzewski, J. Gao, N. Rega, , W. L. G. Zheng, M. Hada, M. Ehara, K. Toyota, R. Fukuda, , M. I. J. Hasegawa, T. Nakajima, Y. Honda, O. Kitao, H. Nakai, , K. T. T. Vreven, J. A. Montgomery, Jr., J. E. Peralta, , M. J. B. F. Ogliaro, J. J. Heyd, E. N. Brothers, K. N. Kudin, , T. A. K. V. N. Staroverov, R. Kobayashi, J. Normand, , A. P. R. K. Raghavachari, J. C. Burant, S. S. Iyengar, , M. C. J. Tomasi, J. M. Millam, M. Klene, C. Adamo, R. Cammi, , R. L. M. J. W. Ochterski, K. Morokuma, O. Farkas, , a. D. J. F. J. B. Foresman, *Gaussian, Inc.* **2016**, *Wallingford CT*.

[14] D. Stuart, S. D. Wetmore, M. Gerken, *Angew. Chem. Int Ed.* **2017**, *56*, 16380-16384.

[15] T. S. Sorensen, *J. Am. Chem. Soc.* **1969**, *91*, 6398-6403.

Entry for the Table of Contents

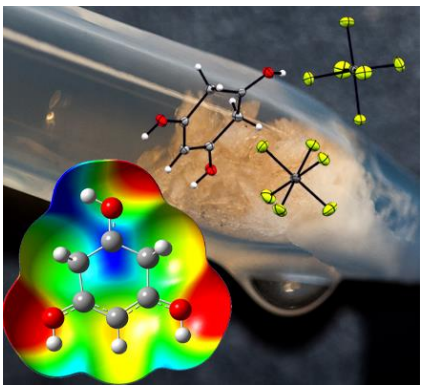

1,3,5-trihydroxy- and 1,3,5-trimethoxybenzene were mono- and diprotonated in superacidic media. Arenium monocations and cyclohexenyl carboxonium dications were isolated, the latter for the first time. The experimental data, namely vibrational and NMR spectroscopy together with single crystal X-ray diffraction, are expanded by quantum chemical calculations.

RESEARCH ARTICLE

Arenium, oxononium and arenium oxonium cations – Protonation of 1,2,3- and 1,2,4-trihydroxybenzene

A. Nitzer,[a] M. Cornelsen,[a] C. Jessen,[a] R. Haiges,[b] K. O. Christe[b] and A. J. Kornath[a]

[a] A. Nitzer, M. Cornelsen, C. Jessen, Prof. Dr. A. Kornath
Department of Chemistry and Pharmacy
LMU Munich
Butenandtstrasse 5-13, 81377 Munich, Germany
E-mail: alexander.nitzer@cup.uni-muenchen.de, malte.cornelsen@cup.uni-muenchen.de, christoph.jessen@cup.uni-muenchen.de, akoch@cup.uni-muenchen.de

[b] Prof. Dr. R. Haiges, Prof. Dr. K. O. Christe
Loker Hydrocarbon Research Facility
University of Southern California
837 Bloom Walk, Los Angeles CA 90089-1661, USA
E-mail: haiges@usc.edu, kchriste@usc.edu

Supporting information for this article is given via a link at the end of the document.

Abstract: 1,2,3- and 1,2,4-trihydroxybenzene were reacted in various superacidic media. Monoprotonation was observed in pure *a*HF, addition of BF_3, GeF_4, AsF_5 or SbF_5 enabled isolation of synthesized arenium ions. When employing at least two equivalents of AsF_5 or SbF_5 diprotonation of both benzenes was detected, leading to the isolation of salts containing arenium oxonium dications. Characterization was done by vibrational and NMR spectroscopy as well as single crystal X-ray diffraction. To further elucidate on experimental results, quantum chemical calculations are employed. NPA charges and Mapped Electrostatic potentials were computed to evaluate charge distribution.

Introduction

A large variety of arenium ions has been prepared, quite a few were also isolated in solid-state and crystallographically characterized.[1] The resonance structures used to describe the arenium ion, also named Wheland intermediate due to the significance in electrophilic substitution mechanism, do fit the cyclohexadienyl cation. When attaching various substituents to the ring, not only the position of electrophilic attack becomes interesting. Also the respective valence bond structures of the arenium ions deviate from typical cyclohexadienyl character, leading to more energetically stable species.[2]

Gillespie and co-workers protonated phenol and other hydroxybenzenes in a mixture of fluorosulfuric acid and 70% perchloric acid.[3] Phenol itself is protonated at the *para*-position to the hydroxy group. Upon employing HF with 5% SbF_5, being a stronger superacid, *O*-protonation of phenol can be observed at low temperatures.[4] When the solution is warmed up, the equilibrium is shifted towards *C*-protonated phenol. For anisol, in HF/BF_3 an equilibrium between *C*- and *O*-protonated species is observed at –40 °C. In other superacidic media like fluorosulfuric acid, be it with or without SbF_5, only the arenium ion is present. Protonation of the dihydroxybenzenes depends on the substitution pattern, as *C*-protonation occurs for Catechol and Resorcinol, while Hydroquinone is *O*-protonated.[4] Generally, the site of protonation of the (di)hydroxy- and (di)methoxybenzenes is depending on the strength of the superacidic system, *C*-protonation achieved in stronger, *O*-protonation in weaker superacid systems.[4]

The protonation of trihydroxy- and trimethoxybenzenes have been NMR spectroscopically studied in solution.[5] Also, kinetic studies[6] and quantum chemical calculations[7] have been employed to describe the findings. Regardless of substitution pattern, monoprotonation occurs at a ring carbon, leading to arenium ions. The cations are still basic enough, that diprotonation is observed in sufficiently strong superacidic media. We recently reported the mono- and diprotonation of 1,3,5-trihydroxy- and 1,3,5-trimethoxybenzene and isolated the synthesized mono- and dications for the first time.[8] So it was only consequent to investigate the behavior of 1,2,3- and 1,2,4-trihydroxybenzene in superacidic media, in particular isolation of the cations. While the 1,3,5-isomer is double *C*-protonated, the 1,2,3-isomers` second protonation occurs at an oxygen. Olah and co-workers have not observed diprotonation in case of the 1,2,4-isomer, so we wanted to check if not a sufficiently strong superacidic medium could enable that and if *C*- or *O*-protonation would occur.

Results and Discussion

1,2,3-trihydroxybenzene **1** and 1,2,4-trihydroxybenzene **2** were monoprotonated (Equations 1 and 2). Therefore, superacidic mixtures in *a*HF were prepared. When employing at AsF_5 or SbF_5, one equivalent in respect to **1** or **2** was used, BF_3 and GeF_4 were used in excess compared to the starting materials. The superacids were mixed at 0 °C, then frozen to –196 °C so **1** or **2** could be added. After warming up to 0 °C, the samples were stirred until complete solution of the trihydroxybenzenes occurred. The solutions were cooled down to –78 °C and the solvent was removed, leading to precipitation of salts containing **[1+1H]** and **[2+1H]**.

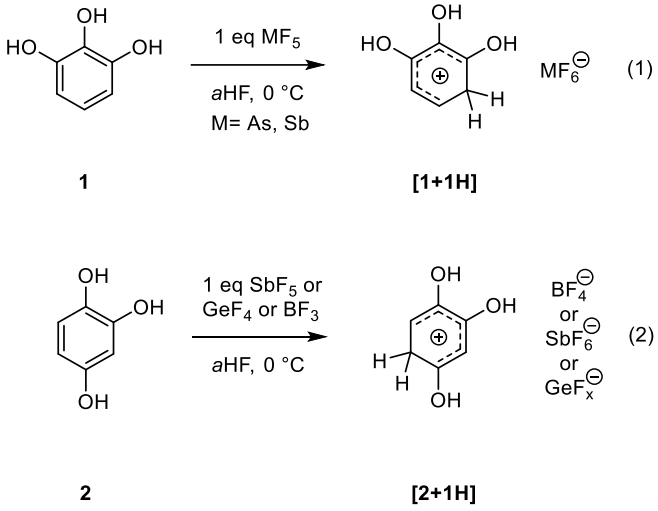

Diprotonation of **1** and **2** was achieved when employing at least two equivalents of AsF_5 or SbF_5 in respect to the starting materials (Equations 3 and 4). The superacids were mixed at 0 °C and then frozen to –196 °C, so that the starting materials could be added. The mixtures were warmed up to –60 °C in case of **1**, –40°C for **2** and stirred. The samples were cooled to –78 °C, the solvent removed and received salts characterized.

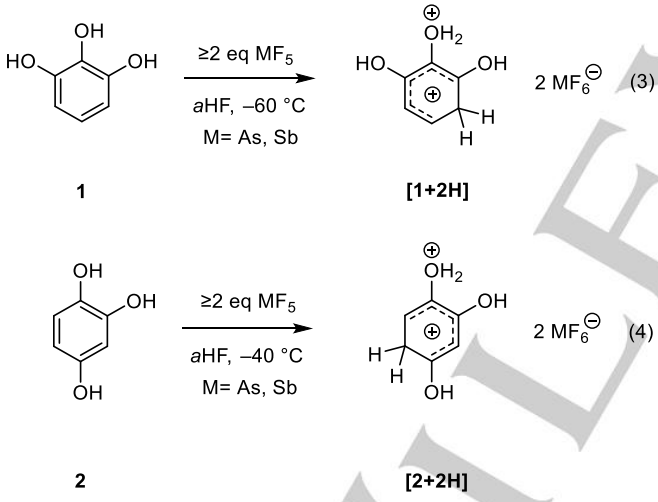

The synthesized salts were characterized by vibrational spectroscopy. Arenium cations are formed by monoprotonation. In case of 1,2,3-trihydroxybenzene, Raman spectroscopy showed the weakening of the ring breathing by protonation as well as the appearance of methylene group, specifically the CH_2 groups' stretching vibrations. 1,2,4-trihydroxybenzene was slightly fluorescent, for the protonated compounds fluorescence was increased, so that Raman spectroscopy was unsuitable for characterization. Therefore IR spectroscopy was used, where the weakening of the ring breathing by monoprotonation was also observed for **2**. NMR spectroscopy showed the resonance of the CH_2 group in both ^1H and ^{13}C NMR for **[1+1H]** and **[2+1H]**.

Diprotonation of 1,2,3- and 1,2,4-trihydroxybenzene results in the formation of arenium oxonium dications. The main difference between mono- and diprotonated species regarding characterization by vibrational spectroscopy is the weakening of the CO bond to the OH_2^+ group. As the stretching vibration of the C–O single bond is combined with other modes and/or rather weak, it is rather unsuitable for differentiation. The ^{13}C NMR spectra of **[1+2H]** and **[2+2H]** on other hand are significantly different compared to those of **[1+1H]** and **[2+1H]**. Also, the hydrogens of the OH_2^+ group are detected by ^1H NMR, in case of **[1+2H]** even in *a*HF as a sharp resonance despite exchange with the solvent. 2D NMR experiments enabled complete assignment of resonances for all species.

X-ray Crystal Structure Determination: [1+1H] and **[1+2H]** were crystallized within the same compound, namely $[(1,2,3\text{-}C_6H_4(OH)_3)(1,2,3\text{-}C_6H_4(OH_2)(OH)_2)][(AsF_6)_3]$. It crystallizes in the orthorhombic space group *P*bca ($Z = 8$). The properties, foremost bond lengths, are compared to those of 1,2,3-trihydroxybenzene. Some crystal structures of **1** are published, of which the one reported by Nangia and co-workers is used for comparison.[9] Selected bonds lengths of **1**, **[1+1H]** and **[1+2H]** are shown in Figure 51.

The CC bonds within the ring of **1** are within the standard deviation of equal length. The three CO bonds are not equisized, the CO bond in position 1 is significantly longer compared to the one in position 3. In **[1+1H]**, the CC bonds to the methylene group are elongated, coming closer to C–C single bonds.[10] One CC bond, which is not connected to the methylene group, is with 1.452(3) Å in **[1+1H]** and 1.444(3) Å in **[1+2H]** longer than expected for arenium ions. In **[1+2H]** one CC bond is with 1.637(4) Å even shorter than in **1**. The CO bonds in position 1 and 3 are shortened by mono- and diprotonation. Contrary, the CO bond in position 2 is slightly elongated in **[1+1H]**, significantly in **[1+2H]**.

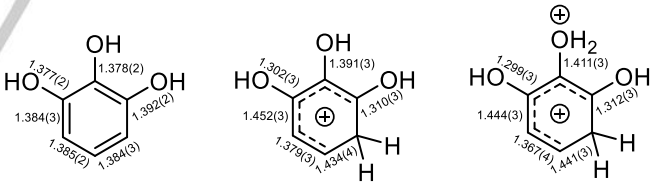

Figure 51. Comparison of bond lengths of **1**, **[1+1H]** and **[1+2H]**, all lengths in Å.

When examining stabilization by resonance, the positive charge may not be located in *meta*-position to the CH_2 group, which is the 2-position. This hydroxy group is then the most basic site, leading to the arenium oxonium dication **[1+2H]**. The CO bond is resembling a typical C–O single bond. All other bonds of the dication are within standard deviation as long as in the monocation. As the ring remains planar, the angles within the cycle do not change significantly compared to the starting material, deviating slightly from the ideal 120°.

As no crystal structure of 1,2,4-trihydroxybenzene was published so far, we recrystallized the powdery starting material from ethyl acetate. Solvent-free $1,2,4\text{-}C_6H_3(OH)_3$ formed as clear brown prisms, which crystallizes in the monoclinic space group *C*2/c ($Z = 8$). **[2+1H]** and **[2+2H]** were crystallized as $[1,2,4\text{-}C_6H_4(OH)_3][BF_4]$, crystallizing in the triclinic space group *P*–1 ($Z = 2$), and $[1,2,4\text{-}C_6H_4(OH_2)(OH)_2][(SbF_6)_2] \cdot 2HF$ in the

monoclinic space group $P2_1$ (Z = 2). Selected bonds lengths are shown in Figure 52.

The CC bonds of **2** are all similarly long, also comparable in length to **1**. The CO bonds are equisized within deviation. In **[2+1H]** the CC bonds to the methylene group become longer in the same order of magnitude compared to **1**. One CC bond, which is not connected to the methylene group quite long compared to other arenium ions with 1.441(3) Å in **[2+1H]** and 1.457(10) Å in **[2+2H]**. The similar observation was made for **1** upon diprotonation. All three CO bonds are decreased in length upon monoprotonation in **1**. The ones at position 2 and 4 the most, the in position only slightly. That CO bond is then connected to the OH_2^+ group in **[2+2H]**, being elongated in a similar fashion compared to **[1+2H]**.

The ring remains planar independent from degree of protonation, the angles within the cycle being close to 120°.

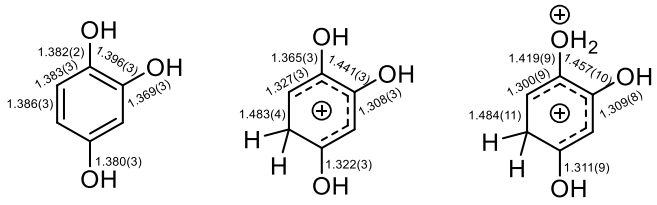

Figure 52. Comparison of bond lengths of **2**, **[2+1H]** and **[2+2H]**, all lengths in Å.

Monoprotonation of **1** and **2** leads to arenium ions, favourable positions of the double bonds are found, the trend amplified by diprotonation (Figure 53).

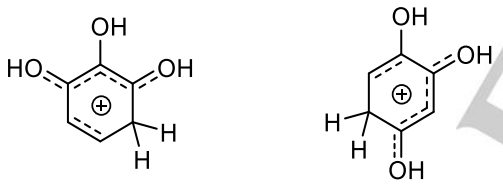

Figure 53. Valence-bond structures for **[1+1H]** and **[2+1H]**.

NMR Spectroscopy: **1** was NMR spectroscopically characterized in SO_2, **2** in DMSO-d_6 and the protonated species in *a*HF. Protonation occurs for both benzenes already in pure *a*HF. The resonances were compared to the data reported by Olah.[5a] The essential ^{13}C NMR data is listed in Table 13, the complete spectra are given in the Supporting Information (Chapter 4). The methylene group is formed by protonation, exhibiting its resonance at 37.1 ppm in **[1+1H]** and 35.5 ppm in **[2+1H]**. The other ^{13}C resonances are deshielded, except C-2 and C-6 for **[1+1H]** and C-1 and C-3 for **[2+1H]**. As shown in Scheme 15, no meaningful resonance can be drawn, where the charge goes in *meta* position to the methylene group. These carbons are therefore not deshielded by monoprotonation.

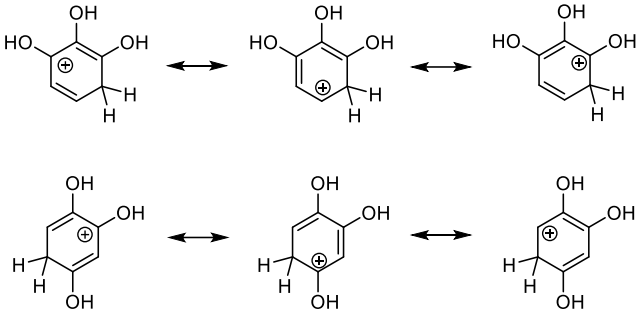

Scheme 15. Selected resonance structures of **[1+1H]** (top) and **[2+1H]** (bottom).

While diprotonation of 1,3,5-trihydroxybenzene takes place at another ring carbon, for **[1+1H]** and **[2+1H]** second protonation occurs at a hydroxyl group. In case of **[1+2H]** the OH_2^+ resonance is found at 10.83 ppm in the ^1H NMR spectrum, although exchange with the solvent is expected to occur even at –60 °C. The hydroxyl groups at which the oxonium group is formed are attached to C-2 for **[1+1H]** and C-1 for **[2+1H]**. These carbons are not deshielded by monoprotonation, so the attached hydroxyl group is more basic than the other two. Incidently, in **[1+1H]** the C2-O2 bond is elongated. In **[2+1H]** the C1-O1 bond is much less shortened than the other C-O bonds. C-2, which is connected to the OH_2^+ group in **[1+2H]**, is shielded by diprotonation. C-3 and C-5 are futher deshielded. Diprotonation of **2** results in a minor shielding of C-2 and deshielding of C-4.

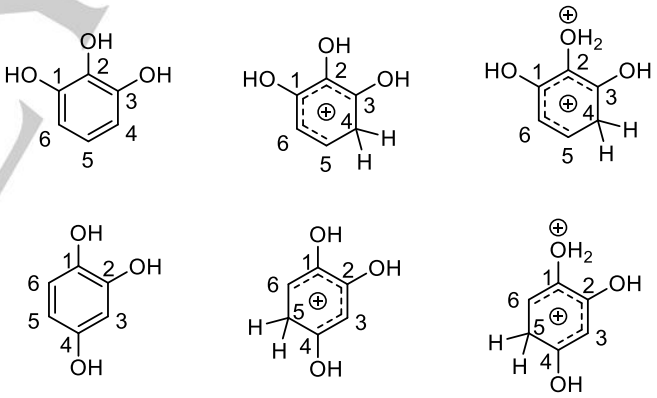

Table 13. NMR shifts of **1**, **2** and their protonated derivatives.[a]

^{13}C	**1**[b]	**[1+1H]**[c]	**[1+2H]**[d]	**2**[e]	**[2+1H]**[f]	**[2+2H]**[g]
C-1	145.9	180.0	180.6	137.7	142.7	142.8
C-2	133.4	131.3	122.8	150.4	183.8	178.0
C-3	145.9	178.6	184.5	103.6	103.1	103.2
C-4	110.2	37.1	38.7	145.8	196.5	199.1
C-5	122.2	149.4	156.3	105.2	35.5	35.6
C-6	110.2	121.9	121.5	116.0	122.7	122.8

[a] All shifts in ppm. [b] In SO_2 at 25 °C. [c] In *a*HF as [AsF_6] species at –20 °C. [d] In *a*HF as [AsF_6] species at –60 °C. [e] In DMSO-d_6 at 26°C. [f] In *a*HF at 26 °C. [g] In *a*HF as [SbF_6] species at –40 °C.

Vibrational Spectroscopy: 1,2,3-trihydroxybenzene has its' ring breathing mode appearing at 713 cm^{-1}. Protonation shifts it to 827 cm^{-1} and decreases its relative intensity. As diprotonation leads to an arenium oxonium species, the main difference is the appearance of a C–O stretching vibration compared to the monoprotonated compound. The C–O stretching vibration is combined with other vibrations, amongst others the CC stretching and CH deformation vibrations, being visible at 1382 cm^{-1} and 1308 cm^{-1} in the hexafluoridoantimonate.

IR spectroscopy had to be employed for vibrational characterization of 1,2,4-trihydroxybenzene (Figure 54), as fluorescence was too intensive in the protonated species, excluding Raman spectroscopy as an analytical method. The ring breathing is too weak to be considered for characterization. The strongest bands of **2** are observed at 1059, 1045 and 1026 cm^{-1}, belonging to combinations of stretching vibrations of the OH and CH groups. Their relative intensity is decreased by monoprotonation. A successful diprotonation of **2** is validated rather indirectly, as the main difference is the overwhelmingly intensive peak of the respective anion, shadowing the peaks of the cation.

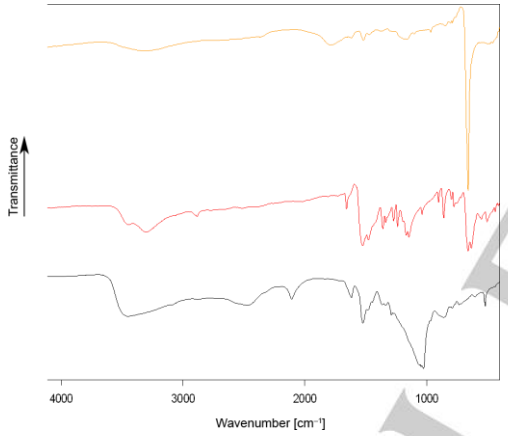

Figure 54. IR spectra of **2**, **[2+1H]**[SbF_6] and **[2+2H]**[$(SbF_6)_2$].

Quantum chemical calculations: The site of protonation(s) were reported correctly by Olah[5a] based on NMR spectroscopy and more recently, the site of first protonation of the 1,3,5- and 1,2,3-trihydroxybenzene was also calculated.[7] Still, our employed DFT calculations sufficiently predict relative energies to exclude the case of various experimentally observable isomers. As diprotonation of **2** has not been achieved until now, different isomers of **[2+2H]** were optimized on DFT/6–311g++(3d2f, 3p2d) level of theory to compare energies (Figure 55). The experimentally observed species is also computed to be the most stable one, the second and third most stable species for **[2+2H]** are also arenium oxonium dications. Second protonation has occurred at the oxygen in position 2 rather than in position 1, that isomer is less stable by 37 kJ/mol, in case of protonation at the oxygen in position 4 that isomer is less stable by 77 kJ/mol. A diarenium species similar to diprotonated 1,3,5-trihydroxybenzene would be the least energetically favourable isomer, by 86 kJ/mol compared to the observed compound.

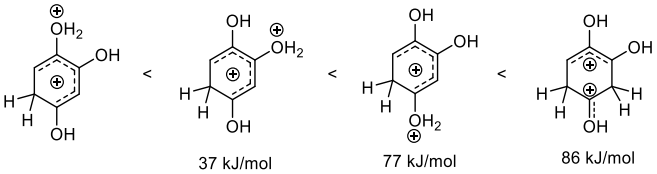

Figure 55. Isomers of **[2+2H]**, sorted by most stable (left) to least stable (right) with energy difference to most stable isomer, calculated on B3LYP/6–311g++(3df,3pd) level of theory.

Aromatic character of the here discussed species was quantified by NICS(0).[11] Calculations for **1**, **2** and their protonated derivatives were done by employing the GIAO method for the optimized structures. All starting materials naturally exhibit aromatic character, their NICS(0) being around –10 ppm. Monoprotonation leads to the non-aromatic Wheland-intermediate, the arenium ion, which has a NICS(0) value close to zero, for **[1+1H]** and **[2+1H]** around –2 ppm. Diprotonation does not significantly change NICS(0) compared to the monoprotonated species. The near constant NICS(0) value can be attributed to a pure oxonium character of the diprotonated compounds, not changing much of the arenium character and thus influencing ring current.

As stated, the charge localization is experimentally observable by ^{13}C NMR spectrosocopy and X-ray crystallography. Mapped Electrostatic Potentials (MEPs) and NPA charges were calculated to further narrow down, which atoms hold the positive charges. The NPA charges of each carbon, where a positive charge may be located due to resonance (Scheme 15), is increased by in **[1+1H]** and **[2+1H]** compared to 1 and 2 respectively (Figure 56, Figure 57). The carbons in meta-position to the methylene group are shielded as observed by ^{13}C NMR, their NPA charge remains constant or is decreased. Formation of the dications, the protonation of the hydroxyl groups, has only a minor effect on the NPA charges.

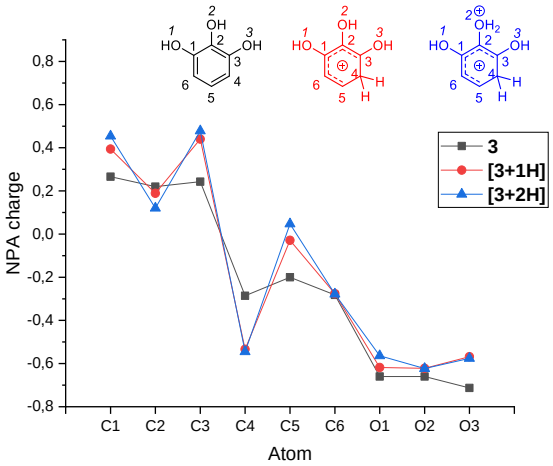

Figure 56. NPA charges of **1**, **[1+1H]** and **[1+2H]**, calculated on B3LYP/6–311g++(3d2f, 3p2d level of theory.

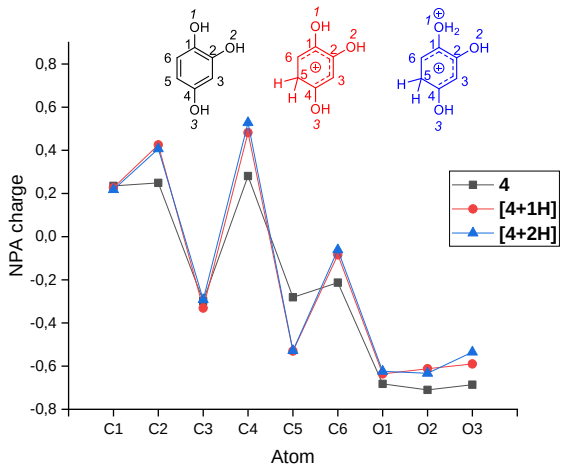

Figure 57. NPA charges of **2**, **[2+1H]** and **[2+2H]**, calculated on B3LYP/6–311g++(3d2f, 3p2d level of theory.

The main difference between mono- and dication is visualized by MEPs of **[1+2H]** and **[2+2H]**. The oxonium character is visible as the protonated hydroxy group is colored in a deep blue, indicating the presence of a positive charge (Figure 58). The other atoms in the dications possess more electron density as indicated by the green and yellow shades, the electron pairs of the unprotonated oxygens are denoted by the red area stretching out.

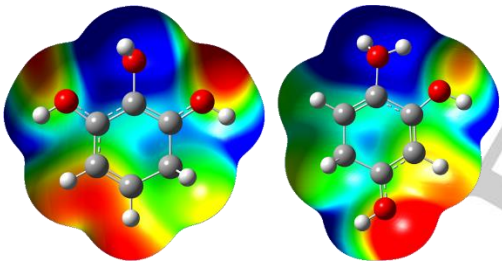

Figure 58. Molecular 0.0004 bohr^{-3} 3D isosurfaces with MEP of **[1+2H]** (0.26 a.u. (red) to 0.32 a.u. (blue)) and **[2+2H]** (0.26 a.u. (red) to 0.32 a.u. (blue)), calculated on B3LYP/6–311g++(3df,3pd) level of theory.

Conclusion

1,2,3- and 1,2,4-trihydroxybenzene were mono- and diprotonated in superacidic media and isolated for the first time. The monocations are arenium ions, which exhibit the predicted cyclohexadienyl character as observed by NMR spectroscopy and single crystal X-ray diffraction. The dications are arenium oxonium dications, where the positive charges in the ring and at the oxonium ring do not influence each other as visualized by MEPs. The monocations form room temperature stable salts with any here employed anion, salts containing any of the two dications are much less stable due to the oxonium character.

Experimental Procedures

Caution! Avoid contact with any of these compounds. Hydrolysis might form HF, which burns skin and causes irreparable damage.

Apparatus and Materials

Standard Schlenk technique with a stainless steel vacuum line was used to perform all reactions. All reactions in superacidic media were carried out in FEP/PFA reactors closed with a stainless steelvalve. HF was dried with F_2 prior to use. Raman spectra were recorded on a Bruker MultiRAM FT-Raman spectrometer with Nd:YAG laser excitation (λ = 1064 nm). For Raman measurements, samples of products were transferred into a cooled glass cell, which were evacuated afterwards. IR spectra were recorded with a Vertex-80V FT-IR spectrometer. Samples were placed on a CsBr single-crystal plate within a cell, which was cooled for the compounds not stable at room temperature. The starting materials were transferred into NMR tubes and measured at room temperature.

NMR spectra at LMU Munich were recorded either on a Jeol ECX400 NMR or a Bruker AV400 NMR. The spectrometers were externally referenced to $CFCl_3$ for ^{19}F and to tetramethylsilane for ^{1}H and ^{13}C NMR spectra. The spectra were recorded inside 4 mm FEP NMR tube inliners. Acetone-d_6 was employed for external shimming when *a*HF or SO_2 was used as solvent for the respective compounds. The starting materials were measured in 9 mm glass NMR tubes. The NMR samples were prepared by redissolving the respective protonated trihydroxybenzene at the designated measuring temperature in *a*HF and transferring the solution into a 4 mm FEP NMR tube inliner. The inliner was then frozen and flame sealed.

At USC Los Angeles either a Varian VNMRS-600 3-Channel NMR Spectrometer, a Varian VNMRS-500 2-Channel NMR Spectrometer or a Varian Mercury 400 2-Channel NMR Spectrometer were employed for NMR spectroscopy.

The low-temperature X-ray diffraction was performed with an Oxford X-Calibur3 equipped with a Kappa CCD detector, operating with Mo-K_α radiation (λ = 0.71073 Å) and a Spellman generator (voltage 50 kV, current 40 mA).

Deposition Numbers 2142684 for **[(1+1H)(1+2H)]**[$(AsF_6)_3$], 2142692 for **2**, 2142685 for **[2+1H]**[BF_4] and 2142686 for **[2+2H]**[$(SbF_6)_2$]·2HF contain the supplementary crystallographic data for this paper. These data are provided free of charge by the joint Cambridge Crystallographic Data Centre and Fachinformationszentrum Karlsruhe Access Structures service www.ccdc.cam.ac.uk/structures.

General Procedure

In a typical experiment, the lewis acid and *a*HF were condensed into a FEP reactor at –196 °C. The mixture was reacted at –40 °C for 15 minutes and frozen to –196 °C. 1,2,3- or 1,2,4-trihydroxybenzene was added under constant N_2-flow. The complete mixture was reacted at before mentioned temperature. The solution was cooled down to –78 °C and the solvent was removed *in vacuo*. Some material of the obtained colorless salts was used for Raman spectroscopy, the rest was redissolved in *a*HF to grow crystals suitable for single crystal X-ray diffraction and transfer material into FEP inliners for NMR spectroscopy.

For all experimental details, see the Supporting Information.

Acknowledgements

We are grateful to the Department of Chemistry and Pharmacy of the Ludwig Maximilians University of Munich, the Deutsche Forschungsgemeinschaft (DFG) and the F-Select GmbH for their financial support. Furthermore, we like to thank Thomas Saal for extensive support during experimentation at USC Los Angeles.

Keywords: Trihydroxybenzenes • Aromaticity • Superacid • Protonation • Quantum chemical Calculations

[1] [a] G. A. Olah, R. H. Schlosberg, R. D. Porter, Y. K. Mo, D. P. Kelly, G. D. Mateescu, *J. Am. Chem. Soc.* **1972**, *94*, 2034-2043; [b] G. A. Olah, R. H. Schlosberg, D. P. Kelly, G. D. Mateescu, *J. Am. Chem. Soc.* **1970**, *92*, 2546-2548; [c] G. A. Olah, J. S. Staral, G. Asencio, G. Liang, D. A. Forsyth, G. D. Mateescu, *J. Am. Chem. Soc.* **1978**, *100*, 6299-6308; [d] C. A. Reed, K.-C. Kim, E. S. Stoyanov, D. Stasko, F. S. Tham, L. J. Mueller, P. D. W. Boyd, *J. Am. Chem. Soc.* **2003**, *125*, 1796-1804; [e] F. Scholz, D. Himmel, L. Eisele, W. Unkrig, I. Krossing, *Angew. Chem. Int. Ed.* **2014**, *53*, 1689-1692.

[2] M. Hadzic, B. Braïda, F. Volatron, *Org. Lett.* **2011**, *13*, 1960-1963.

[3] [a] T. Birchall, A. N. Bourns, R. J. Gillespie, *Can. J. Chem.* **1964**, *42*, 1433–1439; [b] R. W. Alder, F. J. Taylor, *J. Chem. Soc. B* **1970**, 845–848.

[4] G. A. Olah, Y. K. Mo, *J. Org. Chem.* **1973**, *38*, 353-366.

[5] [a] G. A. Olah, Y. K. Mo, *J. Am. Chem. Soc.* **1972**, *94*, 5341-5349; [b] R. F. Childs, B. D. Paddington, *Can. J. Chem.* **1974**, *52*, 3303–3312; [c] J. C. Jacquesy, J. M. Coustard, M. P. Jouannetaud, *Top. Catal.* **1998**, *6*, 1–7.

[6] [a] A. J. Kresge, G. W. Barry, K. R. Charles, Y. Chiang, *J. Am. Chem. Soc.* **1962**, *84*, 4343–4344; [b] A. J. Kresge, H. J. Chen, L. E. Hakka, J. E. Kouba, *J. Am. Chem. Soc.* **1971**, *93*, 6174-6181.

[7] C. M. Mayhan, H. Kumari, J. M. Maddalena, G. N. Borgmeyer, C. A. Deakyne, *J. Coord. Chem.* **2021**, *74*, 61-73.

[8] A. Nitzer, C. Jessen, R. Haiges, K. O. Christe, A. J. Kornath, to be published.

[9] R. Thakuria, S. Cherukuvada, A. Nangia, *Cryst. Growth Des.* **2012**, *12*, 3944-3953.

[10] A. F. Holleman, E. Wiberg, N. Wiberg, *Lehrbuch der Anorganischen Chemie*, Walter de Gryuter & Co., Berlin, New York**, 2007**.

[11] P. V. R. Schleyer, C. Maerker, A. Dransfeld, H. Jiao, N. J. R. Van Eikema Hommes, *J. Am. Chem. Soc.* **1996**, *118*, 6317-6318.

Entry for the Table of Contents

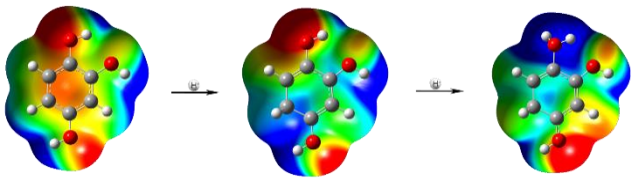

Arenium cation, oxonium cation, why not both? – The protonation of 1,2,3- and 1,2,4-trihydroxybenzene in superacidic media was investigated. The prepared mono- and dications were analyzed in solution by NMR spectroscopy. Characterization in solid-state by vibrational spectroscopy and single crystal X-ray diffraction was combined with quantum chemical calculation to describe charge localization and reactivity.

RESEARCH ARTICLE

Increasing aromaticity by protonation

A. Nitzer, C. Jessen, A. J. Kornath[a]

[a] A. Nitzer, C. Jessen, Prof. Dr. A. Kornath
Department of Chemistry and Pharmacy
LMU Munich
Butenandtstrasse 5–13, 81377 Munich, Germany
E-mail: alexander.nitzer@cup.uni-muenchen.de, christoph.jessen@cup.uni-muenchen.de, akoch@cup.uni-muenchen.de

Supporting information for this article is given via a link at the end of the document.

Abstract: Cyanuric acid was reacted in the superacidic media HF/SbF_5, HF/AsF_5 and HF/GeF_4. The respective mono- and diprotonated species were isolated as $[SbF_6]$, $[AsF_6]$ or $[GeF_6]$ salts. Characterization was achieved by Raman and NMR spectroscopy as well as single crystal X-ray structure determination. Quantum chemical calculations are employed to test for charge localization. NPA charges and MEPs are calculated to evaluate electron distribution. NICS(0) values are computed to quantify aromatic character of the novel compounds. Finally, the causes, why cyanuric acid may not be triprotonated, are discussed.

Introduction

First discovered by Friedrich Wöhler[1] as a product of the thermal decomposition of urea or uric acid, cyanuric acid is a base structure for various compounds with different purposes. For example, cyanuric acid chloride is used in organic syntheses as chlorinating agent, leading to acid chlorides.[2]
Cyanuric acid is present as a keto species, although many studies examine its keto-enol tautomerism (Scheme 16).[3]

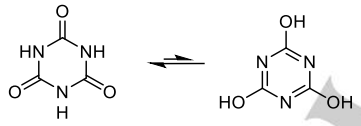

Scheme 16. Keto-enol tautomerism of cyanuric acid.

Although the keto species is more stable by around 130 kJ/mol, the enol form would exhibit aromaticity. All electron pairs of the nitrogen would be in plane, enabling ring current. Planarity, which is essential to aromaticity, is present in the molecule as found in the crystal structure.[4] An extensive study was done to elucidate the possibility of aromaticity by means of ASE and HOMA methods.[5] Showing that the enol form certainly is aromatic. Further calculations were employed for the keto form, but only a slight aromatic character was found to be present. As explanation, frontier molecular orbitals analysis showed two aromatic systems to be present, which oppose each other, decreasing total aromatic character.[5]
Considering the keto-enol tautomerism of cyanuric acid, our question was, if we could induce this kind of effect on the keto form by protonation at the carbonyl group(s) of cyanuric acid. Protonation of ketones[6] leads to the respective protonated species, which can be described as an oxonium or hydroxycarbenium ion (Scheme 17).

Scheme 17. Resonance structures for protonated ketones.

With the respective formation of protonated cyanuric acid, resonance stabilization by the adjacent nitrogen lone pairs is excited. Upon triprotonation, resonance stabilization should lead to a species resembling the enol form and keto-enol tautomerism would simply no longer be possible (Scheme 18). The trication would be aromatic like the enol form of cyanuric acid.

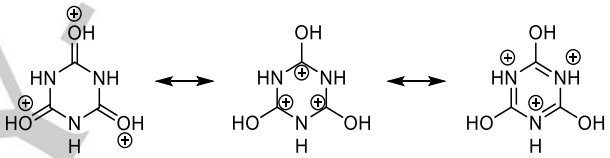

Scheme 18. Resonance structures of triprotonated cyanuric acid.

Results and Discussion

The superacidic mixtures HF/AsF_5, HF/SbF_5 and HF/GeF_4 were prepared by mixing the respective lewis acids with anhydrous hydrogen fluoride (*a*HF) at –40 °C. The mixtures were then frozen to –196 °C and cyanuric acid was added under N_2-flow to the superacid. The mixtures were allowed to warm to 0 °C and vigorously stirred until complete solution was achieved. If one equivalent of AsF_5 or SbF_5 in respect to cyanuric acid was used, monoprotonation of the species was achieved (Equation 1). When employing the superacidic system HF/GeF_4 in any stoichiometric amount of the lewis acid, monoprotonation of cyanuric acid was also enabled.

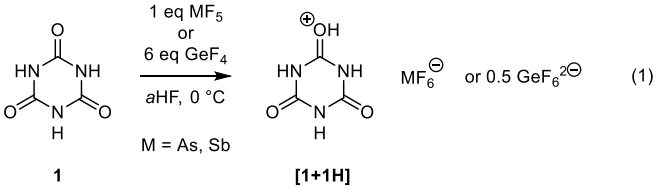

1 **[1+1H]** (1)

By employing at least two equivalents of SbF_5 or AsF_5 in respect to cyanuric acid, diprotonation of cyanuric acid was observed (Equation 2).

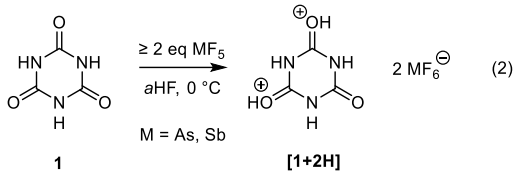

The mixtures were cooled down to –78 °C and the solvent was slowly removed *in vacuo*. Mono- and diprotonated salts of cyanuric acid were all room-temperature stable, colorless solids. Low-temperature Raman spectroscopy showed a shift of the C=O stretching vibrations for the monoprotonated species, visible as a broadening of the lines with the formation of two close lines emerging from the main one. Diprotonation leads to a distinctly visible shift of the CO stretching vibrations, as two separable lines are detectable. Triprotonation at 0°C or –78°C as reaction temperature was not observed, even with more than eightfold excess of SbF_5. NMR data was gathered only for the diprotonated species in *a*HF. All three synthesized salts containing **[1+1H]** are not sufficiently soluble in *a*HF or SO_2.

X-ray Crystal Structures: Recrystallization from *a*HF led to the isolation of **[1+1H]**[SbF_6], **[(1+1H)$_2$]**[GeF_6] and **[1+2H]**[$(SbF_6)_2$] · HF as determined by single crystal X-ray diffraction. As the deviations in bond length and angles for **[1+1H]** are the smallest for the hexafluoridogermanate, that data are used in the following discussion. A comparison of bond lengths between the [GeF_6] and [SbF_6] species as well as extensive crystallographic data are listed in the Supporting Information (Chapter 3). To summarize, the two cations differ not significantly regarding bond lengths and angles.

A crystal structure of cyanuric acid was reported by Verschoor in 1964[4] and in 1971.[7] It has to be noted, that the molecule is no perfect, symmetric hexagon. The low temperature crystal structure shows, that the angles within the ring vary from 115.30(13)° to 124.79(10)°. The C-N bonds are not of equal length, as one bond is with 1.347(1) Å shorter than the other two with 1.372(1) Å and 1.370(1) Å. Two different types of hydrogen bonds are found on **1**, further decreasing symmetry. The molecule is thus better described by C_{2v} symmetry contrary to D_{3h}.

[(1+1H)$_2$][GeF_6] · 4HF crystallizes in the triclinic space group *P*-1 (*Z* = 1), the cation found by X-ray diffraction is depicted in Figure 59. Distortion is slightly increased compared to **1**, the smallest angle N2-C2-N1 being 114.2(2)° and the largest angle C3-N2-C2 being 125.5(2)°. Upon protonation, the C=O(H) bond is elongated from 1.217(2) Å in **1** to 1.274(2) Å. The adjacent C-N bonds, C1-N1 and C1-N3, are 1.331(2) Å and 1.336(3) Å long. In case for C1-N1, the distance is decreased compared to a CN distance of 1.347(1) Å in cyanuric acid. The C2-N2 and C3-N2 distances amounting to 1.374(3) Å and 1.367(3) Å are within deviations of equal length compared to 1.370(1) Å in **1**. The longest CN bonds, C2-N1 and C3-N3 are with 1.388(3) Å longer than the longest CN distance in **1**. The unprotonated C=O bonds are with 1.210(2) Å and 1.213(2) Å shortened compared to 1.223(1) Å in **1**. Overall, the divergence of the ring from an ideal hexagon is greater in **[1+1H]** compared to **1**, as the difference between longest and shortest CN bond is increased.

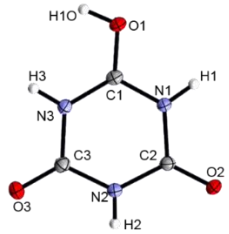

Figure 59. [1+1H] from the asymmetric unit of [$(C_3N_3H_3O_2(OH))_2$][GeF_6] · 4HF, view along *b*. Displacement ellipsoids at 50% probability.

[1+2H][$(SbF_6)_2$] · HF crystallizes in the monoclinic space group $P2_1$ (*Z* = 4) (Figure 60). The asymmetric unit contains two independent cations. The complete list of bond distances and angles is listed in the SI (Chapter 3.3), but as the cations are not significantly different, for clarity only bond lengths and angles of one cation are taken discussed here. Distortion from an ideal hexagon is still present, the smallest angle N1-C1-N2 being 112.2(6)° and the largest being 124.6(6)°. Both protonated C=O bonds are with 1.266(9) and 1.268(9) Å of similar length compared to the protonated C=O bond in **[1+1H]**. With a distance of 1.182(9) Å, the unprotonated C=O bond is only slightly shorter compared to the ones in **[1+1H]**. The C-N bonds adjacent to the unprotonated CO moiety are with distances of C1-N1 1.398(9) Å and C1-N2 1.406(10) Å slightly longer than the longest C-N bonds in **1** and **[1+1H]**. The respectively adjoining C-N bonds C1-N3 and C2-C2 are 1.322(10) Å and 1.324(9) Å long, shorter than C1-N1 and C1-N2. The distances C2-N3 and C3-N3 are with 1.349(10) Å and 1.356(9) Å in length between the other C-N bond lengths.

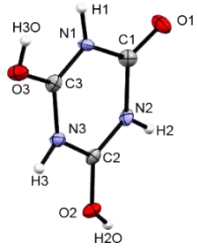

Figure 60. One cation of [$C_3N_3H_3O(OH)_2$][$(SbF_6)_2$] · HF, view along *b*. Displacement ellipsoids at 50% probability.

An overview of all bond lengths as well as selected angles of **1**, **[1+1H]** and **[1+2H]** is given in Figure 61. While in **1** all C-N bonds have the same length within deviations, in **[1+1H]** those CN bonds close to the COH^+ moiety are shortened. The adjacently located CN bonds in **[1+1H]** are elongated. In **[1+2H]**, all CN bonds close or in between the COH^+ moieties are at least slightly decresed in length. Those at the unprotonated CO group are elongated. When comparing to monoprotonated urea,[8] the C-N bonds are even shorter in [$H_2NC(OH)NH_2$] with 1.321(1) and 1.313(1) Å, while the C-O bond is with 1.316(1) Å quite longer. The bonding nature in protonated urea thus seems to be quite different to mono- and diprotonated cyanuric acid, disfavouring further comparison. The longest C-N bonds of **1** are between a formal C-N single and C=N double bond, although in length closer to the first.[9] With protonation, CN distances of the shorter CN bonds in **[1+1H]** and **[1+2H]** do come closer to C=N double bonds, while the longest ones more resemble single bonds.

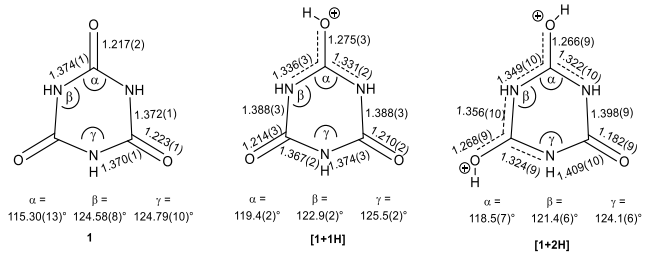

Figure 61. Overview of selected bond lengths for **1**, **[1+1H]** and **[1+2H]** in Å.

Raman Spectra: For a clear overview and discussion only the lines observed in the hexafluoridoantimonates of **[1+1H]** and **[1+2H]** are summarized in Table 14. Assignment is done with calculated frequencies of quantum-chemically optimized structures on DFT, B3LYP/6–311g++(3d2f,3p2d) level of theory. Protonation of cyanuric acid is illustrated by the shift of the CO stretching vibrations. The symmetric and antisymmetric stretching modes of the C-O bonds are situated closely together at 1727 and 1688 cm^{-1} in **1**. In **[1+1H]** the stretching mode assigned to the protonated CO group is slightly redshifted by 15 cm^{-1} compared to **1**. The CO stretching mode assigned to the unprotonated carbonyl groups is blueshifted by 17 cm^{-1}. The protonated C=O bond is weakened, the unprotonated ones are strengthened. The hydrogen bonding already leads to deformation in **1**, suggesting C_{2v} symmetry compared to D_{3h}, as seen in the crystal structure.[7] In **[1+2H]** even more hydrogen bonds at the CO and the $CO(H)^+$ groups are present than in **1** or **[1+1H]**. Consequently, the CO stretching modes are different for each cation. In case of **[1+2H]** even two independent cations are present in the asymmetric unit, enabling more different CO stretching modes than are expected. These are observed from 1688 to 1832 cm^{-1}. As the CO stretching modes are highly depending on the hydrogen bonding in the salts, another way of comprehending the protonation of cyanuric acid by Raman spectroscopy had to be found. The CN bonds are mostly unaffected by the strong hydrogen bonds, so their stretching vibration modes were investigated. A single CN stretching mode is observed at 1419 cm^{-1} in **1**. Two modes are expected in **[1+1H]**. One line is observed at 1515 cm^{-1}, a blueshift of 96 cm^{-1} compared to **1**. It is assigned to the stretching mode of the shortened, strengthened C-N bonds. The other mode is computed to be at 1194 cm^{-1}, belonging to the stretching mode of the elongated, weakened C-N bonds. The latter mode is not found in the spectra, it was also computed to be very weak regarding intensity. The divergence of the modes of the C-N stretching vibration is increased in **[1+2H]**. One stretching mode which is assigned to the strengthened C-N bonds appears at 1688 cm^{-1}, being combined with as CO stretching mode. The mode assigned to the stretching vibrations of the weakened C-N bonds is combined with an OH deformation, appearing at 1094 cm^{-1}. The ring breathing vibration exhibits a slight blueshift of 9 cm^{-1} by monoprotonation and an additional 8 cm^{-1} by diprotonation (Table 14). The complete list of vibrational frequencies, including salts containing the hexafluoridogermanates and hexafluoridoarsenates, together with their assignments are given in the Supporting Information (Chapter 2).

Table 14. Selected experimental Raman frequencies [cm^{-1}] of **1**, **[1+1H]**, **[1+2H]** and assignments based on respective calculated vibrational frequencies [cm^{-1}].[a]

1	**[1+1H]**[SbF_6]	**[1+2H]**[$(SbF_6)_2$]	Assignment[a]
		1832(32)	v (CO)
		1805(22)	
	1742(57)	1786(20)	
		1764(52)	
1727(37)	1710(15)		
1688(2)		1688(17)	v (CO(H)) + v (CN)
702(100)	711(73)	717(26)	ring breathing
		1688(17)	v (CO(H)) + v (CN)
1419(4)	1515(5)		v (CN)
		1094(28)	v (CN) + δ (OH)

[a] Calculated on B3LYP/6–311g++(3d2f, 3p2d) level of theory. Raman intensity in $Å^4/u$.

NMR spectroscopy: **1** and **[1+2H]** were NMR spectroscopically characterized in *a*HF. For **[1+2H]** *O*-Protonation becomes apparent by ^1H NMR, as the diprotonated species displays a signal at 8.37 ppm, which is assigned to the oxonium hydrogens. The ^{13}C and ^{14}N NMR data show a slight shift of resonances by protonation. The ^{13}C nuclei are shifted by around 2.5 ppm downfield, all carbons being magnetically equivalent. The ^{14}N nuclei exhibits a shift downfield by around 6.5 ppm, which is rather small due to the great range of ^{14}N NMR shifts. Also in both **1** and **[1+2H]** broad peaks are observed, which are inherent to low-symmetric environment of the ^{14}N nuclei. Still, this excludes *N*-protonation to be existent at least in solution, as otherwise N-H coupling would be observable. A complete list of resonances together with the spectra is given in the Supporting Information (Chapter 4).

Quantum Chemical Calculations: Quantum chemical calculations were carried out on DFT, B3LYP/6–311g++(3d2f, 3p2d) level of theory to support vibrational assignment. While the CO stretching modes are heavily influenced by hydrogen bonding in the crystal, amongst other things the CN stretching modes are mostly unaffected by solid states effects. In general the predicted frequencies of the computed structure fit the experimental data. The full list of parameters is given in the Supporting Information (Chapter 5).

For assessment of aromaticity NICS(0) value calculations were employed.[10] **1** is with a NICS(0) –2.43 ppm only slightly aromatic. The triol species has a NICS(0) of –5.81 ppm, thus being aromatic. For **[1+1H]** the NICS(0) is –2.44 ppm, for **[1+2H]** it amounts to –2.55 ppm. The decrease in NICS(0), which is an increase in aromatic character, is minimal for these two species. For **[1+3H]**, the NICS(0) drops to –3.62 ppm. A significant increase in aromatic character would occur only upon triprotonation. Still, it is only a 35% increase in aromaticity compared to the triol species

of **1**. X-ray data is considered to find the cause why aromaticity is not drastically increased in **[1+1H]** and **[1+2H]**. Conjugation of all bonds as well as same size of all angles within the ring is needed. This is not present in **[1+1H]** and **[1+2H]**. X-ray data shows for both cations, that some C-N bonds are shortened, others are elongated. For a perfectly conjugated system all bonds within the ring have to be of equal length. In the case of cyanuric acid that would mean a general decrease of all C-N bonds by monoprotonation. Diprotonation should further shorten the C-N bonds. Each angle should amount to 120° in a symmetric hexagon. This is not present in **1**, **[1+1H]** or **[1+2H]**. Only for **[1+3H]** conjugation over the whole ring would arise. The C-N bonds become equally long, shorter than in **1**, thus aromatic character is increased.

NPA charges and Mapped Electrostatic Potentials (MEPs) are computed to understand the nature of charge distribution. The MEPs together with selected NPA charges of **1**, **[1+1H]**, **[1+2H]** as well as **[1+3H]** are visualized in Figure 62. In **1** the blue colour in the middle of the ring shows an electron-hole to be present. The presence of the lone pairs of the oxygen atoms is observable as red zones. The carbon and nitrogen atoms are highlighted in green.

The blue area in the MEP of **[1+1H]** denoting few electron density is not limited to the ring center as it was observed in **1**. It stretches to the carbon and even to the oxygen of the protonated CO group. The NPA charge of that carbon is increased. Denotable by increased NPA charge and the colour change from green to light blue, the neighboring nitrogens do become more positively charged compared to **1.**

In the MEP of **[1+2H]** the blue electron sparse area is more restricted to the ring center, stretching only faintly to the two carbons of the protonated CO groups. All nitrogens have similar electron density, denoted by the green to light blue colour. The NPA charge of all nitrogen atoms is increased compared to **1**. The lone pairs of all oxygens are deeply red coloured, denoting zones of higher electron density, for the unprotonated oxygen in a greater area. The NPA charge of the single unprotonated oxygen is at –0.344, much higher than in **[1+1H]**. This might explain why cyanuric acid cannot be triprotonated. The oxygen O3, which is the only remaining protonable site, is simply not basic enough. In **[1+3H]** the deep blue area expands from the central area, enveloping all three carbon atoms. The oxygens and nitrogens are not part of the blue area, denoting more electron density to be present at these atoms compared to the carbon atoms.

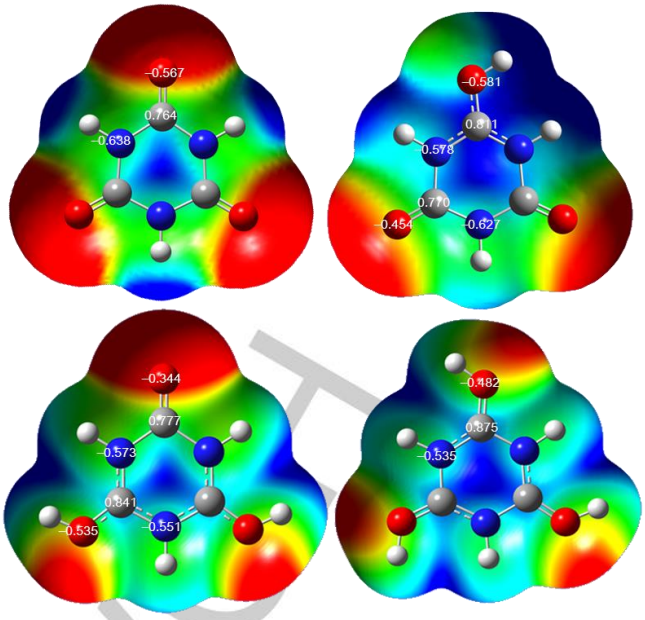

Figure 62. Molecular 0.0004 bohr^{-3} 3D isosurfaces with mapped electrostatic potential of **1**[a] (top left), **[1+1H]**[b] (top right), **[1+2H]**[c] (bottom left) and **[1+3H]**[d] (bottom right) (color scale ranging from [a] 0.00 a.u. [red] to 0.05 a.u. [blue]; [b] 0.1 a.u. [red] to 0.2 a.u. [blue]); [c] 0.28 a.u. [red] to 0.37 a.u. [blue]; [d] 0.40 a.u. [red] to 0.52 a.u. [blue]).

Conclusion

Cyanuric acid was successfully mono- and diprotonated and its salts characterized by Raman and NMR spectroscopy as well as single crystal X-ray diffraction of selected salts. With the support of quantum-chemical calculations, the aromatic character and charge stabilization were evaluated. The experimental data, foremost X-ray crystallography, show an increased asymmetry of the mono- and dication compared to cyanuric acid. Mono- or diprotonation increases conjugation of the C-N bonds, but not in the whole ring. Only triprotonation would have enabled resonance through the ring, but we showed that the remaining unprotonated oxygen of **[1+2H]** is not basic enough.

Experimental Procedures

Caution! Avoid contact with any of these compounds. Hydrolysis might form HF, which burns skin and causes irreparable damage.

Apparatus and Materials

Standard Schlenk technique with a stainless steel vacuum line was used to perform all reactions. All reactions in superacidic media were carried out in FEP/PFA reactors closed with a stainless steelvalve. HF was dried with F_2 prior to use. Raman spectra were recorded on a Bruker MultiRAM FT-Raman spectrometer with Nd:YAG laser excitation (λ = 1064 nm). For Raman measurements, samples of products were transferred into a cooled glass cell, which were evacuated afterwards. The starting materials were transferred into NMR tubes and measured at room temperature. NMR spectra were recorded either on a Jeol ECX400 NMR or a Bruker AV400 NMR instrument. The spectrometers were externally referenced to $CFCl_3$ for ^{19}F, CH_3NO_2 for ^{14}N and to tetramethylsilane for ^{1}H and ^{13}C NMR

spectra. The spectra were recorded inside 4 mm FEP NMR tube inliners. Acetone-d_6 was employed for external shimming when *a*HF was used as solvent for the respective compounds. The NMR samples were prepared by (re-)dissolving the respective compound at the designated measuring temperature in *a*HF and transferring the solution into a 4 mm FEP NMR tube inliner. The inliner was then frozen and flame sealed. The low-temperature X-ray diffraction was performed with an Oxford X-Calibur3 equipped with a Kappa CCD detector, operating with Mo-K_α radiation (λ = 0.71073 Å) and a Spellman generator (voltage 50 kV, current 40 mA).

Deposition Numbers 2072529 for **[1+1H]**[SbF_6], 2072530 for **[(1+1H)$_2$]**[GeF_6]·4HF and 2072531 for **[1+2H]**[$(SbF_6)_2$]·HF contain the supplementary crystallographic data for this paper. These data are provided free of charge by the joint Cambridge Crystallographic Data Centre and Fachinformationszentrum Karlsruhe Access Structures service www.ccdc.cam.ac.uk/structures.

General Procedure

In a typical experiment, the lewis acid and *a*HF were condensed into a FEP reactor at –196 °C. The mixture was reacted at –40 °C for 15 minutes and frozen to –196 °C. Cyanuric acid (~0.5–3.0 mmol) was added under constant N_2-flow. The complete mixture was reacted at before mentioned temperature. The solution was cooled down to –78 °C and the solvent was removed *in vacuo*. Some material of the obtained colorless salts was used for Raman spectroscopy, the rest was redissolved in *a*HF. A part of the solution was transferred into a FEP NMR tube, the rest was used to grow crystals suitable for single crystal X-ray diffraction.

For all experimental details, see the Supporting Information.

Acknowledgements

We are grateful to the Department of Chemistry and Pharmacy of the Ludwig Maximilians University of Munich, the Deutsche Forschungsgemeinschaft (DFG) and the F-Select GmbH for their financial support.

Keywords: Aromaticity • Cyanuric acid • Keto enol tautomerism • Protonation • Superacids • Quantum chemical calculations

[1] F. Wöhler, *Ann. Phys. (Leipzig)* **1829**, *15*, 619-630.
[2] K. Venkataraman, D. R. Wagle, *Tetrahedron Lett.* **1979**, *20*, 3037-3040.
[3] [a] A. Zabardasti, *Chem heterocycl. Comp.* **2007**, *43*, 1344-1346; [b] X. Liang, X. Pu, H. Zhou, N.-B. Wong, A. Tian, *J. of Mol. Struct. THEOCHEM* **2007**, *816*, 125-136.
[4] G. C. Verschoor, *Nature* **1964**, *202*, 1206-1207.
[5] L. Pérez-Manríquez, A. Cabrera, L. E. Sansores, R. Salcedo, *J. Mol. Model.* **2011**, *17*, 1311-1315.
[6] D. Stuart, S. D. Wetmore, M. Gerken, *Angew. Chem. Int. Ed.* **2017**, *56*, 16380-16384.
[7] E. Keulen, G. C . Verschoor, *Acta Cryst.* **1971**, *27*, 134-145.
[8] J. Axhausen, PhD thesis, LMU Munich, **2013**.
[9] A. F. Hollleman, E. Wiberg, N. Wiberg, *Lehrbuch der Anorganischen Chemie*, Walter de Gryuter & Co., Berlin, New York, **2007**.
[10] P. V. R. Schleyer, C. Maerker, A. Dransfeld, H. Jiao, N. J. R. Van Eikema Hommes, *J. Am. Chem. Soc.* **1996**, *1A18*, 6317-6318.
[11] I. Reva, *Spectrochim. Acta A* **2015**, *151*, 232-236.

Entry for the Table of Contents

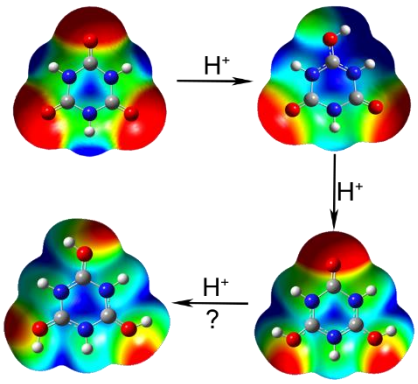

Protonation of cyanuric acid was accomplished in superacidic media. The salts were characterized by vibrational and NMR spectroscopy as well as single crystal X-ray crystallography. The stabilization of positive charge is examined by comparing experimental results to quantum chemical calculations including NPA charges and Mapped Electrostatic Potentials.

RESEARCH ARTICLE

N, C, O – distribution of charge in protonated urazole

A. Nitzer, C. Jessen and A. J. Kornath*[a]

[a] A. Nitzer, C. Jessen, Prof. Dr. A. Kornath
Department of Chemistry and Pharmacy
LMU Munich
Butenandtstrasse 5–13, 81377 Munich, Germany
E-mail: alexander.nitzer@cup.uni-muenchen.de, christoph.jessen@cup.uni-muenchen.de, akoch@cup.uni-muenchen.de

Supporting information for this article is given via a link at the end of the document.

Abstract: Urazol was reacted in various superacidic media. Its` mono- and diprotonated species were isolated and characterized by Raman and NMR spectroscopy as well as single crystal X-ray structure determination. Quantum chemical calculations are employed to characterize charge localization with Mapped Electrostatic Potentials and NPA charges. NICS(0) is calculated to evaluate aromatic character of urazole and its` cations. The results are used to compare the protonation of urazole to that of parabanic acid.

Introduction

Urazole (1,2,4-triazolidine-3,5-dione) is a key component in organic chemistry, a variety of compounds can be prepared from its` host compound 1,2,4-triazole.[1] Applications of the derivatives include usage as herbicides, polymer precursors or pharmaceuticals. The high polarity together with its aromatic character are emphasized, the latter is caused by the inclusion of a nitrogen lone pair into aromatic system. Infrared spectra of 1,2,4-triazole and its` derivatives thus show bands typical for aromatic compounds. As the compound contain a high percentage of nitrogen, of several derivatives heats of combustion have been studied.[1] More recently urazole and its derivative urazine, which has an amino group instead of a hydrogen attached at its` 4-position, were examined as a potential energetic material.[2] With either modification of the 4-position of urazine and/or formation of salts containing suitable counterions, desirable energetic compounds are synthesizable.

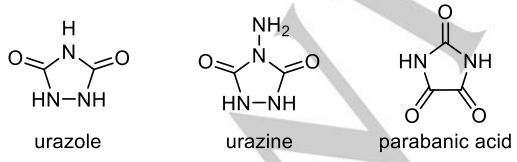

Figure 63. Overview of discussed compounds.

While anions of urazole are widely present, as it is a weak monoprotic acid, cations were not reported so far. The nitrogens are rather basic, the protonation of one of them could hinder aromatic character. Contrary, protonation at an oxygen would enable resonance stabilization of the formed carbocation. As the protonation of parabanic acid was recently reported by our group,[3] comparison is apt. Both being five-membered, heterocyclic rings, the difference is the exchange of a CO group for an NH moiety in urazole. Diprotonation of parabanic acid leads to a vicinal 1,2-dication, both protonations occurring at the neighboring CO groups. As from urazole, a 1,3-dication could be formed by diprotonation, the stabilization of charge should lead to an increased participation of the nitrogen lone pairs into the π-system.

Results and Discussion

Monoprotonation of urazole was carried out (Equation 1). Anhydrous hydrogen fluoride (*a*HF) was first mixed with one equivalent of antimony pentafluoride or four equivalents of boron trifluoride, in respect to urazole **1**, at –40 °C. The superacids were then frozen to –196 °C and urazole was added under N_2-flow. Reacting at 0 °C, clear solutions were formed. Cooling down to –78 °C and removing the solvent led to the formation of colorless salts containing **[1+1H]**, which were stable up to room temperature.

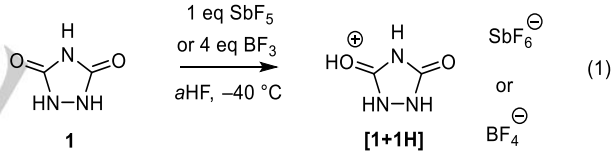

(1)

Diprotonation of **2** was performed (Equation 2). A mixture of *a*HF with at least two equivalents of antimony or arsenic pentafluoride or three equivalents of germanic tetrafluoride was prepared. The superacids were frozen to –196 °C and urazole added under N_2-airstream. In case of HF/SbF_5 and HF/AsF_5, the mixtures then allowed to warm to 0 °C, for HF/GeF_4 to –40 °C. Following complete solution of urazole, the samples were cooled down to –78 °C and the solvent was removed. Colorless salts containing **[1+2H]** were precipitated, which were stable up to room temperature.

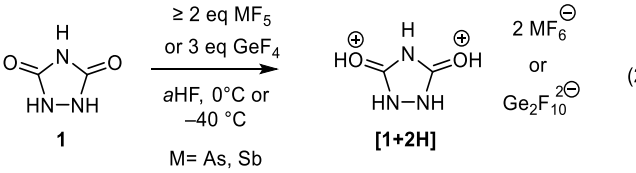

(2)

X-ray Crystallography: Recrystallization from *a*HF allowed to grow crystals suitable for single crystal X-ray diffraction. Of the monoprotonated species, crystals of **[1+1H]**$[SbF_6]$ were grown. Of the diprotonated species, **[1+2H]**$[(AsF_6)_2]$, **[1+2H]**$[Ge_2F_{10}]$ and **[1+2H]**$[(SbF_6)_2] \cdot 2HF$ were characterized. As standard deviations

in bond lengths and angles are the smallest in the hexafluoridoarsenate of **[1+2H]**, it is taken into account for the following explanations. The complete crystallographic data of all species is listed in the Supporting Information (Chapter 3). For comparison the crystal structure of urazole reported by Belaj[4] derived from low-temp diffraction of a single crystal is used.

[1+1H][SbF_6] crystallizes in the monoclinic space group $P2_1/c$ ($Z = 4$) (Figure 64). The C1-O1 distance increases from 1.232(1)/1.237(1) Å in **1** to 1.284(3) Å. This elongation shows the site of protonation to be the oxygen O1. The other C-O bond C2-O2 stays with 1.233(3) Å within range of urazoles' C-O distances. The CN bonds adjacent to the protonated CO moiety, C1-N1 and C1-N2, are reduced in length compared to **1**, from 1.378(1) and 1.367(1) Å to 1.347(3) and 1.315(3) Å respectively. Already in **1**, these CN distances are in length between a standard C–N single bond with 1.47 Å and a representative C=N double bond with 1.22 Å.[5] In **[1+1H]** these bonds come closer to a C=N double bond, especially C1-N2. The N-N bond is with 1.380(3) Å much shorter than in **1**, where it is 1.410(1) Å long. A standard N–N single bond is 1.48 Å long, a characteristic N=N double bond 1.22 Å,[5] in **[1+1H]** it is in between those two. The C-N bonds adjacent to the unprotonated carbonyl moiety, C2-N1 and C2-N3, are with 1.389(3) and 1.342(3) Å only slightly longer than in urazole, where they are 1.380(1) and 1.354(1) Å long.

Angles in **1** are not of equal size, as in an ideal symmetric pentagon, each angle would be 108°. The angles at the carbonyl moieties, N1-C1-N2 and N1-C2-N3 are 106.6(1)° and 106.3(1)° respectively. C1-N1-C2 amounts to 110.2(1)°. In **[1+1H]**, N1-C1-N2 is with 108.3(2)° within deviation ideal. C1-N1-C2 with 109.5(2)°, but especially N1-C2-N3 with 104.6(2)° does stray away from an ideal symmetric pentagon.

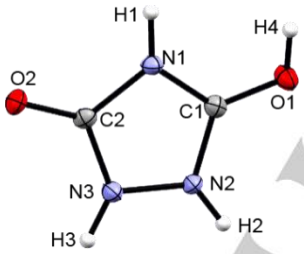

Figure 64. [1+1H], derived from the asymmetric unit of [$C_2N_3H_3O(OH)$][SbF_6], view along *a*. Displacement ellipsoids at 50% probability.

[1+2H][$(AsF_6)_2$] crystallizes in the orthorhombic space group *P*bca (*Z* = 8) (Figure 65). Protonation occurring at the second CO group is detected by the elongation of that CO bond. Ultimately, both CO distances are with 1.282(3) and 1.278(3) Å longer than those in **1**. The C-N bonds to N1, C1-N1 and C2-N1, are with 1.355(3) and 1.354(4) Å equidistant. The NN bond is with 1.372(4) Å of similar length compared to **[1+1H]**. The distances C2-N2 and C1-N3 amount to 1.316(3) and 1.308(4) Å. The decrease in CN bond length which was observed in **[1+1H]** only for the C-N bonds close to the COH^+ moiety is in **[1+2H]** occuring for all C-N bonds. Distortion is no longer present in **[1+2H]**. Each angle is within deviations 108°, the dications' ring resembles an ideal, symmetric pentagon.

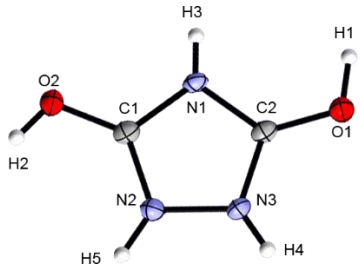

Figure 65. [1+2H], derived from the asymmetric unit of [$C_2N_3H_3(OH)_2$][$(AsF_6)_2$], view along *c*. Displacement ellipsoids at 50% probability.

In Figure 66, selected bond lengths of the here discussed species are visualized. The CO bonds are elongated by protonation, the CN bonds (at the protonated CO group) shortened.

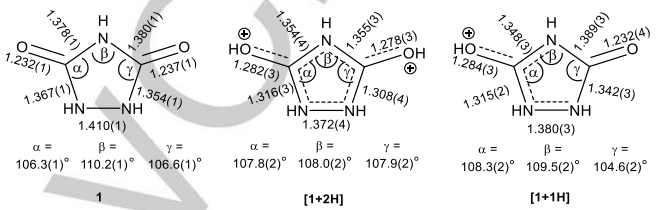

Figure 66. Overview of bond lengths (Å) and selected angles of **1**, **[1+1H]** and **[1+2H]**.

The protonation of urazole is compared to that of parabanic acid. The C=O bonds where protonations occurs, are elongated less in parabanic acid than in urazole. The CN distances within the ring, which are close to the protonated CO groups are shortened to a similar extent as observed in urazole. The C-N bonds to the unprotonated CO moiety in parabanic acid are elongated, in urazole they are shortened. The C-C bond between the protonated CO groups is slightly shortened, but with 1.511(3) Å still resembling much more a C–C single than a C=C double bond.[5] The equivalent in urazole, the N-N bond, comes significantly closer to an N=N double bond in length. At any degree of protonation, the angles within the ring of parabanic acid do not come close to ideal 108°, distortion is prevalent.

Raman Spectra: Urazole and all salts containing [1+1H] or [1+2H] were characterized by Raman spectroscopy. Quantum-chemically optimized structures were used to compute Raman frequencies and to enable assignment of experimentally found lines. In case of urazole itself a vibrational study by Jensen[6] was published in 2003, which was consulted for this work. For clarity, of **[1+1H]** and **[1+2H]** the experimental frequencies of the [SbF_6] and [SbF_6][Sb_2F_{11}] species are discussed. An overview of selected vibrations is given in Table 15, a complete list of assigned vibrational data together with the spectra is given in the Supporting Information (Chapter 2). Rather than a shift of the CO stretching modes by protonation of **1**, a change in the lines assigned to the CN stretching modes enabled comprehension of protonation of urazole. In **1** a single line assignable to the CN stretching vibration was found at 1258 cm^{-1}, which is in between a typical C–N single and C=N double bond stretching mode.[7] In **[1+1H]** two lines belonging to the CN stretching vibrations are detected, one blueshifted by

311 cm^{-1}, the other redshifted by 237 cm^{-1} compared to **1**. That shows that some CN bonds are strengthened, resembling C=N double bonds, while others are weakened, coming closer to C–N single bonds. For **[1+2H]** only one CN stretching mode is expected, the assigned line is observed at 1570 cm^{-1}. So no more C–N single bonds are present, only C=N double bonds.

A consecutive blueshift is observed for the NN stretching mode. The mode is shifted by 16 cm^{-1} due to monoprotonation and an additional 31 cm^{-1} by diprotonation compared to urazole. A typical N–N stretching mode is expected at around 930 cm^{-1}, a standard N=N stretching mode at 1570 cm^{-1}. With 1170 cm^{-1} in **[1+2H]**, Raman spectroscopy expects the NN bond to be in between a single and double bond in strength. X-ray crystallography shows that the N-N bond is shortened by protonation, the observed blueshift of the respective line fits well to the crystallographic data.

1 has a ring breathing mode, the assigned line is found at 1010 cm^{-1}. The mode vanishes by monoprotonation, the ring has lost symmetry. It is detected again by diprotonation as two lines at 1057 and 1039 cm^{-1} are assigned to the two ring breathing modes. The ring has regained symmetry and its ring breathing mode reapppears.

Table 15. Selected experimental Raman frequencies [cm^{-1}] of **1**, **[1+1H]** and **[1+2H]** as well as their assignment based on respective calculated vibrational frequencies [cm^{-1}]. [a]

1	**[1+1H]**[SbF_6]	**[1+2H]** [$(Sb_2F_{11})(SbF_6)$]	Assignment[a]
1258(2)	1569(10)	1570(6)	v (CN)
	1021(15)		v (CN)
1123(8)	1139(13)	1170(11)	v (NN)
1010(52)	-	1057(22) 1039(4)	ring breathing

[a] Calculated on B3LYP/6–311g++(3d2f, 3p2d) level of theory. Raman intensity in $Å^4/u$.

NMR Spectra: NMR spectroscopy of **1**, **[1+1H]**[SbF_6] and **[1+2H]**[$(SbF_6)_2$] was carried out in *a*HF. Only one signal each was detected by ^{14}N and ^{13}C NMR spectroscopy (Table 16), independent from degree of protonation. The broad signals in the ^{14}N NMR spectra of **[1+1H]** and **[1+2H]** point against *N*-protonation, as a doublet with a significant N-H coupling would then be visible. The single ^{13}C resonance does not shift significantly upon protonation. The presence of an oxonium hydrogen resonance was observed at 10.09 and 10.17 ppm for **[1+2H]** in dependence on temperature. NMR spectroscopy shows the diprotonated species to be a double *O*-protonated dication. The list of resonances as well as the spectra are given in the Supporting Information (Chapter 4).

Table 16. ^1H, ^{14}N and ^{13}C NMR shifts of **1** and its protonated species in *a*HF.[a]

	1[b]	**[1+1H]**[b] [SbF_6]	**[1+2H]** [$(SbF_6)_2$]
$\delta\,^1H$ (OH^+)	-	-	10.09[c]/10.17[b]
$\delta\,^{14}N$	–244.69	–246.67	–241.55[b]
$\delta\,^{13}C$	151.75	151.60	151.12[d]

[a] all shifts in ppm. [b] at 25 °C or 20°C. [c] at –40 °C. [d] at –30 °C.

Quantum chemical calculations: Quantum chemical calculations are employed using DFT, B3LYP/6–311G++(3d2f, 3p2d) level of theory for **1**, **[1+1H]** and **[1+2H]**. The calculations were foremost employed to assign observed Raman lines to calculated vibrational modes. The prediction of the increasing C-N or N-N bond strength and the resulting conjugation of bonds in the ring is computed by the used method. To ascertain charge distribution and to evaluate aromatic character, further calculation based on the previously optimized structures, the complete data is in the Supporting Information (Chapter 5).

Urazole itself is an aromatic compound. Crystallography indicates for **[1+2H]** an increased C=N double bond character. Also all angles within the ring each amount to the ideal 108°. These observations indicate increased conjugation, thus increased aromatic character of **[1+2H]** compared to **1**. So it was in our interest to quantify aromaticity by employing NICS(0) calculations.[8] A NICS(0) of –8.24 ppm is computed for urazole. For **[1+1H]** it decreases to –9.51 ppm and for **[1+2H]** to –11.32 ppm. A more negative NICS(0) value indicates increased aromatic character. The aromaticity of urazole is increased the most by diprotonation. Parabanic acid on the contrary has a NICS(0) of –2.93 ppm, which decreases to –3.02 ppm for the monocation and to –4.65 ppm for the dication. It is from the start much less aromatic compared to urazole, almost non-aromatic. A significant decrease of NICS(0) occurs only by diprotonation, which still a much more positive value compared to **[1+2H]**.

Mapped Electrostatic Potentials of **1**, **[1+1H]** and **[1+2H]** together with the NPA charges visualize charge stabilization (Figure 67). A light green to blue zone is visible in **[1+1H]** at the protonated carbonyl moiety. The positive charge introduced by monoprotonation is evenly distributed over the protonated carbonyl moiety and its' adjacent nitrogens. The NPA charges of the closeby nitrogens are increased more than that of the carbon. The light blue zone is present over the whole ring in **[1+2H]**. In the center, denoted by the deep blue colour, the least electron density is found. Conjugation of the whole ring in tandem with the carbonyl groups occurs. The NPA charges of the carbons are only slightly increased, most of the positive charges is distributed onto the nitrogens. For parabanic acid the positive charge is much more distributed on the carbons than on the nitrogens, for urazole it is vice versa. The charge is much more localized in diprotonated parabanic acid compared to diprotonated urazole, where the whole ring stabilizes the whole charge.

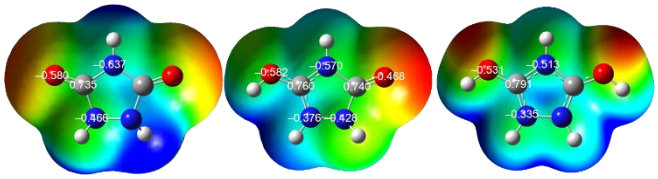

Figure 67. Molecular 0.0004 bohr^{-3} 3D isosurfaces with mapped electrostatic potentials and NPA charges of **1**,[a] **[1+1H]**[b] and **[1+2H]**[c] (color scale ranging from [a] –0.05 a.u. [red] to 0.05 a.u. [blue]; [b] 0.07 a.u. [red] to 0.24 a.u.;[c] 0.26 a.u. [red] to 0.38 a.u. [blue]).

Conclusion

Mono- and diprotonation of urazole was achieved for the first time in the superacidic media HF/BF_3, HF/GeF_4, HF/AsF_5 and HF/SbF_5. Room temperature stable salts containing mono- and diprotonated urazole were isolated. The compounds were characterized by Raman and NMR spectroscopy as well as single-crystal X-ray diffraction, confirming the protonations to occur at the carbonyl moieties. The increasing bond conjugation in the system with higher degree of protonation is mirrored by increase in aromatic character calculated by NICS(0). Charge stabilization occurs readily by all nitrogen atoms, in case of the dication, the whole ring stabilizes the positive charge.

Experimental Procedures

Caution! Avoid contact with any of these compounds. Hydrolysis might form HF, which burns skin and causes irreparable damage.

Apparatus and Materials

Standard Schlenk technique with a stainless steel vacuum line was used to perform all reactions. All reactions in superacidic media were carried out in FEP/PFA reactors closed with a stainless steelvalve. HF was dried with F_2 prior to use. Raman spectra were recorded on a Bruker MultiRAM FT-Raman spectrometer with Nd:YAG laser excitation (λ = 1064 nm). For Raman measurements, samples of products were transferred into a cooled glass cell, which were evacuated afterwards. The starting materials were transferred into NMR tubes and measured at room temperature. NMR spectra were recorded on a Jeol ECX400 NMR instrument. The spectrometer was externally referenced to $CFCl_3$ for ^{19}F, CH_3NO_2 for ^{14}N and to tetramethylsilane for ^{1}H and ^{13}C NMR spectra. The spectra were recorded inside 4 mm FEP NMR tube inliners. Acetone-d_6 was employed for external shimming when *a*HF was used as solvent for the respective compounds. The NMR samples were prepared by (re-)dissolving the respective protonated compound at the designated measuring temperature in *a*HF and transferring the solution into a 4 mm FEP NMR tube inliner. The inliner was then frozen and flame sealed. The low-temperature X-ray diffraction was performed with an Oxford X-Calibur3 equipped with a Kappa CCD detector, operating with Mo-K_α radiation (λ = 0.71073 Å) and a Spellman generator (voltage 50 kV, current 40 mA).

Deposition Numbers 2072534 for **[1+1H]**[SbF_6], 2072535 for **[1+2H]**[Ge_2F_{10}], 2072533 for **[1+2H]**[$(AsF_6)_2$] and 2072532 for **[1+2H]**[$(SbF_6)_2$]·2HF contain the supplementary crystallographic data for this paper. These data are provided free of charge by the joint Cambridge Crystallographic Data Centre and Fachinformationszentrum Karlsruhe Access Structures service www.ccdc.cam.ac.uk/structures.

General Procedure

In a typical experiment, the lewis acid and *a*HF were condensed into a FEP reactor at –196 °C. The mixture was reacted at –40 °C for 15 minutes and frozen to –196 °C. Urazole (~0.5–3.0 mmol) was added under constant N_2-flow. The complete mixture was reacted at before mentioned temperature. The solution was cooled down to –78 °C and the solvent was removed *in vacuo*. Some material of the obtained colorless salts was used for Raman spectroscopy, the rest was redissolved in *a*HF. A part of the solution was transferred into a FEP NMR tube, the rest was used to grow crystals suitable for single crystal X-ray diffraction.
For all experimental details, see the Supporting Information.

Acknowledgements

We are grateful to the Department of Chemistry and Pharmacy of the Ludwig Maximilians University of Munich, the Deutsche Forschungsgemeinschaft (DFG) and the F-Select GmbH for their financial support.

Keywords: Urazole • Single-crystal X-ray diffraction • Quantum chemical calculations • Superacids • Protonation

[1] K. T. Potts, *Chem. Rev.* **1961**, *61*, 87-127.
[2] T. M. Klapötke, B. Krumm, C. Riedelsheimer, J. Stierstorfer, C. C. Unger, M. H. H. Wurzenberger, *Eur. J. Org. Chem.* **2020**, *2020*, 4916-4924.
[3] S. Beck, M. Raljic, C. Jessen, A. J. Kornath, *Eur. J. Org. Chem.* **2020**, *2020*, 4521-4527.
[4] F. Belaj, *Acta Cryst.* **1992**, *48*, 1088-1090.
[5] A. F. Hollleman, E. Wiberg, N. Wiberg, *Lehrbuch der Anorganischen Chemie*, Walter de Gryuter & Co., Berlin, New York, **2007**.
[6] J. O. Jensen, *Spectrochim. Acta A* **2003**, *59*, 637-650.
[7] J. Weidlein, K. Dehnike, U. Müller, *Schwingungsspektroskopie. Eine Einführung*, Thieme Stuttgart **1988**.
[8] P. v. R. Schleyer, C. Maerker, A. Dransfeld, H. Jiao, N. J. R. Van Eikema Hommes, *J. Am. Chem. Soc.* **1996**, *118*, 6317-6318.

Entry for the Table of Contents

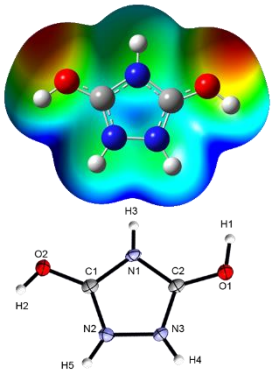

Mono- and diprotonation of urazole was achieved. The colorless salts were isolated and characterized by Raman and NMR spectroscopy as well as single-crystal X-ray crystallography. N, C or O – the localization and distribution of charge was investigated by quantum chemical calculations.

RESEARCH ARTICLE

Diaminomaleonitrile – mono-, di- …and tetraprotonation?!

A. Nitzer, P. Manhart, C. Jessen and A. J. Kornath*[a]

[a] A. Nitzer, C. Jessen, Prof. Dr. A. Kornath
Department of Chemistry and Pharmacy
LMU Munich
Butenandtstrasse 5–13, 81377 Munich, Germany
E-mail: alexander.nitzer@cup.uni-muenchen.de, christoph.jessen@cup.uni-muenchen.de, akoch@cup.uni-muenchen.de

Supporting information for this article is given via a link at the end of the document.

Abstract: The successful mono- and diprotonation of DAMN showed first site of protonation to be an amino group, second protonation occurs at a nitrile group. The prepared salts were characterized by vibrational spectroscopy and single crystal X-ray crystallography. Under strong superacidic conditions and with sufficient time cyclization of two (di)protonated molecules of DAMN is observed, leading to a tetracationic pyrazine species. Quantum chemical calculations are employed to explain reactivity and properties of here showed compounds.

Introduction

Diaminomaleonitrile (Figure 68) - commonly abbreviated as DAMN (**1**) - is of key interest in organic chemistry. First report in 1873 suggested a polymer of hydrogen cyanide,[1] which was later found to be its tetramer.[2] Further studies including IR and UV/VIS spectroscopy as well as ultimately X-ray crystallography show, that the compound is in fact the tetramer. The molecule is present exclusively in the *cis* conformation.[3] Although the *cis* conformation is far more stable than the *trans* one, attempts were made to synthesize diaminofumaronitrile (DAFN, Figure 68, **2**). In 1968, as the irradiation of an aqueous solution of **1** with UV radiation led to an imidazole, which had to proceed via **2**. Further experiments enabled isolation of DAFN,[4] although being labile in any solution, isomerizing back to DAMN.

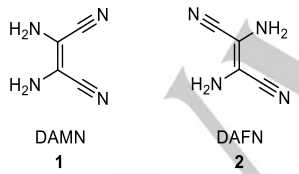

Figure 68. Structures of Diaminomaleonitrile (**1**) and Diaminofumaronitrile (**2**).

Under the aspect of chemical evolution, the compound is of high importance. Starting from hydrogen cyanide, which DAMN is the tetramer of, the nucleobases or α-amino acids can be formed (Scheme 19). As DAFN is obtainable by UV-radiation induced photoisomerization, follow-up reactions are possible.

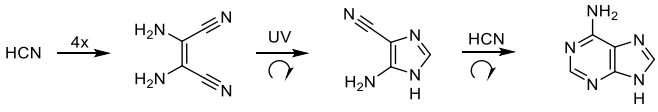

Scheme 19. Polymerization of hydrogen cyanide.[5]

Hydrogen cyanide and various nitriles are found in space, most prominently in the atmosphere of Saturns` moon Titan[6] or comets. The theory was sparked, that on the surface of those stellar bodies, for example the black crust, polymers may be found.[7] As HCN, and consecutively DAMN, polymerize to such a black solid, called azulmic acid, a source for more complex molecules is given.[8] It is suggested, that DAMN may be the main precursor for the formation of pyrimidines and purines.[9] As tested, reactions leading to nucleobases may simply occur from an aqueous NH_4CN solution even under icing conditions, which are present on icy moons, foremost Europa.[9] Volcanic activity as a cyanide source is present in various forms throughout the solar system. Hot volcanoes are found on Io, erupting sulfur clouds which contain cyanides. Cryovolcanoes, which emit slurries and aqueous solutions including HCN, are present on Triton, Ganymede, Pluto and other stellar bodies.[10]

As compounds in space are often protonated because of the huge abundance of solar radiation, e.g. protons, we wanted to examine DAMN under superacidic conditions. Most moons do not have a sufficiently strong magnetic field to shield the surface from radiation. The atmospheric cyanides are even more exposed to cosmic radiation than those in the crust. Furthermore, gas clouds, stellar and planetary nebulae do contain HCN.[11] Protonated hydrogen cyanide[12] as well as protonated cyanamide (H_2N-CN)[13] have been investigated. As the sensible next step, our interest was to protonate DAMN, perhaps even find heterocyclic compounds.

Results and Discussion

Diaminomaleonitrile was reacted in the superacidic media HF/SbF_5 and HF/AsF_5 at –40 °C (Equation 1), employing one or two equivalents of lewis acid.

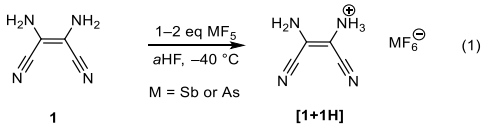

The starting material was quite insoluble in anhydrous HF (*a*HF) at –40°C, but reacted consequently as off-white brownish solids were precipitated. After removing the solvent at –78 °C, the hexafluoridoarsenate and hexafluoridoantimonate were characterized by IR and Raman spectroscopy and found to contain **[1+1H]** as cationic species. Protonation occurs at an amino group. Of the hexafluoridoantimonate, crystallization was

successful and enabled single crystal X-ray crystallography, determining **[1+1H]**[SbF_6] · 2HF to be present.

While monoprotonation of DAMN is possible with one or two equivalents of lewis acid, diprotonation is only observed with four or more equivalents at otherwise similar conditions. So **1** was reacted with four equivalents of lewis acid in *a*HF, resulting in off white-solids to be formed immediately (Equation 2).

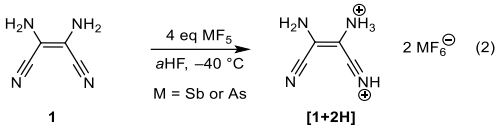

After removing the solvent at –78 °C, the off-white solids where characterized by IR and Raman spectroscopy. Second protonation occurs at the nitrile group which is on the same side of the double bond with the ammonium group. Of the hexafluoridoarsenate, suitable crystals for single crystal X-ray crystallography were grown, characterizing the diprotonated compound as **[1+2H]**[$(AsF_6)_2$] · 3HF.

When using at least four equivalents of SbF_5, reacting the mixture at up to 0 °C, then keeping the reactor stored at –70 °C for at least a week, crystals of a deeply yellow/orange color were found amongst the off-white bulk material (Equation 3). Single crystal X-ray crystallography identified the compound as **[1`+4H]**[$(SbF_6)_4$] · 3HF. The bulk material was characterized by IR and Raman spectroscopy and found to be mainly **[1+2H]**[$(SbF_6)_2$]. The tetracationic species was reproducable under similar conditions.

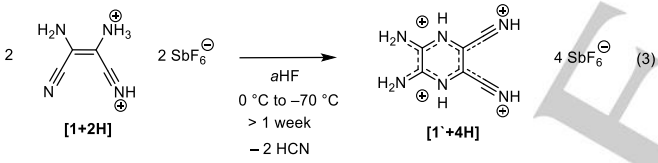

The tetracation was surprisingly stable, at room temperature for more than 15 minutes no decomposition was observed.

Crystal structure of monoprotonated DAMN: **[1+1H]**[SbF_6] · 2HF crystallizes in the monoclinic space group *C*2/c (*Z* = 8). In the asymmetric unit are besides the cation and two co-crystallized HF molecules two independent halfs of the anion. Depicted in Figure 69 is the cation **[1+1H]** with its closest contacts. The complete list of crystallographic details can be found in the Supporting Information (Chapter 3).

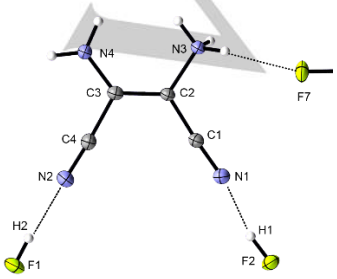

Figure 69. Section of the crystal structure of **[1+1H]**[SbF_6] · 2HF, view along *a*, displacement ellipsoids at 50% probability.

The starting molecule is symmetric regarding its` crystal structure within the bond length deviations, a mirror plane could be placed through the C=C double bond.[3b] That symmetry is lost by protonation. The C=C double bond in the monocation is 1.365(2) Å long, around the same length as in the starting material[3b] with 1.363(3) Å. These are values for a slightly elongated C=C double bond.[14] The C–N bond to the ammonium group, C2-N3, is 1.4589(18) Å long, the C-N(H_2) bond to the amino group, C3-N4, 1.338(2) Å. The first is elongated, the latter shortened, compared to the neutral compound with distances of 1.398(3) and 1.387(3) Å. The C≡N distances amount to 1.142(2) and 1.146(2) Å, both decreased in length compared to 1.166(3) and 1.164(3) Å in the starting material. The adjacent C–C bond length does slightly increase in the protonated half of the cation, e.g. C3-C4 is 1.454(2) Å long, while C1-C2 decreases in length to 1.416(2) Å compared to 1.434(3) and 1.441(3) Å.

Crystal structure of diprotonated DAMN: **[1+2H]**[$(AsF_6)_2$] · 3HF crystallizes in the orthorhombic space group *P*ca2_1 (*Z* = 4), the cation with its' closest contacts is depicted in Figure 70.

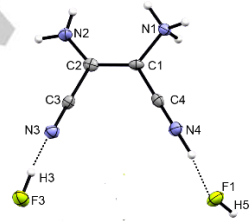

Figure 70. Section of the crystal structure of **[1+2H]**[$(AsF_6)_2$] · 3HF, view along *a*, displacement ellipsoids at 50% probability.

The C=C bond in **[1+2H]** is 1.380(6) Å long, which is around the same length as observed in **1** and **[1+1H]**. C1-N1, the C–N bond to the ammonium group, is 1.465(6) Å long, of similar length as in the monocation. The C–N bond to the NH_2 group, C2-N2, is 1.317(6) Å long, slightly shortened compared to **[1+1H]**. The C≡N distances amount to 1.133(6) Å and 1.130(6) Å, second protonation does not change bond lengths compared to the monoprotonated compound. The C-N bond adjacent to the nitrilium group, C1-C4, is further shortened, the trend observed before in **[1+1H]** is amplified. The other C–N bond, C2-C3, located next to the unprotonated nitrile group stays with 1.454(7) Å within same range of length as seen in **[1+1H]**.

When comparing all bond lengths of **1**, **[1+1H]** and **[1+2H]** (Figure 71), first, increase of the respective C–N distance by appearance of the ammonium group is observed. Second, quite possibly due to HF-coordination, the C≡N bonds decrease in length already in **[1+1H]**. Third, the C-N bond to the NH_2 group decreases in length, amplified by diprotonation. Fourth, the C–N bonds adjacent to the nitrile groups change length, the one at the protonated nitrile group is shortened, the other elongated.

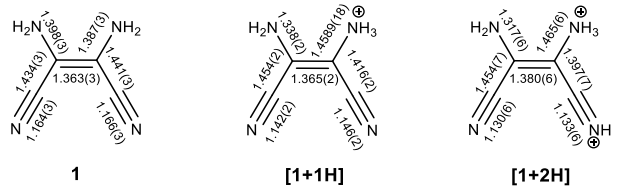

Figure 71. Bond lengths (Å) of **1**, **[1+1H]** and **[1+2H]** (left to right).

Crystal structure of cyclodimerized protonated DAMN: [1`+4H][$(SbF_6)_4$] · 3HF crystallizes in the triclinic space group *P*1 (*Z* = 1), the cation is depicted in Figure 72.

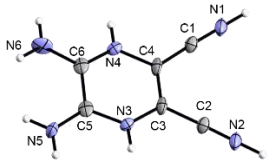

Figure 72. Cation derived from the asymmetric unit of **[1`+4H]**[$(SbF_6)_4$] · 3HF, view along *a*, displacement ellipsoids at 50% probability.

Bond lengths within the cycle (Table 17) were compared to the parent compound pyrazine (1,4-diazabenzene).[15] While C4-C3 is with 1.38(2) Å of similar length compared to 1.378(3) Å in pyrazine, the other C-C bond C5-C6 is with 1.50(2) Å much longer, more in range of a C–C single bond.[14] The C-N distances within the ring are in between C–N single and C=N double bond length.[14] Compared to pyrazine, when taking standard bond errors into consideration, the longest C-N bond C4-N4 is longer than in the parent compound. Assuming a mirror plane through the system, all C-N distances within the ring are slightly elongated compared to pyrazine. The C≡N distances are similar compared to **[1+1H]** and **[1+2H]**, the adjacent C-C bonds are in length between a C–C single and C=C double bond.[14] The C-N bonds to the NH_2 groups are with 1.34(3) and 1.32(2) Å length in between a C=N double and C–N single bond.[14] The angles within the ring are distorted like in pyrazine, which possesses a C-N-C angle of 115.8°. In **[1`+4H]** C6-N4-C4 amounts to 122.6(15)°. Reversal of distortion is likely caused by the lack of the two nitrogens' lone pairs, which are incorporated in the C-N bonds.

Table 17. Selected bond lengths of **[1`+4H]**[$(SbF_6)_4$] · 3HF.

Bond[a]	Length [Å]	Bond[b]	Length [Å]	Bond[c]	Length [Å]
N1-C1	1.15(2)	C3-C4	1.38(2)	C6-N6	1.34(3)
C1-C4	1.38(3)	C4-N4	1.41(2)	C5-N5	1.32(2)
C2-N2	1.11(3)	N4-C6	1.29(2)		
C2-C3	1.41(2)	C3-N3	1.33(2)		
		N3-C5	1.36(2)		
		C6-C5	1.50(2)		

[a] of the nitrile moiety. [b] of the ring. [c] of the imine moiety.

Vibrational spectroscopy: The protonation of DAMN is comprehended by Raman spectroscopy. Exemplary, a section from the Raman spectra of the hexafluoridoantimonates are depicted besides the starting material (Figure 73). The complete list of vibrational data is given in the Supporting Information (Chapter 2), selected frequencies are listed in Table 18.

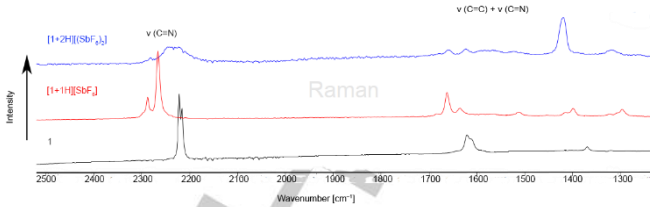

Figure 73. Section from the Raman spectra of **1**, **[1+1H]**[SbF_6] and **[1+2H]**[$(SbF_6)_2$].

Both lines assigned to the C≡N stretching modes are blueshifted by monoprotonation, although it occurs at the amino group. Second protonation, which results in the formation of a nitrilium group, then broadens the lines of these stretching vibrations. One broad line is thus observable, which is slightly redshifted compared to **[1+1H]**. In the range from 1300 to 1700 cm^{-1} the lines belonging to the deformation vibrations of the NH_2/NH_3 group as well as the C=C and C=N stretching vibrations are located. Monoprotonation leads to a strengthening of the C=C bond, the presence of the NH_3 group increases the respective C-N single bond length, thus blue-shifting the C=C stretching vibration. Diprotonation leads to a drastic change in bonding character in the molecule. The C=C stretching vibration is coupled with a C=N stretching vibration, leading to an overall redshift of the lines in that range, the C=C bond is weakened. Note that both C=C and C=N stretching vibration are always coupled with the deformation of the NH_2 and/or NH_3 group, independent from protonation degree.

Table 18. Selected experimental frequencies [cm^{-1}] of **1, [1+1H]**[SbF_6] and **[1+2H]**[$(SbF_6)_2$] and their assignment based in calculated vibrational frequencies [cm^{-1}].[a]

	1	**[1+1H]**[SbF_6]	**[1+2H]**[$(SbF_6)_2$]
ν (C≡N)		2289(35)	2282(16)
ν (C≡N)	2222(100)	2266(100)	2243(14)
ν (C≡N)	2216(81)		2226(28)
ν (C=C) + δ (NH_2/NH_3)	1646(s) 1617(s) 1621(46)	1715(vs) 1662(42)	
ν (C=C) + ν (C=N) + δ (NH_2/NH_3)			1558(w) 1552(w) 1420(60) 1319(26)

[a] Calculated on B3LYP/6–311g++(3d2f, 3p2d) level of theory, IR intensities in km/mol, Raman intensities in $Å^4/u$; abbreviations for IR intensities: vs – very strong, s – strong, w – weak.

Quantum chemical calculations: First, **1**, **[1+1H]** and **[1+2H]** were optimized on B3LYP/6–311g++(3d2f,3p2d) level of theory. That monoprotonation leads to an ammonium ion and not to a nitrilium species is perhaps on the first sight intuitive due to the obvious basicity of an amine. Contrary, protonation of cyanamide H_2N-CN occurs at the nitrile group. Furthermore, DFT calculations on the mentioned level of theory expect the nitrilium species to be energetically more favorable by 14.95 kcal/mol. As this contradicts experimental results, we employed MP2/6–311g++(3d2f, 3p2d) level of theory to obtain much more exact energies of both nitrilium and ammonium species of **[1+1H]**. Still the nitrilium species was calculated to be more favoured, although now only by 1.02 kcal/mol.

When examining the different diprotonated isomers, the dinitrilium species is expected to be the most stable when using DFT method on the mentioned level of theory (Scheme 20, top). The found ammonium nitrilium dication is 3.41 kcal/mol less stable. The other two possible species are much less energetically favorable, the *trans* ammonium nitrilium dication by 12.29 kcal/mol and the diammonium dication by 38.73 kcal/mol, each compared to the dinitrilium species. Again MP2/6–311g++(3d2f, 3p2d) was also employed to optimize the structures and compute energies. That method expects the experimentally found isomer to the have the lowest energy (Scheme 20, bottom). The dinitrilium species would be by 1.61 kcal/mol less stable, the *trans* ammonium nitrilium by 3.32 kcal/mol. The di ammonium species is considerably less favoured by 24.21 kcal/mol.

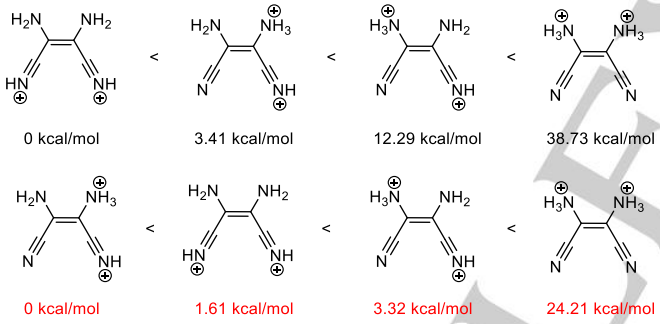

Scheme 20. Isomers of **[1+2H]** ordered by energy, lowest (left) to highest (right); top with black values: Energies calculated on B3LYP/6–311g++(3d2f, 3p2d) level of theory; bottom with red values: Energies calculated on MP2/6–311g++(3d2f, 3p2d) level of theory

While both methods fail to predict correct site of first protonation, MP2 fairs better to compute **[1+2H]** than DFT. Actually the MP2 method just inverts protonation sequence. To explain the discrepancy between experimental observations and quantum chemical calculations, a look on the crystal structures may enlighten. The calculations optimize the molecules in the gas phase. In both crystal structures of **[1+1H]** and **[1+2H]** the nitrile group(s) are strongly coordinated by hydrogen fluoride molecules, showing a possible cause by a solid-state effect. This adduct formation likely stabilizes the ammonium species over the nitrilium species, as the CN groups are blocked from protonation. Also a kinetic effect may lead to the formation of experimentally found species, which traps both mono- and dication with an ammonium species. As the calculated vibrational modes are far better predicted by DFT, especially in **[1+2H]**, for the following calculations B3LYP/6–311g++(3d2f, 3p2d) level of theory is employed.

To fathom the observations made by Raman spectroscopy and X-ray crystallography, NBO calculations were carried out to comprehend bond conjugation. NBO 6.0 with an explicit Natural Resonance Theory Analysis[16] was used to compute, how the bonding situation as well as bond occupation would be in **1**, **[1+1H]** and **[1+2H]**. While for DAMN and **[1+1H]** no unusual types of bonds were found, for **[1+2H]** two 3-center-4-electron bonds were detected, their key properties are listed in Table 19. One hyperbond (1.) is located from the NH_2 group to the C=C moiety, the other (2.) includes the nitrilium CN bond and the adjacent CC bond. While in the first the weighting between C=C and C=N bond is almost similar, for the second the weighting between C≡N vs C=C is more in favor for the CN triple bond. Occupation is below four electrons due to the species being a dication, lacking electrons.

Table 19. Hyperbonds detected by NBO analysis.[a]

	Hyperbond A:-B-:C	%A-B/%B-C[b]	occupation
1.	$(H_2)N\cdots C\cdots C$	51.0/49.0	3.78
2.	$(H)N\cdots C\cdots C$	66.4/33.6	3.61

[a] Structures were optimized before, B3LYP/6–311g++(3d2f, 3p2d) level of theory. [b] Threshold for detection 33.3%.

For **1**, **[1+1H]** and **[1+2H]**, Natural Resonance Theory (NRT) analysis included in NBO 6.0 generated the main contributing resonance structures together with their weighting. They are visualized in Scheme 21, Scheme 22 and Scheme 23. For DAMN (Scheme 21), the neutral structure is the leading one with 61.39%. Two zwitterionic ones with 7.33% weighting show a carbanion at the ethylene moiety together with an iminium cation. With 4.79% and 1.82% weighting, heterocumulenic structures, where ethylene carbons and nitrile nitrogens have alternatingly positive and/or negative charge, are computed.

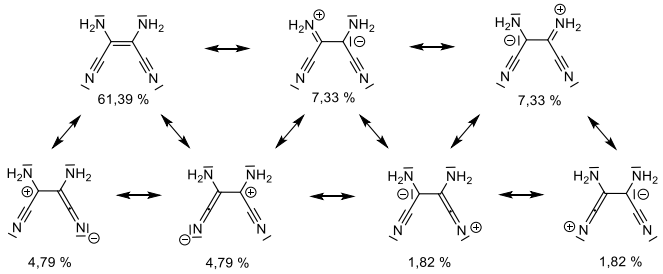

Scheme 21. Most important resonance structures of **1** with weighting.

For the monocation (Scheme 22), the resonance structure with the only positive charge at the ammonium group is the most important one with 69.52%. The heterocumulenic structures are of similar importance compared to the starting material, no iminium character is found in the five most weighted resonance structures.

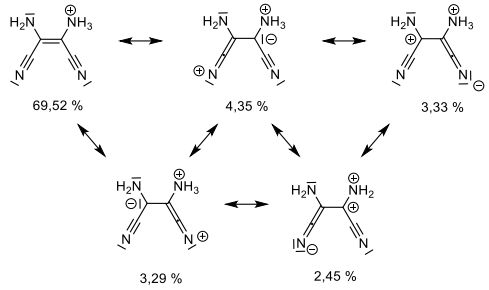

Scheme 22. Most important resonance structures of **[1+1H]** with weighting.

A drastic change in conjugation is observed for the dication (Scheme 23). The ammonium nitrilium structure with 34.55% weighting is only the second most important structure. The most important one with 36.53% predicts the ethylene carbon to have carbanionic character and three positive charges on three nitrogens to be present. The term of nitrilium iminium ammonium trication ethylene carbanion describes the leading resonance structure best. The heterocumulenic structures are calculated to be of similar importance compared to **1** and **[1+1H]**.

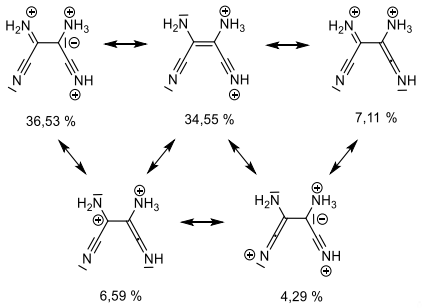

Scheme 23. Most important resonance structures of **[1+2H]** with weighting.

As shown by NRT calculations, DAMN undergoes a drastic change on mesomeric character by diprotonation. To exactly locate positive and negative charges, Mapped Electrostatic Potentials in conjunction with NPA charges were calculated for **1**, **[1+1H]** and **[1+2H]** and are visualized in Figure 74 and Figure 75. Overall changes in NPA charge are rather small by monoprotonation of DAMN. The ethylene carbons and nitrile nitrogens become more positive, the same is found for the ammonium nitrogen. The nitrile carbons and the amine nitrogen become slightly more negatively charged. Diprotonation drastically changes charge distribution. The iminium character is quite detectable, as the amine nitrogen becomes even more positively charged than the ammonium nitrogen. While the nitrogen of the unprotonated nitrile group has its NPA charge increased, the nitrilium nitrogens` one is decreased, becoming even more negative than in the starting material. The carbon at the nitrilium group is much more positively charged, the one at the unprotonated nitrile group becomes more negative. The carbanionic character of the ethylene carbon is validated, as that carbon becomes quite negatively charged. The ethylene carbon in the unprotonated moiety increases its NPA charge.

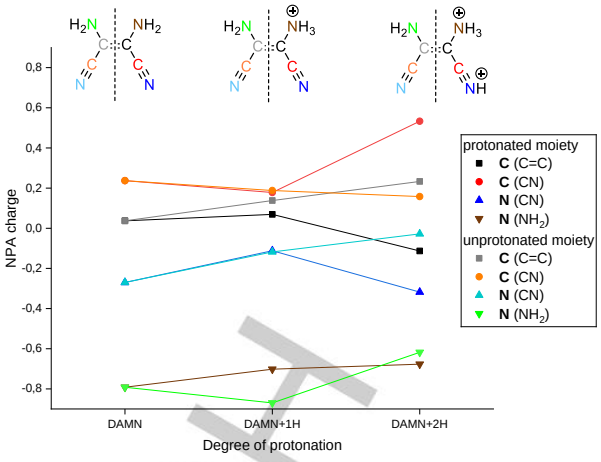

Figure 74. Plot of the NPA charges of **1**, **[1+1H]** and **[1+2H]**.

With the Mapped Electrostatic Potentials (MEPs) depicted in Figure 75 the change of conjugation and charge localization is recognizable. In **1** and **[1+1H]** each atom has its distinct charge. The lone pairs of the nitrile nitrogens are visible as red areas, the zone around the amino nitrogens is coloured blue, denoting less electron density to be present. The main difference between starting material and **[1+1H]** is the lower electron density at the ammonium group compared to the amino group. Otherwise, both MEPs are very similar. In **[1+2H]** all atoms from the amine/iminium group over C=C bond to the nitrilium group show the same potential, visible as a green area diagonally spanning the dication. Only ammonium and nitrile group have less or more electron density, which indicates their removal from conjugated system.

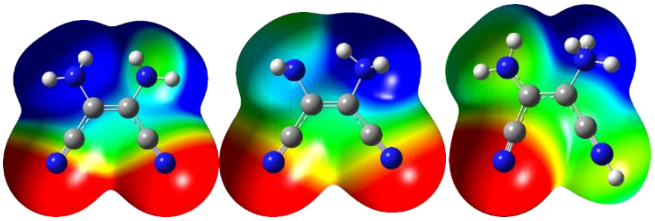

Figure 75. Molecular 0.0004 bohr^{-3} 3D isosurfaces with Mapped Electrostatic Potentials of **1**[a] (left), **[1+1H]**[b] (middle) and **[1+2H]**[c] (right); color scale ranging from [a] –0.02 a.u. (red) to 0.02 a.u. (blue), [b] 0.1 a.u. (red) to 0.22 a.u. (blue) and [c] 0.24 a.u. (red) to 0.36 a.u. (blue)

The mesomerism and charge distribution investigated by NRT and NBO calculations together with MEPs explains the change of bond lengths in the crystal structures, most prevalent in the dication. The imine and carbanionic character stand out in the diprotonated species, with the heterocumulenic character of importance at the protonated nitrile group. Due to that type of ionic character, triprotonation of DAMN was not achievable, but another observation was made, namely the mentioned cyclodimerazation to **[1`+4H]**.

Based on the findings regarding the tricationic carbanionic of **[1+2H]**, **[1`+4H]** may be explained as a dimerization and cyclization of two dications. As the carbanionic and iminium

character is increasingly present only in the diprotonated species, it may be essential for the formation of **[1`+4H]**. Quantum-chemical calculations using B3LYP/6–311g++(3d2f, 3p2d) level of theory were employed to optimize the experimentally found tetracation. With the optimized structure, NBO calculations together with computation of MEPs were carried out to locate the four positive charges. In Figure 76, the MEP of **[1`+4H]** is given with the respective NPA charges. The positive charges are stabilized by the whole system, with locally lowered electron density at the iminium and nitrilium moiety. To evaluate if the compound would not just exhibit a conjugated π-system, but show true aromaticity, a possible driving force for its formation, NICS(0) value[17] was calculated. With –3.90 ppm, the tetracation does have aromatic character, especially when comparing to the value of –4.12 ppm we computed for the parent compound pyrazine. An associated Molecular Orbital is also detected at –0.528 Hartree, encompassing the whole π-system. Fittingly, the MEP shows an electron deficit, deeply blue colored, in the middle of the aromatic ring. Interestingly, the blue zone stretches over the C-C bond close to the iminium moiety. The respective bond is with 1.50(2) Å far too long for a common aromatic C-C bond. The quantum chemical calculation do also expect this bond to be extraordinary long with 1.51 Å, close to a length of a typical C–C single bond.[14] All other bonds within the aromatic system fit better a typical aromatic ring, as they are much shorter.

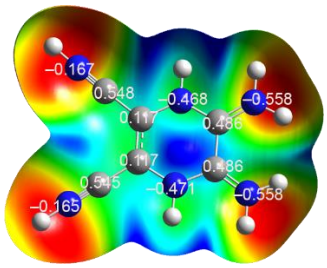

Figure 76. Molecular 0.0004 bohr^{-3} 3D isosurfaces with Mapped Electrostatic Potentials as a color scale ranging from 0.500 a.u. (red) to 0.585 a.u. (blue) of **[1`+4H]** together with NPA charges of respective atoms.

When examining NBOs and occupations, sp^2 hybridization is present for these two carbons, but the CC bond shows no π-bond besides the σ-bond. When assuming two positive charges in rightmost part of the cation (Figure 76), the moiety may be described as an ethane diamine dication, which would be isoelectronic to diboranetetramine (Figure 77). On that type of compound some theoretical studies were carried out.[18] A significant hyperconjugation from the free lone pairs of the nitrogens into the empty p-orbitals of the borons was calculated. Interactions rather showed no inclusion of the B-B bond, thus not changing bond properties. When adapting to our system, we find the lone pair of the nitrogens rather incorporated within C=N double bonds, more exhibiting iminium character. NBO calculation show delocalization from the iminium C=N bonds into the C–C single bond, a total of 2.86 kcal/mol. Further delocalizations include donations from the N-H bonds, be it from the imine nitrogen or the ring nitrogens, with a total of 19.61 kcal/mol. Thus, the C–C single bond is stabilized, although not shortened, but still included into the π-system, enabling ring current and aromatic character.

Figure 77. The section from **[1`+4H]**, the ethane diamine dication (left) and comparison to diboranetetramine (right).

As presence of hydrogen cyanide and subsequently DAMN in space is confirmed, diprotonation of **1** could enable cyclodimerization and formation of heterocycles. While (di)protonated DAMN may be not present on moons with a thick atmosphere and perhaps a small magnet field, stellar and planetary nebulae are a much more suitable environment for this kind of dimerization. Protons are a main component of solar winds, which are there in abundance. As energy difference between ammonium nitrilium and dinitrilium species are quite small, presence in outer space of the first must not be excluded. On the other hand, dimerization of the dinitrilium dication may also be possible, leading to other heterocyclic compounds.

Many extraterrestrial environments, be it Europas' oceans[19] or past Mars' aquatic areas,[20] are expected to be acidic. The cold oceans of Europa could have a pH value of around 2.6 due acidification oxidants.[19] The acidic waters of the Tinto River in spain show pH values as low as 1.05, the authors describe this environment as a possible approximation of the *Terra Meridiani* hematite site of Mars supporting its aqueous origin. While on earth the rivers acidity, mainly at its spring, is caused by chemolithotrophic bacteria,[20] on Mars the cause may be different. Although the discussed aqueous environments are quite less acidic than our employed superacids, reactivity of DAMN may be enabled just enough to start formation of heterocycles. Considering the timescales, if not in our solar system it may happen somewhere else.

Conclusion

We report the first-time protonation of diaminomaleonitrile. First an ammonium cation, then to an ammonium nitrilium dication is formed. The latter is not a simple dication, as ammonium iminium and nitrilium character is detected, while one ethylene carbon is carbanionic. NRT and NBO calculations verify the spectroscopically and crystallographically found bond conjugation. With the cyclodimerization of two dications, leading to a tetracationic pyrazine derivative, a possible way of formation for heterocycles in outer space is presented.

Experimental Procedures

Caution! Avoid contact with any of these compounds. Hydrolysis might form HF, which burns skin and causes irreparable damage.

Apparatus and Materials

Standard Schlenk technique with a stainless steel vacuum line was used to perform all reactions. All reactions in superacidic media were carried out in FEP/PFA reactors closed with a stainless steelvalve. HF was dried with F_2 prior to use. Raman spectra were recorded on a

Bruker MultiRAM FT-Raman spectrometer with Nd:YAG laser excitation (λ = 1064 nm). For Raman measurements, samples of products were transferred into a cooled glass cell, which were evacuated afterwards. IR spectra were recorded with a Vertex-80V FT-IR spectrometer. Samples were placed on a CsBr single-crystal plate within a cell, which was cooled for the compounds not stable at room temperature. The low-temperature X-ray diffraction was performed with an Oxford X-Calibur3 equipped with a Kappa CCD detector, operating with Mo-K_α radiation (λ = 0.71073 Å) and a Spellman generator (voltage 50 kV, current 40 mA).

Deposition Numbers 2120215 for **[1+1H]**[SbF_6]·2HF, 2120216 for **[1+2H]**[$(AsF_6)_2$]·2HF and 2120217 for **[1`+4H]**[$(SbF_6)_4$]·HF contain the supplementary crystallographic data for this paper. These data are provided free of charge by the joint Cambridge Crystallographic Data Centre and Fachinformationszentrum Karlsruhe Access Structures service www.ccdc.cam.ac.uk/structures.

General Procedure

In a typical experiment, the lewis acid and *a*HF were condensed into a FEP reactor at –196 °C. The mixture was reacted at –40 °C for 15 minutes and frozen to –196 °C. Diaminomaleonitrile was added under constant N_2-flow. The complete mixture was reacted at before mentioned temperature. The solution was cooled down to –78 °C and the solvent was removed *in vacuo*. Some material of the obtained colorless salts was used for Raman spectroscopy, the rest was redissolved in *a*HF to grow crystals suitable for single crystal X-ray diffraction.

For all experimental details, see the Supporting Information.

Acknowledgements

We are grateful to the Department of Chemistry and Pharmacy of the Ludwig Maximilians University of Munich, the Deutsche Forschungsgemeinschaft (DFG) and the F-Select GmbH for their financial support.

Keywords: Diaminomaleonitrile • Superacid • Tetracation • Quantumchemistry • Astrochemistry

[1] O. Lange, *Liebigs Ann. Chem.* **1873**, *6*, 99-101.
[2] C. Bedel, *Compte Rendu* **1923**, 168-171.
[3] [a] R. L. Webb, S. Frank, W. C. Schneider, *J. Am. Chem. Soc.* **1955**, *77*, 3941-3943; [b] B. R. Penfold, W. Lipscomb, *Acta Cryst.* **1961**, *14*, 589-597.
[4] Y. Yamada, N. Nagashima, Y. Iwashita, A. Nakamura, I. Kumashor, *Tetrahedron Lett.* **1968**, *9*, 4529-4532.
[5] J. P. Ferris, L. E. Orgel, *J. Am. Chem. Soc.* **1966**, *88*, 1074-1074.
[6] R. N. Clark, J. M. Curchin, J. W. Barnes, R. Jaumann, L. Soderblom, D. P. Cruikshank, R. H. Brown, S. Rodriguez, J. Lunine, K. Stephan, T. M. Hoefen, S. Le Mouélic, C. Sotin, K. H. Baines, B. J. Buratti, P. D. Nicholson, *J. Geophys. Res.* **2010**, *115*.
[7] C. N. Mathhews, *Orig. Life Evol. Biosph.* **1991**, *21*, 421-434.
[8] C. N. Matthews, R. D. Minard, *Faraday Discuss.* **2006**, *133*, 393.
[9] M. R. Marín-Yaseli, E. González-Toril, M. Ruiz-Bermejo, *Front. Astron. Space Sci.* **2020**, *7*.
[10] [a] J. S. Kargel, *Earth Moon Planets* **1994**, *67*, 101-113; [b] S. A. Fagents, *J. Geophys. Res. Planets* **2003**, *108*, 1-19.
[11] *https://phys.org/news/2021-06-molecules-reveal-clues-dying-stars.html* **2021**.
[12] [a] H. Tachikawa, T. Iyama, T. Fukuzumi, *Astron. Astrophys.* **2003**, *397*, 1-6; [b] N. R. Goetz, J. A. H. Axhausen, T. Soltner, C. Rotter, A. J. Kornath, *ChemistrySelect* **2016**, *1*, 5517-5520.
[13] J. Axhausen, *Ph.D. thesis* **2013**.
[14] A. F. Hollleman, E. Wiberg, N. Wiberg, *Lehrbuch der Anorganischen Chemie*, Walter de Gryuter & Co., Berlin, New York, **2007**.
[15] P. J. Wheatley, *Acta Cryst.* **1957**, *10*, 182-187.
[16] [a] E. D. Glendening, C. R. Landis, F. Weinhold, *J. Comput. Chem.* **2013**, *34*, 1429-1437; [b] J. K. B. NBO 6.0. E. D. Glendening, A. E. Reed, J. E. Carpenter, C. M. Morales, C. R. Landis,, U. and F. Weinhold (Theoretical Chemistry Institute, University of Wisconsin, WI, 2013); http://nbo6.chem.wisc.edu/.
[17] P. v. R. Schleyer, C. Maerker, A. Dransfeld, H. Jiao, N. J. R. Van Eikema Hommes, *J. Am. Chem. Soc.* **1996**, *118*, 6317-6318.
[18] C. R. Watts, J. K. Badenhoop, *J. Chem. Phys.* **2008**, *129*, *104307*, 1-7.
[19] M. A. Pasek, R. Greenberg, *Astrobiology* **2012**, *12*, 151-159.
[20] [a] R. Amils, E. González-Toril, A. Aguilera, N. Rodríguez, D. Fernández-Remolar, F. Gómez, A. García-Moyano, M. Malki, M. Oggerin, I. Sánchez-Andrea, J. L. Sanz, in *Advances in Applied Microbiology, Vol. 77* (Eds.: A. I. Laskin, S. Sariaslani, G. M. Gadd), Academic Press, **2011**, pp. 41-70; [b] D. Fernández-Remolar, J. Gómez-Elvira, F. Gómez, E. Sebastian, J. MartíIn, J. A. Manfredi, J. Torres, C. González Kesler, R. Amils, *Planet. Space Sci.* **2004**, *52*, 239-248.

Entry for the Table of Contents

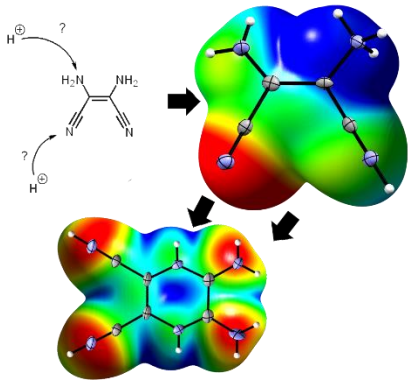

DAMN – that's interesting. Mono- and diprotonation of diaminomaleonitrile were carried out. With two basic sites, where does Protonation occur? And how can a tetracation be formed by these cations? On these topics and much more will be elucidated in this article.